NTNU
Norwegian University of
Science and Technology

Integration of LNG Regasification and Air Separation Units

Roxane Edith Helene Giametta

Natural Gas Technology
Submission date: June 2017
Supervisor: Truls Gundersen, EPT
Co-supervisor: Donghoi Kim, EPT

Norwegian University of Science and Technology
Department of Energy and Process Engineering

Thesis description

Liquefied natural gas (LNG) is a major source of natural gas supply for long-distance transport, typically over 2000 km. After the long travel, the LNG is vaporized in a receiving terminal in order to supply natural gas at desired conditions through domestic pipeline networks. During regasification, the cold energy of the LNG (around -163 ^{o}C) is just released to the environment by heat exchange with seawater or air, wasting a large amount of exergy. Therefore, there have been various attempts to recover such cold exergy in the import terminal.

- Power generation by a cold Rankine cycle.
- Desalination of the seawater using LNG cold energy.
- Food processing (Freezing food using the cold LNG as refrigeration)
- Fractionation of heavier hydrocarbons in the imported LNG using the cold LNG
- Air Separation Unit (ASU) integrated with the cold LNG stream

Due to the low operating temperature of air separation units (from -170 ^{o}C to -190 ^{o}C), these plants can benefit significantly from the supply of cold exergy from an LNG regasification plant. Thus, the integration of LNG regasification with an ASU is regarded as a promising alternative for utilizing the cold energy of LNG. Air separation has various process schemes such as one-column, two-column, and even three-column distillation. This increases the complexity of design in the LNG regasification system when integrated with an ASU. Thus, process providers and academic researchers have suggested a number of LNG regasification processes integrated with an ASU. However, there seems to be a lack of fair comparison between the systems suggested. The fact that each system brings different products makes setting a reasonable objective function difficult.

The main objective of this Master thesis is to perform a fair comparison between various process concepts for LNG regasification integrated with an air separation unit by using mathematical optimization, considering exergy as an objective function. The process modeling, optimization, and exergy analysis will be performed in commercialized simulation tools, such as Aspen HYSYS and MATLAB.

The following tasks are to be considered:

1. Literature review of current technical trends in utilization of LNG cold energy and make a survey of LNG regasification processes integrated with air separation units.
2. Select and categorize the most promising process options for further evaluation.
3. Establish process models and design basis for a robust and rigorous optimization study on an LNG regasification process integrated with various air separation schemes.

4. Perform optimization by Aspen HYSYS or MATLAB for the processes with different objective functions and constraints, such as exergy efficiency (Exergy Transfer Effectiveness).

5. Present and analyze the optimization results for the process options and different objective functions. If possible, compare the results with relevant literature. The optimization work performed must be reproducible.

6. Discuss analysis results and give a recommendation for selection of an LNG regasification system integrated with an air separation process. Evaluate the use of exergy efficiency (Exergy Transfer Effectiveness) as an objective function and/or constraints in optimization for complicated processes with distillation columns.

Department of Energy and Process Engineering, 15 January 2017

__Truls Gundersen___
Academic Supervisor

Research Advisor:

PhD student Donghoi Kim, Department of Energy and Process Engineering
E-mail: donghoi.kim@ntnu.no

Abstract

Through the various LNG cold recovery applications, cryogenic air separation is the only one recovering the coldest range of temperature-based exergy, which is also the most valuable. Several designs of integrated ASU and LNG regasification have been proposed but there is still a lack of fair comparison between the existing options. In this study, promizing configurations have been selected and classified according to the number of columns in the ASU block and the use of LNG cold exergy either for feed air cooling or in the nitrogen liquefaction loop. Each case has been modelized in the commercialized software Aspen HYSYS and evaluated thanks to a range of performance indicators: LNG cold exergy use, work requirement per amont of liquid nitrogen produced, Exergy Transfer Effectiveness and the decomposition of material stream exergy variations both at stream level and at component level. The two first indicators where insufficient to compair fairly the cases and required to scale the designs to a common set of constraints. ETE provided a tool to fairly compare the designs, with regards to all the ASU products, without re-scaling the original models. Yet, the high energy requirements for ASU processes overweighted material stream exergy variations in ETE results, making it close to a ratio of expansion to compression work. Further decomposition of material exergy variations confirmed that exergy analysis at component level was more consistant than stream level calculation for processes with a chemical change. Single column designs were more efficient than two-column ASU configurations, the best performing cases among integrated designs being the recuperative vapor recompression ASU using heat pump effect proposed by Fu and Gundersen (2013) followed by the integration of column draws coupled to compression-expansion described by Mehrpooya et al. (2015).

Table of Contents

Thesis description **1**

Abstract **i**

Table of Contents **v**

List of Tables **viii**

List of Figures **xi**

Nomenclature **xii**

1 Preliminary literature review - trends and technologies **1**
- 1.1 LNG regasification . . . 1
  - 1.1.1 Regasification market . . . 1
  - 1.1.2 LNG import terminals . . . 3
  - 1.1.3 LNG vaporization processes . . . 3
- 1.2 Utilization trends of LNG cold energy other than ASU . . . 5
  - 1.2.1 Power generation . . . 6
  - 1.2.2 Seawater desalination . . . 10
  - 1.2.3 Food processing . . . 12
  - 1.2.4 NGL extraction and fractionation from LNG feed . . . 13
- 1.3 Cryogenic Air separation processes . . . 13
  - 1.3.1 Single-column processes . . . 15
  - 1.3.2 Two-column processes . . . 15
  - 1.3.3 Multiple-column processes . . . 17

2 Survey of existing integrated ASU and LNG regasification technologies **21**
- 2.1 Two-column processes . . . 23
  - 2.1.1 Small capacity two-column ASU with nitrogen cycle and LNG cold recovery, Xu et al. (2014) . . . 23

2.1.2 Two-column ASU with large capacity fully integrated LNG cold recovery, Tesch et al. (2016) 23
2.2 Single-column processes 25
2.2.1 Single-column heat pump ASU and LNG cold recovery with cyclic nitrogen, Zheng et al. (2015) 25
2.2.2 Single-column ASU with LNG cold recovery and power cycle, Mehrpooya et al. (2015) 26

3 Selection of processes and parameter sets for a fair comparison 29
3.1 Selection of ASU and LNG regasification configurations 29
3.2 Method for the selection of parameter sets 31
3.3 Inlet parameters 31
3.3.1 LNG feed specifications 31
3.3.2 Air feed specifications 32
3.4 Product specifications 33
3.4.1 Regasified LNG 33
3.4.2 ASU products 33
3.5 Machinery and equipment design 34
3.5.1 Compressors, pumps and expanders 34
3.5.2 Heat exchangers 35
3.5.3 Distillation columns 35

4 Modelization 37
4.1 Adaptation of integrated models from literature 38
4.1.1 CASE IMHE-1C - Single column ASU, LNG in the MHE, based on the work by Mehrpooya et al. (2015) 38
4.1.2 CASE IMHE-2C - Two-column ASU, LNG in the MHE, based on the work by Xu et al. (2014) 39
4.1.3 CASE ILoop-1C - Single column ASU, LNG in the nitrogen loop, based on the work by Zheng et al. (2015) 39
4.1.4 CASE ILoop-2C - Two-column ASU, LNG in the nitrogen loop, based on the work by Xu et al. (2014) and Ebrahimi et al. (2015) . 40
4.2 Introduction of expansion work 40
4.2.1 CASE IMHE-2Cexp 40
4.2.2 CASE ILoop-2Cexp 41
4.3 Adaptation of stand-alone models 41
4.3.1 CASE Alone-1C - Single column ASU, based on the work by Fu and Gundersen (2013) 41
4.3.2 CASE Alone-2C - Two-column ASU, based on the work by Ebrahimi et al. (2015) 41

5 Cases comparison and performance indicator analysis 53
5.1 Utilization of LNG cold exergy 53
5.2 Work per amont of liquid nitrogen produced 55
5.3 Exergy efficiency 56
5.3.1 ETE calculation for the study 57

5.3.2 ETE result analysis 60
5.4 Material stream exergy ratio 64

6 Conclusion **71**
6.1 Key results and comments 71
6.2 Further work 72

Bibliography **74**

7 Appendix **77**
7.1 Exergy presentation 77
7.2 Decomposition of exergy sinks and sources of the overall process into ASU, LNG and energy contributions 80
7.3 Decomposition of exergy contribution per exergy term per ASU product stream at stream level and at component level 82

List of Tables

1.1 Cryogenic power plants using LNG exergy in Japan, Gomez et al. (2014). 8

2.1 Air separation units using LNG cold energy, Xu et al. (2014). 22

3.1 Classification of reviewed integrated ASU and LNG regasification configurations. 30
3.2 LNG feed stream composition. 32
3.3 Air feed stream composition. 33
3.4 Summary of specifications for ASU products. 34

4.1 Summary of simulated cases. 37

5.1 Work required per amont of liquid nitrogen produced, in kW per ton per hour. 56
5.2 Exergy efficiency at stream level, with sinks and sources in TW and ratio ETE2 in %. 61
5.3 Exergy efficiency at component level, with sinks and sources in TW and ratio ETE3 in %. 61
5.4 Material stream exergy ratio, in %. 65

7.1 ETE2 decomposition in GW. 80
7.2 ETE3 decomposition in GW. 81
7.3 Decomposition of exergy flow terms for ASU products at stream level in case IMHE-1C, in kW. 83
7.4 Decomposition of exergy flow terms for ASU products at component level in case IMHE-1C, in kW. 83
7.5 Decomposition of exergy flow terms for ASU products at stream level in case ILoop-1C, in kW. 84
7.6 Decomposition of exergy flow terms for ASU products at component level in case ILoop-1C, in kW. 84

7.7 Decomposition of exergy flow terms for ASU products at stream level in case Alone-1C, in kW. 85
7.8 Decomposition of exergy flow terms for ASU products at component level in case Alone-1C, in kW. 85
7.9 Decomposition of exergy flow terms for ASU products at stream level in case IMHE-2C, in kW. 86
7.10 Decomposition of exergy flow terms for ASU products at component level in case IMHE-2C, in kW. 86
7.11 Decomposition of exergy flow terms for ASU products at stream level in case IMHE-2C exp, in kW. 87
7.12 Decomposition of exergy flow terms for ASU products at component level in case IMHE-2C exp, in kW. 87
7.13 Decomposition of exergy flow terms for ASU products at stream level in case ILoop-2C, in kW. 88
7.14 Decomposition of exergy flow terms for ASU products at component level in case ILoop-2C, in kW. 88
7.15 Decomposition of exergy flow terms for ASU products at stream level in case ILoop-2C exp, in kW. 89
7.16 Decomposition of exergy flow terms for ASU products at component level in case ILoop-2C exp, in kW. 89
7.17 Decomposition of exergy flow terms for ASU products at stream level in case Alone-2C, in kW. 90
7.18 Decomposition of exergy flow terms for ASU products at component level in case Alone-2C, in kW. 90

List of Figures

1.1 LNG supply chain, Mokhatab et al. (2014). 2
1.2 LNG regasification capacity (MTPA) and utilization by country (%), IGU (2016). 2
1.3 LNG onshore import terminal, Mokhatab et al. (2014). 3
1.4 Open Rack Vaporizer overview, Egashira (2013). 4
1.5 Submerged Combustion Vaporizer, Egashira (2013). 5
1.6 Ambient Air Vaporizer schematic, Mokhatab et al. (2014) 6
1.7 Intermediate Fluid Vaporizer schematic using seawater heating, Egashira (2013). 6
1.8 LNG temperature and duty during regasification depending on the distribution pressure, Mokhatab et al. (2014). 7
1.9 LNG pressure-based exergy use in direct expansion, Gomez et al. (2014). 9
1.10 Cold Rankine cycle options for cryogenic power production from LNG cold exergy, Gomez et al. (2014). 10
1.11 Combined regenerative cold RC and direct expansion using LNG thermomechanical exergy for cryogenic power production, Gomez et al. (2014). . 10
1.12 Open Brayton cycle using LNG cold exergy to cool the compressor suction stream, Gomez et al. (2014). 11
1.13 Closed Brayton cycle with LNG precooling and intercooling combined to direct expansion, Gomez et al. (2014). 11
1.14 Indirect contact freeze desalination process using a glycol solution regenerated by LNG cold, Efrat (2011). 12
1.15 Evaporation-condensation seawater desalination using a glycol solution regenerated by LNG cold, Efrat (2011). 13
1.16 Main steps of a cryogenic air distillation plant, Agrawal and Herron (2000). 14
1.17 Single-column ASU with recuperative vapor recompression and distributed reboiling, Fu and Gundersen (2013). 16
1.18 Simplified flow diagram of a basic two-column ASU, distillation part, Agrawal and Herron (2000). 17

1.19 Simplified flow diagram of a two-column ASU with turbo-expander, reflux sub-cooling and oxygen internal compression, Agrawal and Herron (2000). 18
1.20 ASU three-column configuration for crude argon recovery, Agrawal and Herron (2000). 19
1.21 ASU four-column configuration for pure argon recovery, Moll (2014). . . 20

2.1 Conventional process of two-column ASU integrated with LNG, Xu et al. (2014). 24
2.2 Novel process of two-column ASU integrated with LNG, Xu et al. (2014). 24
2.3 Conceptual design 1 - two-column ASU with LNG integrated in the MHE and gaseous product HE, Tesch et al. (2016). 25
2.4 Conceptual design 2 - two-column ASU with LNG integrated in all the heat exchangers, Tesch et al. (2016). 26
2.5 Flowsheet of a single-column heat pump ASU with LNG cold recovery through nitrogen cycle, Zheng et al. (2015). 27
2.6 Flowsheet of a single-column ASU with LNG cold recovery through nitrogen cycle and power cycle, Mehrpooya et al. (2015). 28

4.1 CASE IMHE-1C - Flowsheet of a single column ASU with LNG integrated in the MHE, adapted from the work by Mehrpooya et al. (2015). . 43
4.2 CASE IMHE-2C - Flowsheet of a two-column ASU with LNG integrated in the MHE, adapted from the work by Xu et al. (2014). 44
4.3 CASE ILoop-1C - Flowsheet of a single column ASU with LNG integrated in the nitrogen loop, adapted from the work by Zheng et al. (2015). 45
4.4 CASE ILoop-2C - Flowsheet of a two-column ASU with LNG integrated in the nitrogen loop, adapted from the work by Xu et al. (2014) and Ebrahimi et al. (2015). 46
4.5 CASE IMHE-2Cexp - Flowsheet of a two-column ASU with LNG integrated in the MHE, adapted from the work by Xu et al. (2014). 47
4.6 CASE ILoop-2Cexp - Flowsheet of a two-column ASU with LNG integrated in the nitrogen loop, adapted from the work by Xu et al. (2014) and Ebrahimi et al. (2015). 48
4.7 CASE Alone-1C - Original design of single column stand-alone ASU by Fu Chao. 49
4.8 CASE Alone-1C - Flowsheet of a stand-alone single column ASU, adapted from the work by Fu and Gundersen (2013). 50
4.9 CASE Alone-2C - Original design of two-column stand-alone ASU, proposed by Ebrahimi et al. (2015). 51
4.10 CASE Alone-2C - Flowsheet of a stand-alone two-column ASU, adapted from the work by Ebrahimi et al. (2015). 52

5.1 Details of LNG cold exergy utilization, in %. 54
5.2 Decomposition of ETE3 sink terms, in %. 62
5.3 Decomposition of ETE3 source terms, in %. 63
5.4 ETE2, ETE3 and work ratio, in %. 64

5.5 Comparison of material exergy ratio based on stream-level (ETE2) and component-level (ETE3) exergy terms, in %. 65
5.6 ASU sink decomposition per product at stream level (ETE2), in kW. . . . 68
5.7 ASU sink decomposition per product at component level (ETE3), in kW. . 68
5.8 ASU source decomposition per product at stream level (ETE2), in kW. . . 69
5.9 ASU source decomposition per product component level (ETE3), in kW. . 69

7.1 Decomposition of exergy proposed by Marmolejo-Correa and Gundersen (2015). 78

Nomenclature

Superscripts and Subscripts
i = sum indice for stream components
j = sum indice for exergy terms
k = sum indice for streams
l = sum indice for expanders
z = sum indice for compressors and pumps
$comp$ = compressor
exp = expander
T = temperature-based
P = pressure-based
CH = chemical
Parameters
W = Work in kW
$\dot{m}$ = mass flow in ton per second
$\dot{n}$ = molar flow in kmol per second
n = molar quantity in kmol
E_x = exergy in kJ
e_x = molar exergy in kJ per kmol
$\tilde{e_x}$ = partial molar exergy in kJ per kmol
h = molar enthalpy in kJ per kmol
s = molar entropy in kJ per kmol per K
P = pressure in kPa
T = temperature in ^{o}C or K
Abreviations
LNG = Liquefied Natural Gas
ASU = Air Separation Unit
MTPA = Million Tons Per Annum
FSRU = Floating Storage and Regasification Units
GBS = Gravity Based Structures
ORV = Open Rack Vaporizers
SCV = Submerged Combustion Vaporizers
AAV = Ambient Air Vaporizers
STV = Shell and Tube exchange Vaporizers
IFV = Intermediate Fluid Vaporizers
RC = Rankine Cycles
BC = Brayton Cycles
NGL = Natural Gas Liquids
NBP = Normal Boiling Point
DCAC = Direct Contact After-Cooler
PPU = Pre-Purification Unit

DE = Direct expansion
MHE = Main Heat Exchanger
HP = High Pressure
LP = Low Pressure
JT = Joule-Thomson
HE_{Loop} = Heat Exchanger in the process nitrogen loop
LHV = Low Heating Value
ETE = Exergy Transfer Effectiveness
ETE3 = ETE at component level
ETE2 = ETE at stream level
$Work_{N_2}$ = Work required in kW per ton per hour of liquid nitrogen produced
AP-DMR = Air Product Dual Mixed Refrigerant natural gas liquefaction process

Chapter 1

Preliminary literature review - trends and technologies

Before focusing in details on the opportunity of using the cold exergy available from Liquefied Natural Gas (LNG) regasification to fulfil cold exergy needs in cryogenic air separation units, a preliminary study of the processes involved in LNG regasification and air separation units separatly, as well as an overview of the other trends in LNG regasification integration and markets appear appropriate.

1.1 LNG regasification

In order to bring remoted natural gas reserves into the network and to achieve flexible and long distance distribution, transporting natural gas in liquefied form can be the most economic and convenient solution. LNG is transported at -162 ^{o}C and slightly above atmospheric pressure, on vessels called LNG carrier. According to IGU (2016), 410 carriers were in activity in 2015 with an average capacity of 164,000 cubic meters, transporting LNG over the mean distance of 7,640 nautic miles per trip. Most often the tail end of the distribution network and the end users require the LNG to be transformed back to natural gas. Regasification is achieved at import terminals. The LNG supply chain is summarized on Fig. 1.1.

1.1.1 Regasification market

As shown in Fig. 1.15, Japan has the biggest regasification capacity in the world, followed by South Korea and China in Asia, with a fairly high utilization rate for the three countries. The USA have the second biggest regasification capacity, but since they have now a large domestic gas production, it is barely used. In Europe, most of the regasification capacity is in Spain, followed by the UK and France. The total world regacification capacity was 757.1 MTPA in 2015 with 108 regasification terminals. During this year, three onshore

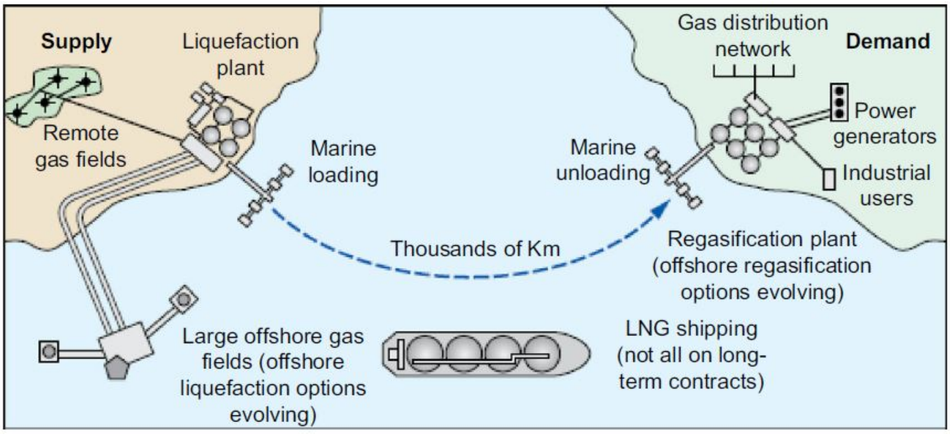
Supply
Liquefaction plant
Remote gas fields
Marine loading
Thousands of Km
Marine unloading
Gas distribution network
Demand
Power generators
Industrial users
Regasification plant (offshore regasification options evolving)
Large offshore gas fields (offshore liquefaction options evolving)
LNG shipping (not all on long-term contracts)

Figure 1.1: LNG supply chain, Mokhatab et al. (2014).

terminals have been built (two in Japan and one in Indonesia) and four FSRU put into operation in Egypt, Jordan and Pakistan according to IGU (2016).

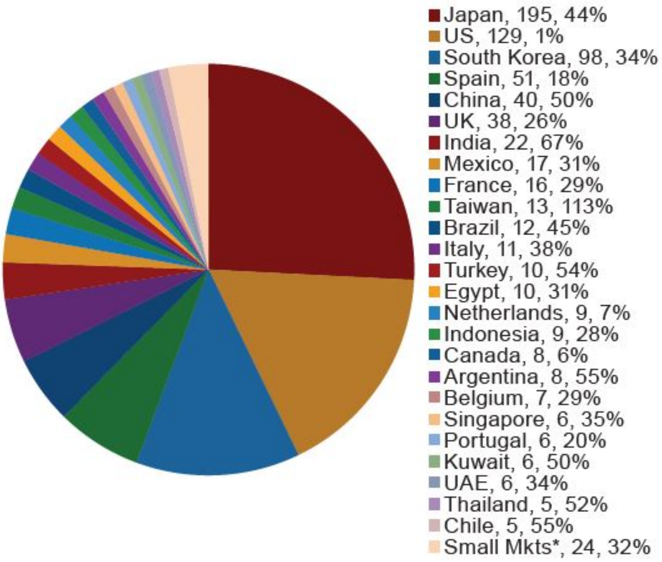

Note: "Smaller Markets" includes Jordan, Pakistan, the Dominican Republic, Greece, Israel, Lithuania, Malaysia, and Puerto Rico. Each of these markets had 4 MTPA or less of nominal capacity in 2015. Sources: IHS, IGU

Figure 1.2: LNG regasification capacity (MTPA) and utilization by country (%), IGU (2016).

1.1.2 LNG import terminals

A few LNG import facilities have favored offshore LNG terminals over the onshore alternative, as it can mitigate the difficulties linked to shore access or environmental and safety constraints in densly populated area. It is also a good option for new or less mature import countries by its flexibility and its relatively quick putting into service period. The two main offshore options proposed by Mokhatab et al. (2014) are Gravity Based Structures (GBS), which are fixed structure in concrete laying on the sea floor, and Floating Storage and Regasification Units (FSRU). Yet, risk and complexity are both increased in offshore designs, as well as capacity limitation, so most of the import LNG installations are onshore.

A simplified layout for onshore terminals is shown on Fig. 1.3. LNG is unloaded from the carrier vessel through several arms at a typical flow rate of 12,000 m^3/h and files up a storage tank. The average regasification terminal storage capacity of LNG was 500,000 m^3/h in 2015. Part of the boil off gas is expanded and used as return vapor to file up the free volume consequently to LNG unloading in the carrier vessel, avoiding void conditions. The major part is compressed and used as fuel gas or condensed and mixed with the pumped LNG toward vaporization at a pressure between 80 and 120 barg depending on the gas export requirements.

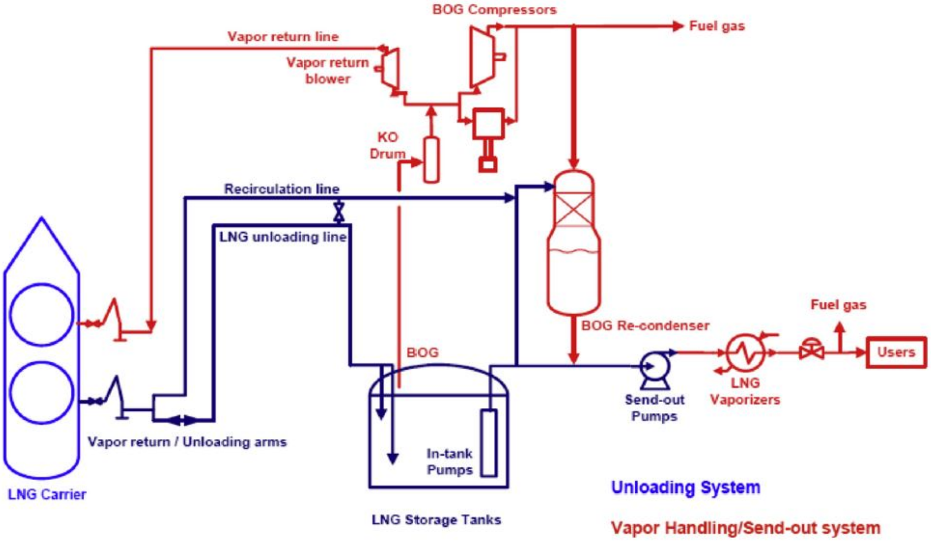
BOG Compressors
Fuel gas
Vapor return line
Vapor return blower
KO Drum
Recirculation line
LNG unloading line
BOG
BOG Re-condenser
Fuel gas
Users
Send-out Pumps
LNG Vaporizers
Vapor return / Unloading arms
In-tank Pumps
LNG Carrier
LNG Storage Tanks
Unloading System
Vapor Handling/Send-out system

Figure 1.3: LNG onshore import terminal, Mokhatab et al. (2014).

1.1.3 LNG vaporization processes

After being pressurized, the LNG is turned back to gas by heat exchange in the vaporizers. There are two main types of vaporizers on the market: Open Rack Vaporizers (ORV), which represent around 70 % of the installations and Submerged Combustion Vaporizers

(SCV), representing a 20 % share. The other options are Ambient Air Vaporizers (AAV), Shell and Tube Exchange Vaporizers (STV) and Intermediate Fluid Vaporizers (IFV) as decribed by Mokhatab et al. (2014). Several vaporizers are required to achieve the total regasification capacity of a mean import terminal. The best combination of vaporizer types depends on site ambient conditions as described by Patel et al. (2013).

ORV use sea water as a heat source. The LNG feed is divided by a bottom manifold and flows upward through curtains composed of hundreds of tubes, where it is heated up by downward water films as shown in Fig. 1.4. Water freezing can restrict the flow and limit the heat transfer at the bottom of the curtains due to low temperature. It can be remediated by using duplex pipe structure in this part as described by Egashira (2013). Nevertheless, ORV is the most used type as seawater allows to have low operating costs and makes the capacity easily adaptable. The downward is the need for water intake and outlet infrastructures, large pumping costs and environmental constraints due to the release of cold water. STV operate similarly to ORV in open loop mode, seawater being pumped into the shell tube heat-exchanger. The maximum capacity of this vaporizer type is 300 tons of LNG per hour according to Patel et al. (2013), which is the biggest capacity among current vaporizer technologies.

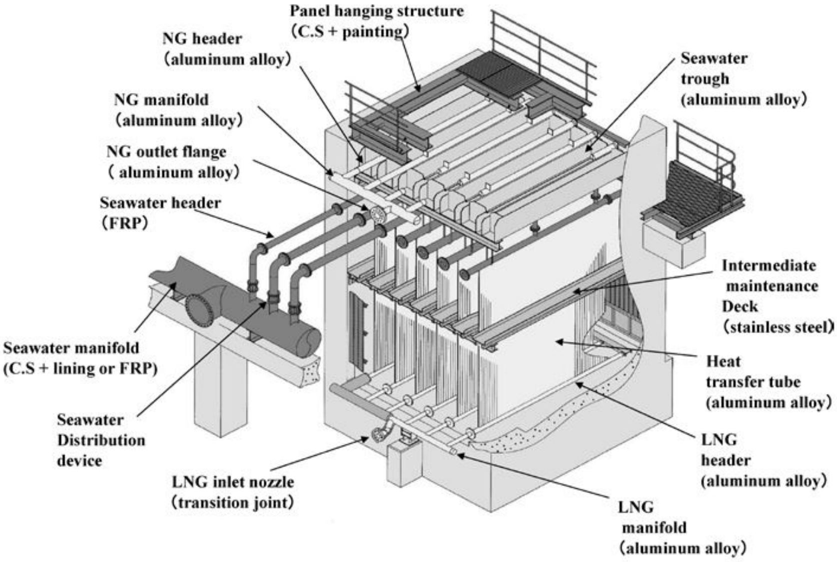
Panel hanging structure (C.S + painting)
NG header (aluminum alloy)
Seawater trough (aluminum alloy)
NG manifold (aluminum alloy)
NG outlet flange (aluminum alloy)
Seawater header (FRP)
Intermediate maintenance Deck (stainless steel)
Seawater manifold (C.S + lining or FRP)
Heat transfer tube (aluminum alloy)
Seawater Distribution device
LNG header (aluminum alloy)
LNG inlet nozzle (transition joint)
LNG manifold (aluminum alloy)

Figure 1.4: Open Rack Vaporizer overview, Egashira (2013).

SCV use the flue gases of gas fuel combustion to warm up water which is used as a heating media in order to vaporize LNG. It is refered to as submerged combustion as the burner is lying directly in the water tank. The LNG circulates in a tube bundle imerged in the water tank as shown in Fig. 1.5.The use of combustion gas allows SCV to be more compact that the other vaporizer alternatives. Moreover, SCV do not require water intake and discharge infrastructures. Yet, the use of fuel gas, which can amount up to 1.5 % of the vaporized LNG, largely increases the running costs. The largest SCV available can regasify 200 tons of LNG per hour according to Patel et al. (2013).

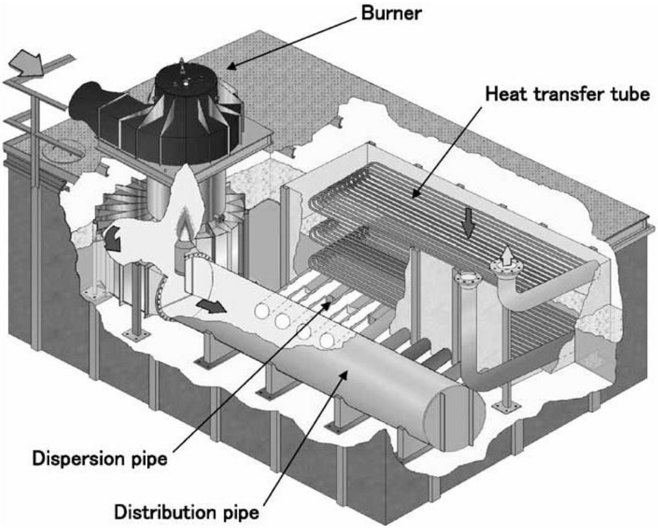

Figure 1.5: Submerged Combustion Vaporizer, Egashira (2013).

AAV use air as a heat source. Thus, they are considered as the most environment friendly option, avoiding water and fuel systems. They can be configurated for direct heat exchange or use an intermadiate heating media, with natural draft or forced draft. A schematic is shown on Fig. 1.6. Yet, AAV require a larger footprint as a bigger number of units is needed and are limited to warm climates, or might need additional heating in cold climates. Indeed the largest AAV units available today can regasify only 5 tons LNG per hour according to Patel et al. (2013). Another drawback of AAV is their tendency to freeze: half of the trains should usually be held in defrosting mode during operations.

IFV use the sensible heat of an intermediate heating media to pre-heat the LNG in a first heat exchanger. The condensed intermediate is vaporized by air or seawater before recirculating in the heat exchanger. Finally, pre-heated LNG is vaporized by air or seawater as displayed in Fig. 1.7. The intermediate fluid can be a glycol-water mixture, which amounts for 5 % of global LNG vaporization capacity, or hydrocarbons. The advantage of using propane or butane as the intermediate fluid is to avoid freezing problems and to allow maintaining throughput even with seawater temperatures down to 1 ^oC as described by Mokhatab et al. (2014). IFV units available today can regasify a maximum of 200 tons of LNG per hour according to Patel et al. (2013).

1.2 Utilization trends of LNG cold energy other than ASU

As described in the previous paragraphs, pressurized LNG represents both a pressure-based exergy source and a temperature-based exergy source, which can be integrated to save energy and utilities in various processes, instead of being wasted to seawater or air in classic regasification processes. Yet, there are drawbacks in LNG cold recovery that

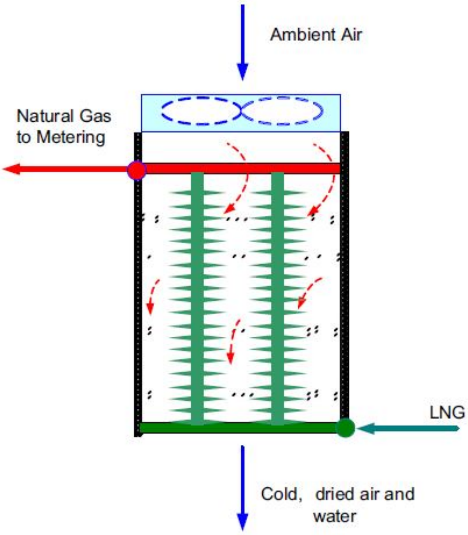
Ambient Air
Natural Gas to Metering
LNG
Cold, dried air and water

Figure 1.6: Ambient Air Vaporizer schematic, Mokhatab et al. (2014)

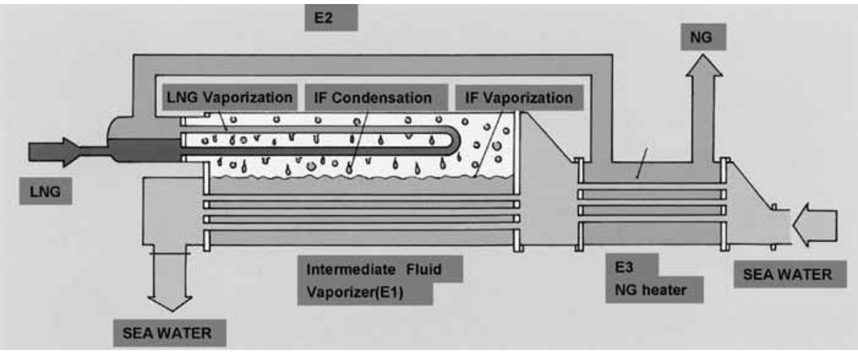
E2
NG
LNG Vaporization
IF Condensation
IF Vaporization
LNG
Intermediate Fluid Vaporizer(E1)
E3 NG heater
SEA WATER
SEA WATER

Figure 1.7: Intermediate Fluid Vaporizer schematic using seawater heating, Egashira (2013).

have to be thought of in integration projects. Each integration project needs to analyze the match between the cold user requirements and the LNG exergy available, both for duty and for temperatures. As an example, Fig. 1.8 shows the duty and temperatures available for heat integration during LNG regasification, depending on the gas distribution pressure. An other constraint is that the cold exergy is available directly at the regasification terminal, which can be at a non-neglectable distance from cold users.

1.2.1 Power generation

According to Gomez et al. (2014), power generation is the most widely studied application to use the cold exergy of LNG regasification. The study presents a number of cycle alternatives to recover LNG exergy and increase power production efficiency. Yet, as of

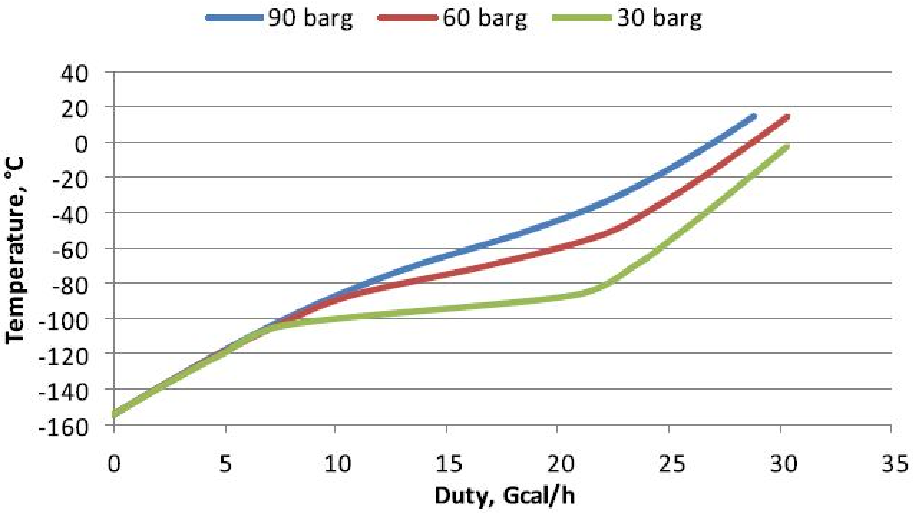

Figure 1.8: LNG temperature and duty during regasification depending on the distribution pressure, Mokhatab et al. (2014).

today, the only options that have been implemented in real cases are LNG exergy use in direct expansion, cold Rankine cycles, and partially in combine cycles.

Japan has been at the forefront of LNG regasification exergy use as shown in table 1.1. Rankine cycles and direct expansion options produce between 1 and 10 MW per installation, which is low compared to the standard 400 MW capacity of gas turbines. In terms of regasification capacity, the LNG flow rates regasified by these plants, ranging between 40 and 175 ton/h, is under the maximum capacities of available ORV and SCV, butin a comparable range.

In Europe, Enagas has installed a Rankine cycle in Huelva LNG terminal in Spain. South Hook (UK), Zeebrugge (Belgium) and Montoir de Bretagne (France) LNG terminals use exhaust gases from combine cycles instead of seawater as a heat source to vaporize LNG. Yet, this option is still wasting LNG cold exergy. On the other hand, EcoElectrica Company has integrated LNG vaporization to glycol condensation, which is used as an intermediate fluid to cool down the compressor suction stream, thus improving the combine cycle efficiency in Penuelas facility in Puorto Rico.

Table 1.1: Cryogenic power plants using LNG exergy in Japan, Gomez et al. (2014).

Company	Terminal	Operation start	Cycle type	Power (kW)	$\dot{m}_{LNG}$ (t/h)	P_{NG} (bar)
Osaka Gas	Senboku	1979	RC	1450	60	30
Toho Gas	Chita Kydo	1981	RC	1000	40	14
Osaka gas	Senboku	1982	RC, DE	6000	150	17
Kyushu	Kitakyushu LNG	1982	RC, DE	9400	150	9
Chubu Power	Chita LNG	1984	RC, DE	$2 * 7200$	150	9
Touhoku Power	Niigata	1984	DE	5600	175	9
Tokyo Gas.	Negishi	1985	RC	4000	100	24
Tokyo Power	Higasi Ougishima	1986	DE	3300	100	8
Osaka Gas	Himeji	1987	RC	2500	120	40
Chubu Power	Yokkaichi	1989	RC, DE	7000	150	9
Tokyo Power	Higasi Ougashima	1991	DE	8800	170	4
Osaka Gas	Himeji	2000	DE	1500	80	15

Direct expansion (DE), shown on Fig. 1.9, is the most straightforward use of LNG exergy. To meet export requirements, LNG pressure is increased thanks to pumping work, which is below the compression work that would be needed if it was in gaseous state. The pressure in liquid state can be increased above distribution specifications (1-2) and the excess pressure-based exergy can be recovered by expansion (3-4) after vaporization (2-3). This method is still quite inefficient on an exergy efficiency view point as LNG cold exergy is entirely lost to the heat source.

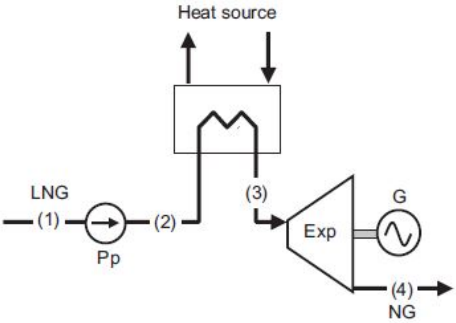

Figure 1.9: LNG pressure-based exergy use in direct expansion, Gomez et al. (2014).

Cold Rankine cylces (RC), as shown on Fig. 1.10, use LNG cold exergy in order to cool down the working fluid in the condenser (Cd). In the basic cycle (a), the condensed fluid is pumped then vaporized in a boiler, using for example seawater as a medium, and finally expanded in a turbine to create work. In order to improve RC efficiency, one can use a regenerator (b) to preheat the working fluid, by heat exchange with the turbine outlet stream, before it enters the boiler. The fluid is then precooled before entering the condenser, which means that a smaller LNG mass flow is necessary. To also recover LNG pressure-based exergy, an option is to use a regenerative cold Rankine cycle combined with direct expansion as displayed on Fig. 1.11. The usual working fluids used in cold RC are ethane or ethylene when the heat source is at low temperature, or carbon dioxide for a higher temperature heat source. One can also use mixtures, like ammonia-water or a binary mixture of hydrocarbons, to reduce irreversibilities by sliding-temperature vaporization and more importantly condensation temperatures matching the LNG vaporization temperatures as described in the synthetic study of Gomez et al. (2014).

Brayton cycles (BC), as shown on Fig. 1.12, are another alternative, yet to be implemented, recovering LNG cold exergy. They work when a higher grade heat source is available. In the simple cycle, LNG cold exergy is used to cool down the air intake before compression, thus improving the gas turbine efficiency. A more complexe option, presented on Fig. 1.13, is to use two-stage compression with LNG precooling and intercooling in a closed BC, integrated with direct expansion of the vaporized LNG. In the study by Gomez et al. (2014), Helium and nitrogen, eventually combined to flue gas, are described as the best working fluids for BC.

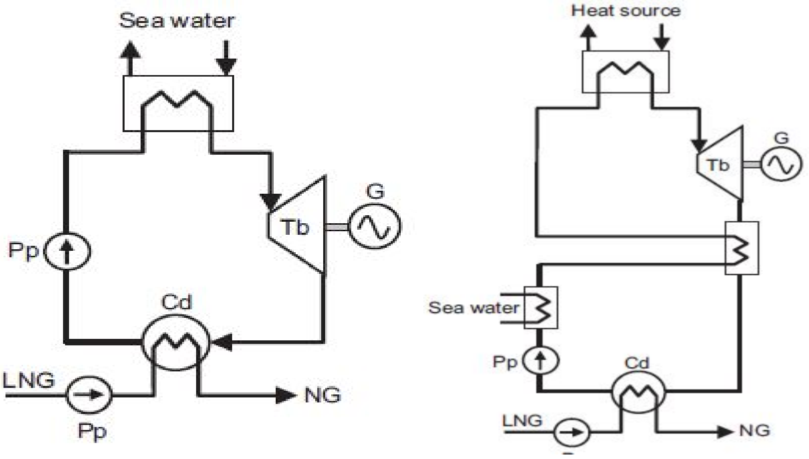
Sea water
G
Tb
Pp
Cd
LNG
NG
Pp
Heat source
G
Tb
Sea water
Pp
Cd
LNG
NG

(a) Basic Rankine cycle **(b)** Regenerative RC

Figure 1.10: Cold Rankine cycle options for cryogenic power production from LNG cold exergy, Gomez et al. (2014).

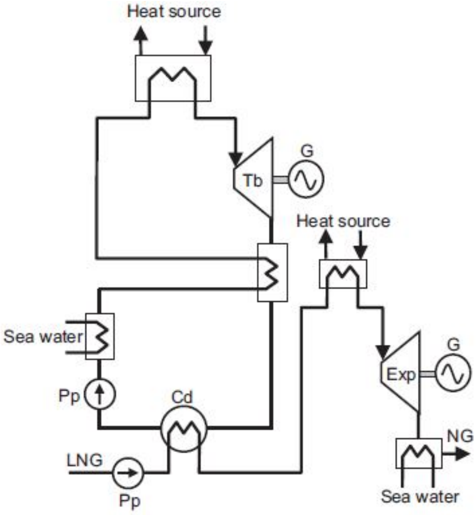
Heat source
G
Tb
Heat source
Sea water
G
Exp
Pp
Cd
NG
LNG
Pp
Sea water

Figure 1.11: Combined regenerative cold RC and direct expansion using LNG thermo-mechanical exergy for cryogenic power production, Gomez et al. (2014).

1.2.2 Seawater desalination

The main desalination technologies in market shares, Multi-Effect Desalination and Reverse Osmosis, are not combined with cold recovery. Yet, two other processes, still at experimental stage, are using LNG cold exergy in order to produce fresh water. As described by Efrat (2011) and shown on Fig. 1.14, **indirect contact freeze desalination**

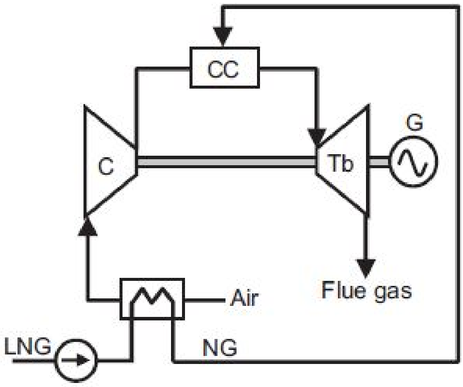

Figure 1.12: Open Brayton cycle using LNG cold exergy to cool the compressor suction stream, Gomez et al. (2014).

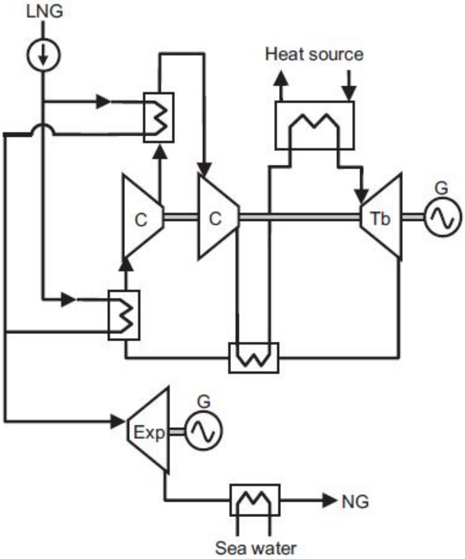

Figure 1.13: Closed Brayton cycle with LNG precooling and intercooling combined to direct expansion, Gomez et al. (2014).

uses a cooling media, typically a water-glycol solution, in order to form ice slurry in seawater. The formed slurries are pumped to a concentrator and rinsing batch where a ice cake forms and rises into the unit, being watched from residual brine by injection of fresh water at the top. The concentrated brine is pumped out to disposal at the tank bottom while the ice cake pieces are directed to the melting unit where they precool the feed seawater. LNG cold exergy is used to condense the water-glycol solution which is providing the heat sink in the ice slurry generator.

The other process is **evaporation-condensation** of seawater, shown on Fig. 1.15, usually used in Multi Flash Distillation. Seawater is flashed in a chamber. The formed vapor flows through a demister before being condensed by heat exchange with a glycol solution. Brine is formed at the bottom of the flash chamber while freshwater is obtained after demisting in the condensing section. To improve the produced water purity, several effects can be used in series. LNG cold exergy is used to cool the glycol solution. Though the achieved purity by multi-effect use can be higher than the water purity obtained in the freezing process, the energy consumption is significantly higher as the latent heat of water vaporization is 7 times higher than the latent heat of ice fusion.

Efrat (2011) study the integration of freeze desalination and evaporation-condensation desalination with a LNG import facility. The receiving terminal would be able to supply 1750 ton/h of water-glycol solution at -15 ^oC using the cold from LNG regasification. The first option would generate 6300 m^3/h of desalinated ice, needing a major scale up of the currently available ice-generator units, while the second would provide a maximum of 960 m^3/h. Assuming the same flow of LNG and water-glycol solution in the IFV units, the studied case corresponds to an import terminal using a minimum of 9 IFV units.

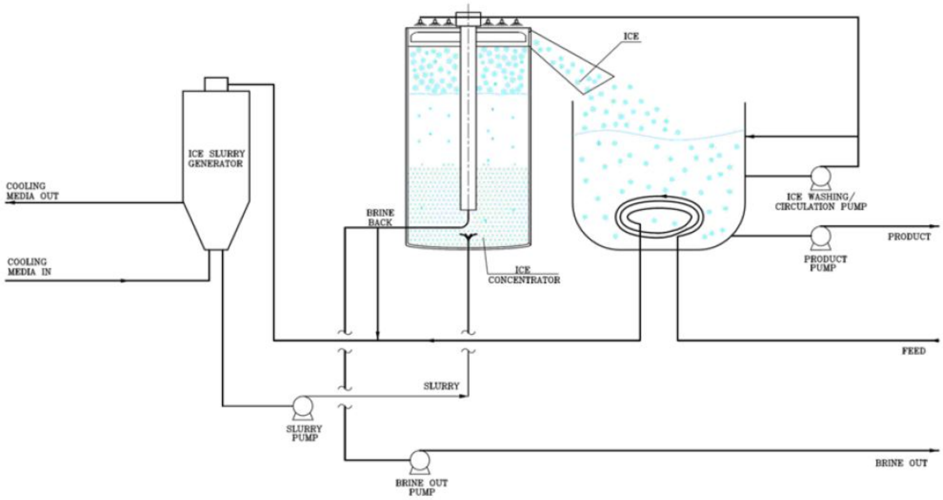

Figure 1.14: Indirect contact freeze desalination process using a glycol solution regenerated by LNG cold, Efrat (2011).

1.2.3 Food processing

As presented by La Rocca (2011), deep freezing in food processing and air conditionning are two cold sinks that could be integrated with LNG regasification at higher temperature levels. The study proposes to use carbon dioxide as an intermediate fluid: it would be liquefied at the terminal by heat exchange with LNG and carried into pipelines over a range of two kilometers to the food processing facilities or buildings requiring air conditioning, thus overcoming the distance constraint between cold availability and cold demand loca-

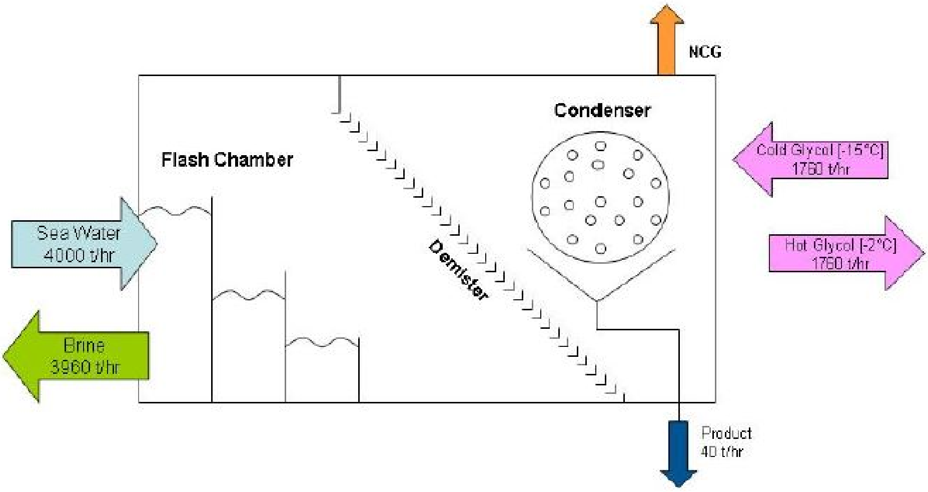

Figure 1.15: Evaporation-condensation seawater desalination using a glycol solution regenerated by LNG cold, Efrat (2011).

tions. Based on the case, the cold requirements for a deep freezing food processing facility would be around 9 MW at the mean temperature of - 43 ^{o}C. For hypermarkets, the required duty would be 7 MW for space conditioning and 0.5 MW for refregiration utilities (150 kW at -35 ^{o}C and 350 kW at -15 ^{o}C). On the other hand, for the studied regasification process, around 14 MW is available between -90 and -35 ^{o}C and around 40 MW from -35 to 0 ^{o}C from LNG regasification.

1.2.4 NGL extraction and fractionation from LNG feed

Uwitonze et al. (2014) describe two processes using LNG cold energy to decrease power consumption of heavy hydrocarbon extraction from an LNG feed with a heating value above the distribution requirements. The products are separated liquid petroleum gases, liquefied ethane and a lean LNG (i.e. with a lower heating value) at a temperature around -105 ^{o}C. Therefore this option does not replace classic vaporization processes: there is still a large amount of cold exergy to recover from the products temperature of -105 ^{o}C up to ambient. Yet, low temperature cold exergy is recovered for liquefaction of the separated products. According to the economic analysis in the study, performing NGL extraction with the decribed process increases the economic value of the products by around 10 % compared to the LNG feed.

1.3 Cryogenic Air separation processes

As the aim of the master thesis is to study integration of air separation to LNG regasification, only cryogenic air separation processes will be developed. Indeed, they require cold down to around -170 ^{o}C to -190 ^{o}C, which matches the available cold temperatures of LNG (around -160 ^{o}C). The main steps of cryogenic air separation, displayed on Fig. 1.16, are air filtration and compression, precooling with water or air, drying and purification by adsorption on molecular sieves in the warm part; followed by cooling down to dewpoint temperature and separation by cryogenic distillation in the cold box, which is the enclosure insulated to limit losses at low temperatures.

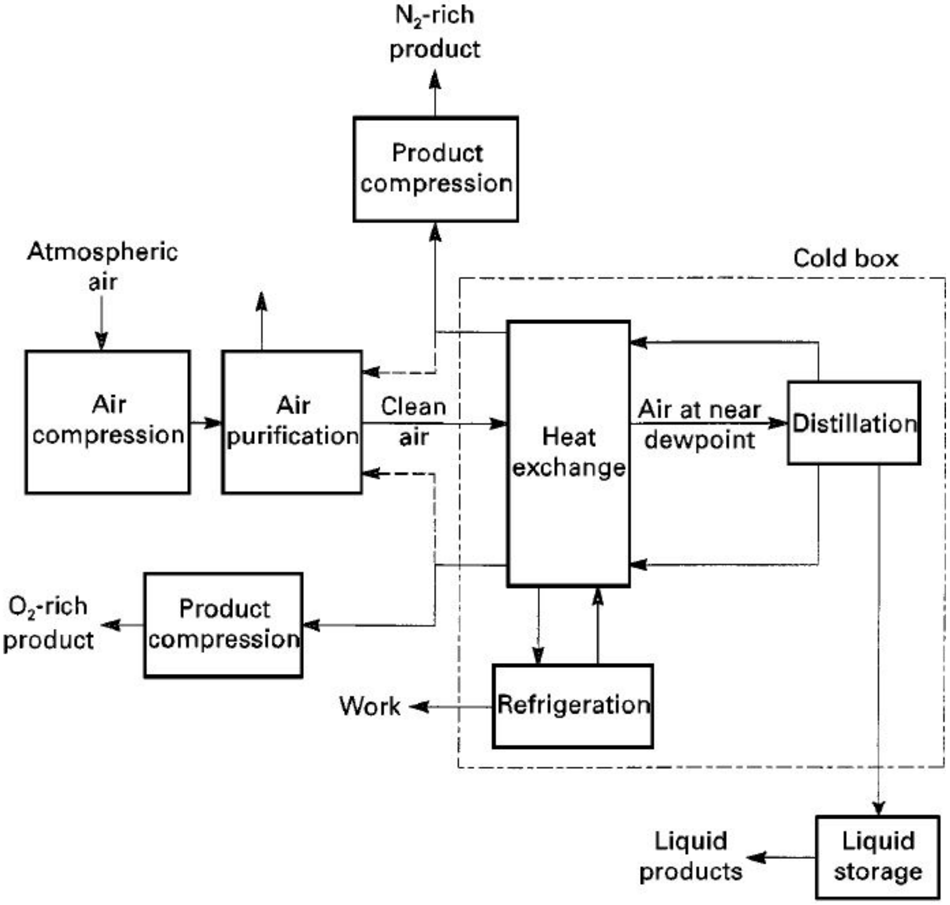
N₂-rich product
Product compression
Atmospheric air
Cold box
Air compression
Air purification
Clean air
Heat exchange
Air at near dewpoint
Distillation
O₂-rich product
Product compression
Work
Refrigeration
Liquid products
Liquid storage

Figure 1.16: Main steps of a cryogenic air distillation plant, Agrawal and Herron (2000).

Processes differ mainly by the number of distillation columns in the cold box and the pressure levels. These differences affect the products (purity, state, pressure) as well as the energy performance and the cost of the Air Separation Units (ASU). Nitrogen (78.12 mol % concentration and NBP at -195.9 ^{o}C) and oxygen (20.95 mol % concentration and NBP at -182.9 ^{o}C) are the main two components usually recovered. Argon (0.93 mol % concentration and NBP at -185.9 ^{o}C) can also be extracted by multi-column processes at various purity levels. More seldomly, noble gases present in air at ppm concentrations are extracted by further purification of the product streams for specific applications. This last option will not be studied. A classification of the existing ASU technologies according to the number of distillation columns in the cold box is presented in the next paragraphs.

1.3.1 Single-column processes

A study by Fu and Gundersen (2013) proposes a single-column ASU process using recuperative vapor recompression and distributed reboiling, as shown on Fig. 1.17. This new configuration produces pure nitrogen and intermediate purity oxygen (about 95 mol %) at atmospheric pressure, which matches the requirements for oxy-combustion applications. The advantages of this process, compared to traditional ASU processes, are the reduced number of columns and the reduced energy consumption as there is almost no more air feed compression required. The feed air is slightly compressed, to compensate for pressure losses in the process, and pre-cooled by water before purification in the pre-purification unit (PPU). After being cooled by the main heat exchanger (MHE) and the sub-cooler to dewpoint temperature, it is fed to the distillation column at an intermediate level. The nitrogen vapor is warmed back to atmospheric conditions in the two heat exchangers. Part of the nitrogen product stream is compressed to two different pressure levels and after-cooled back to cryogenic temperatures in the heat exchangers. Higher pressure stream A5-1 condenses through condenser 1 which is integrated with bottom reboiler 1, while lower pressure stream A7-1 is condensed in condenser 2 integrated with intermediate reboiler 2. Both streams are expended to a pressure slightly above atmospheric before being mixed and used as a reflux in the distillation column. Distributed reboiling reduces irreversibilities in the distillation column. Another portion of the nitrogen product stream can be used through a turbo-expander to provide refrigeration power for the cold box (stream A15-1).

1.3.2 Two-column processes

The conventional two-column air separation process shown on Fig. 1.18, first developped by Linde group in 1910, allows to recover pure nitrogen and intermediate to high purity pressurized or non-pressurized oxygen (95 up to 99.5 mol %) from the feed air according to Beysel (2009). Air is pre-filtered and compressed in a multistage turbo-compressor to about 5.3 bar. It is then cooled by water in a direct contact after-cooler (DCAC). The pre-cooled air flows through molecular sieve adsorbers in the PPU in order to remove water, carbon dioxide and other impurities which would freeze at cryogenic temperatures. The pre-treated air enters the coldbox through the MHE where it is cooled down near its dewpoint temperature and feeds the high pressure (HP) distillation column, entering at the bottom. Pure nitrogen vapor, with oxygen content down to ppm levels, exits at the top through the integrated heat exchanger (being used as HP column condenser and Low Pressure - LP - column reboiler). Around 60 % of the nitrogen stream are used as reflux in the HP column. The remaining 40 % are used as a reflux for the LP column after JT-expansion. The oxygen sump of the HP column, which contains around 35 mol % oxygen, feeds the LP column at an intermediate level after Joule Thomson (JT) expansion. The vapor nitrogen produced at the top of the LP column is used as a cold stream in the MHE. The bottom oxygen product vaporizes in the integrated reboiler and is heated in the

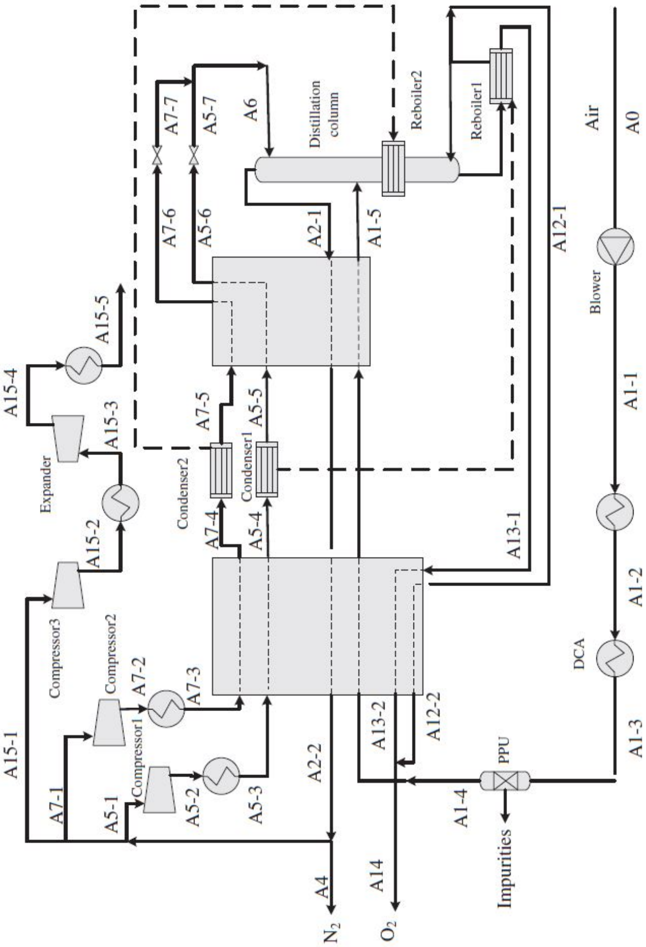
Air
A0
Blower
A1-1
A1-2
DCA
A1-3
PPU
A1-4
Impurities
A12-1
A13-1
A12-2
A13-2
A14
O_2
A4
N_2
A2-2
A2-1
A1-5
Distillation column
Reboiler1
Reboiler2
A6
A5-7
A7-7
A5-6
A7-6
Condenser1
Condenser2
A5-5
A7-5
A5-4
A7-4
A5-3
A5-2
A5-1
Compressor1
A7-3
A7-2
A7-1
Compressor2
Compressor3
A15-1
A15-2
A15-3
Expander
A15-4
A15-5

Figure 1.17: Single-column ASU with recuperative vapor recompression and distributed reboiling, Fu and Gundersen (2013).

MHE. The HP and the LP columns are thermally coupled by the integrated condenser-reboiler. The typical temperature difference in this heat exchanger is 1 K according to Moll (2014). This constraint defines the necessary pressure at the top of the HP column to have a pressure around 1.4 bar in the sump of the LP column.

An improvment alternative, presented by Agrawal and Herron (2000), is to use a turbo-expander in order to provide the needed refregiration for the cold box without additional cooling. At an intermediate temperature around -130 ^{o}C about 10 - 20 % of the clean compressed air stream are extracted and expanded to about 1.4 bar before feeding the LP column at an intermediate level. The power prodruced by the turbo-expander is used for the cold box refrigeration. The remaining cooled air stream feeds the HP column at the bottom as usual.

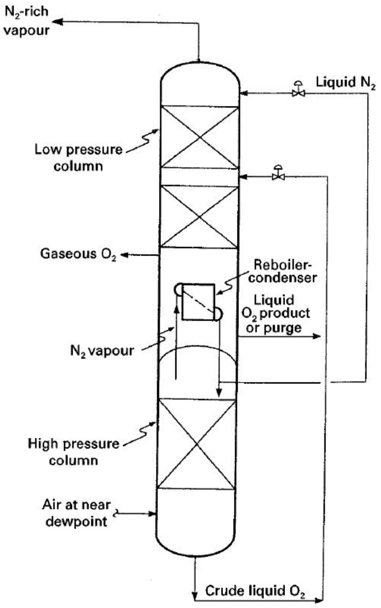

Figure 1.18: Simplified flow diagram of a basic two-column ASU, distillation part, Agrawal and Herron (2000).

To improve the purity of the products, a sub-cooler can be added to cool the nitrogen-rich vapor from the HP column top, using the pure nitrogen distillate from the LP column, before it is expanded and fed to the LP column as a reflux. This provides an increased reflux in the LP column, improving the separation.

An other configuration, for specific applications requiring oxygen at a higher pressure, is internal compression of oxygen compensated by a booster compressor on the air feed. For this alternative process, the oxygen sump of the LP column is extracted in liquid form after condensation in the coupled heat exchanger. It goes through a cryo-pump to be compressed to the desired product pressure before being vaporized in the MHE. Performing the compression with a pump instead of a compressor allows to reduce the power consumption of the ASU. To maintain the refrigeration balance in the MHE, about 30 % of the clean compressed air feed go through a booster compressor before the MHE inlet. The boosted pressure is chosen accordingly to the increase in the oxygen product pressure. The boosted air is then fed to either one or both distillation columns. These options are displayed on Fig. 1.19.

1.3.3 Multiple-column processes

In cases where argon is a desired product, additional distillation columns are required in the process. A first option allows to recover crude argon with an oxygen concentration between 5 and 100 ppm but a nitrogen concentration that can be above 100 ppm. As argon has a Normal Boiling Point (NBP) below nitrogen and slightly above oxygen, its concen-

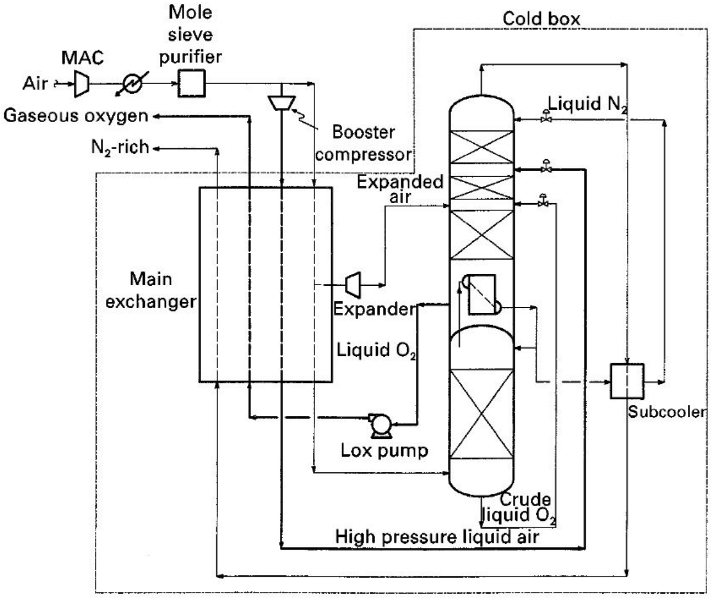
Mole
sieve
purifier
MAC
Air
Gaseous oxygen
N$_2$-rich
Booster
compressor
Cold box
Liquid N$_2$
Expanded
air
Main
exchanger
Expander
Liquid O$_2$
Lox pump
Subcooler
Crude
liquid O$_2$
High pressure liquid air

Figure 1.19: Simplified flow diagram of a two-column ASU with turbo-expander, reflux sub-cooling and oxygen internal compression, Agrawal and Herron (2000).

tration in the conventional two-column process is maximum (up to 18 mol % according to Agrawal and Herron (2000)) a bit below the crude oxygen feed to the LP column. Thus, argon rich vapor (representing about 20 % of the feed air flow) can be extracted at this level of the LP column to feed a side argon column at its bottom as can be seen on Fig. 1.20. The crude liquid oxygen formed at the bottom of this column is pumped back to the LP column below argon rich vapor extraction. Crude argon vapor forms at the top of the side column. It is condensed thanks to the oxygen sump of the HP column before it is fed to the intermediate level of the LP column in vapor and liquid streams. Part of the liquefied distillate is used as reflux in the side column, while the remaining amount is extracted as crude argon.

As generally the specification for argon product is a nitrogen concentration below 5 ppm, a fourth column needs to be added in order to remove the remaining nitrogen in the crude argon stream from the side column. Moll (2014) describes a highly integrated four-column process to fulfil this specification, shown on Fig. 1.21. In the pure argon column, pure liquid argon is recovered at the bottom while sub-cooled crude liquid oxygen from the HP column is used to condense part of the nitrogen rich vapor for the reflux. The remaining top stream is vented to the atmosphere.

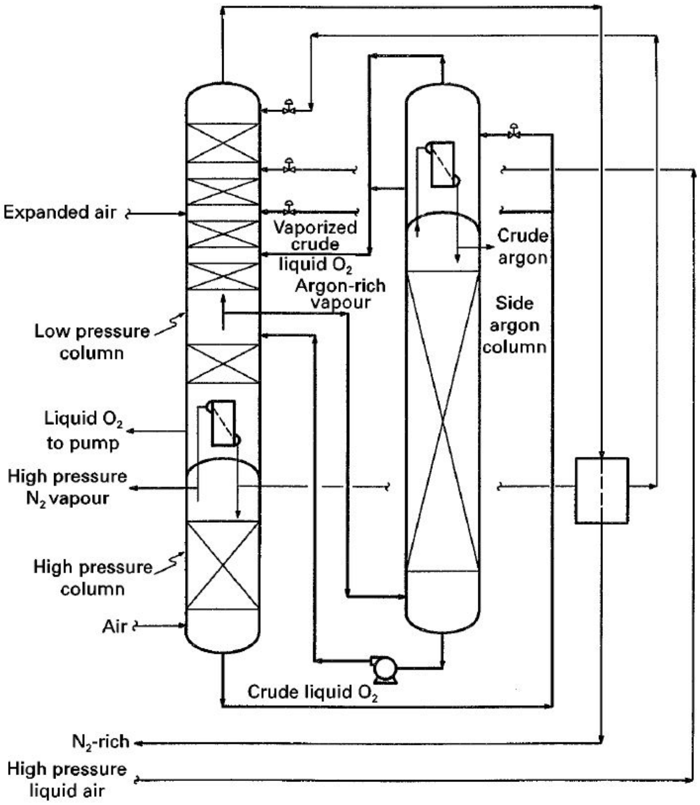
Expanded air
Vaporized crude liquid O_2
Argon-rich vapour
Low pressure column
Liquid O_2 to pump
High pressure N_2 vapour
High pressure column
Air
Crude argon
Side argon column
Crude liquid O_2
N_2-rich
High pressure liquid air

Figure 1.20: ASU three-column configuration for crude argon recovery, Agrawal and Herron (2000).

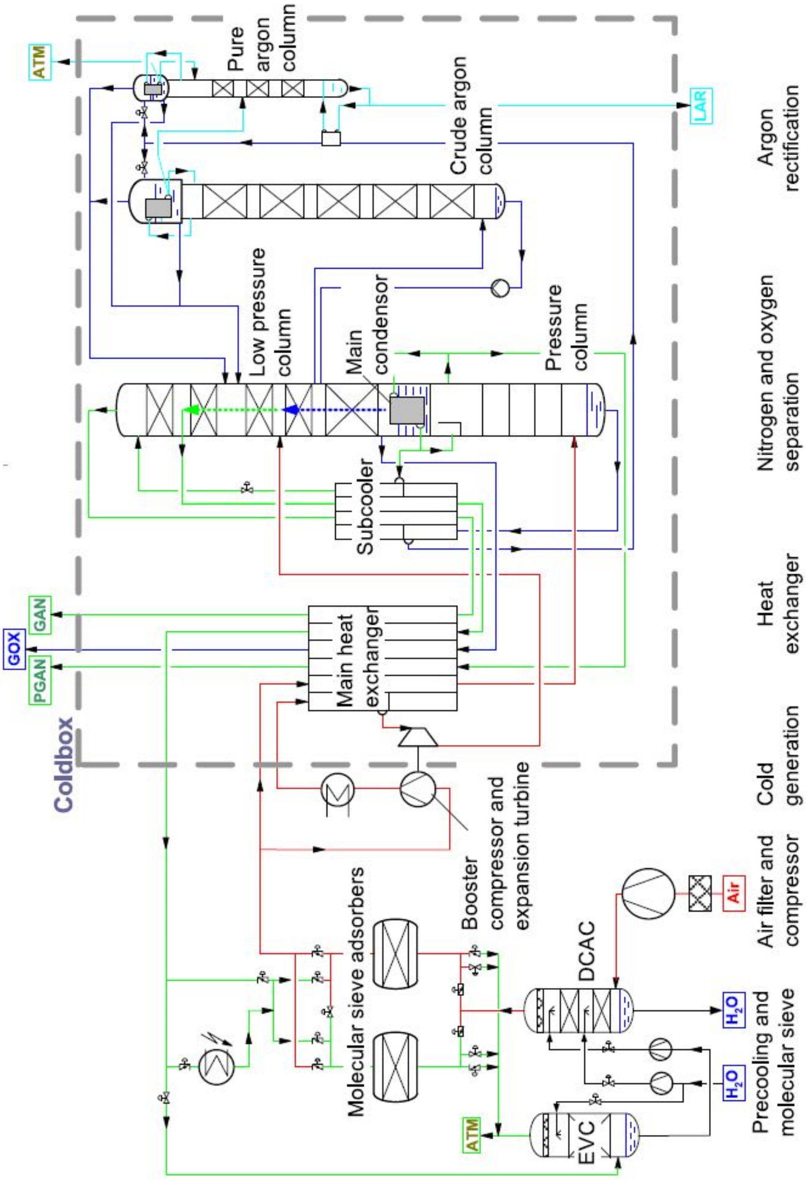
ATM
Pure argon column
Crude argon column
LAR
Argon rectification
Low pressure column
Main condensor
Pressure column
Nitrogen and oxygen separation
Subcooler
GAN
GOX
PGAN
Main heat exchanger
Heat exchanger
Coldbox
Booster compressor and expansion turbine
Cold generation
Molecular sieve adsorbers
Air
Air filter and compressor
DCAC
H2O
H2O
ATM
EVC
Precooling and molecular sieve

Figure 1.21: ASU four-column configuration for pure argon recovery, Moll (2014).

Chapter 2

Survey of existing integrated ASU and LNG regasification technologies

As mentioned in previous chapters, air separation is theoretically the only process that can recover LNG cold exergy on the whole temperature range available during regasification (-160 ^{o}C up to environment temperature). Indeed, typical ASU cold boxes require temperatures down to about -190 ^{o}C for nitrogen liquefaction and up to environment temperature in the warm part.

On the other hand, the refrigeration application described by La Rocca (2011) uses carbon dioxide as an intermediate fluid, which is limited by a freezing point above -60 ^{o}C. Typical low-temperature power generation RC do not go below -90 ^{o}C (when ethane is used as the working fluid) as presented by Gomez et al. (2014). BC could go down to -140 ^{o}C using nitrogen-flue gas as a working fluid but they are not yet implemented in real applications. Desalination options proposed by Efrat (2011) use a glycol-water solution as intermediate with a limit temperature of -15 ^{o}C. Finally, the extraction of NGL from LNG to adjust its heating value, as described by Uwitonze et al. (2014), covers temperatures from -160 ^{o}C but only up to -105 ^{o}C.

Moreover, as described in the study by Xu et al. (2014), ASU using LNG cold exergy have been implemented since the 70s and are already in operation in Japan, South Korea, France and Australia. In addition, there are several projects of integrated ASU and LNG regasification under planning and construction in China. The study gives examples of existing ASU using LNG cold exergy in Japan and South Korea, as shown in table 2.1.

Table 2.1: Air separation units using LNG cold energy, Xu et al. (2014).

LNG receiving bases	Negishi base	Senboku base	Chita base	Sodegaura base	Pyeongtaek base	Putian base	Dapeng base	Ningbo base
LNG flow rate (t/h)	8	23	26	34	50	50	54	68
Power consumption (kW/t/h)	670	500	475	450	-	490	-	-

Several configurations have been studied to integrate LNG regasification to conventional two-column ASU or novel air separation processes as the single-column heat pump described by Fu and Gundersen (2013). All the studies, which will be presented in the next paragraphs, show an improved efficiency compared to traditional processes, thanks to LNG regasification and ASU integration.

2.1 Two-column processes

2.1.1 Small capacity two-column ASU with nitrogen cycle and LNG cold recovery, Xu et al. (2014)

Xu et al. (2014) describe a traditional process integrating a two-column ASU with LNG regasification using a nitrogen loop, shown on Fig. 2.1, and propose a novel integrated process, shown on Fig. 2.2, which decreases the highest operating pressure in the nitrogen loop from 26 to 15 bar and the HP column pressure from the classical 5.3 bar to 3.5 bar. The novel process reduces the LNG flow rate by 44 % for the same air input. The power consumption of the ASU is reduced by 12.6 % and the total exergy efficiency is improved from 38.2 to 66.4 % (calculated as the ratio between total exergy output divided by total exergy input). With its low LNG input flow rate needs (2.778 tons per hour), the novel process described by Xu et al. (2014) could be applied to LNG satellite receiving stations as it could overcome the constraints of a low flow rate of LNG feed and high cold available exergy fluctuations that are serious drawbacks for traditional ASU integration.

In the conventional process, part of the nitrogen product from the HP column is gasified in the MHE and compressed to 26 bar before being after-cooled by seawater and liquefied by the integreted LNG stream in heat exchanger E2. It is then throttled down to the operating pressure of the HP column and used as its reflux. In the novel process as in the traditional one, part of the nitrogen product of the HP column is gasified in the MHE but then compressed to the pressure of 15 bar before being after-cooled in the washing unit. The other main difference is that the LNG cold stream is directly integrated in the MHE where it cools the cyclic nitrogen stream down to dewpoint temperature before going to a gas-liquid flash separator. The vapor nitrogen stream goes back in the nitrogen loop while the liquid is directly extracted as nitrogen product with high purity (99.99 mol %). Liquid oxygen (99.8 mol % pure) is recovered at the bottom of the LP column. No gaseous product are recovered from the novel process.

2.1.2 Two-column ASU with large capacity fully integrated LNG cold recovery, Tesch et al. (2016)

Tesch et al. (2016) describe two alternative possibilities of LNG integration to two-column ASU. The LNG feed pressure is varied between 20 and 120 bar, which is considerably higher than in the options proposed by Xu et al. (2014) (who utilize LNG pressure between 1.2 and 3 bar). The used LNG flow rate is ten times higher (41.4 tons per hour) compared to the conventional option by Xu et al. (2014). In design 1, shown on Fig. 2.3, LNG is used to cool down the clean air inlet at 5.6 bar down to -173 ^{o}C in the MHE as well as the cyclic liquid nitrogen at 8.6 bar. The warmed LNG is then integrated in two other

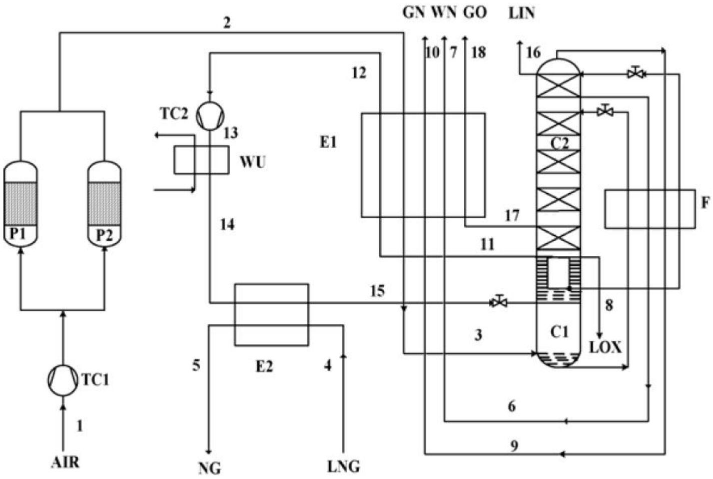
GN WN GO
LIN
10
7
18
16
2
12
TC2
13
WU
E1
C2
F
17
11
14
15
8
P1
P2
C1
LOX
3
5
E2
4
TC1
1
6
9
AIR
NG
LNG

Figure 2.1: Conventional process of two-column ASU integrated with LNG, Xu et al. (2014).

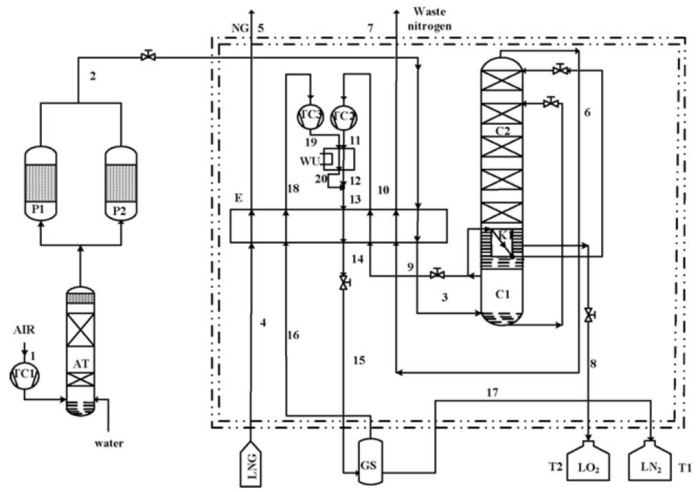
NG
5
7
Waste nitrogen
2
TC3
TC2
19
11
WU
20
12
13
18
10
E
C2
6
P1
P2
K
14
9
3
C1
4
16
15
8
AIR
1
TC1
AT
17
water
LNG
GS
T2
LO2
LN2
T1

Figure 2.2: Novel process of two-column ASU integrated with LNG, Xu et al. (2014).

heat exchangers to gasify the compressed nitrogen and oxygen products. In design 2, displayed on Fig. 2.4, LNG is integrated to all the heat exchangers, including the intercoolers of the feed air compression block and the intercoolers of the cyclic nitrogen compressors. Contrary to design 1, the air is cooled down to -173 ^{o}C in two heat exchangers: the MHE, which is the only one using cyclic nitrogen as a cold stream, stops at -150 ^{o}C for the air outlet temperature. With a LNG feed pressure of 20 bar, designs 1 and 2 have exergetic efficiencies of 49 and 53 % respectively, while the efficiencies go up to 58 and 64 % with a LNG feed at 120 bar. The performance of the integration is better with design 2 but lower than the novel integration design presented by Xu et al. (2014). Even though the configurations proposed by Tesch et al. (2016) produce both liquid and gaseous nitrogen and oxygen, the purity of the oxygen products, ranging from 90 to 97 mol %, is significantly lower than the one achieved by the novel process of Xu et al. (2014). An other difference is that given the large LNG feed flow rate used, the configurations proposed by Tesch et al. (2016) are more relevant for large LNG receiving terminals.

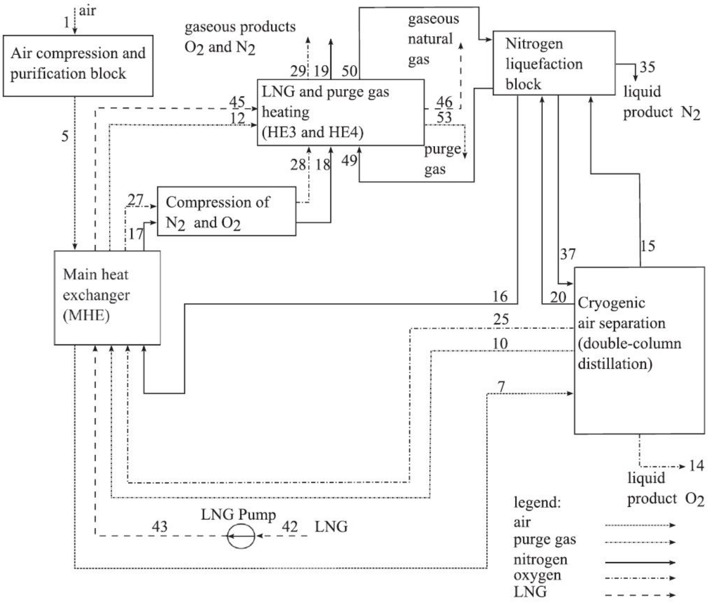
air
1
Air compression and purification block
gaseous products
O2 and N2
29
19
50
gaseous natural gas
Nitrogen liquefaction block
35
liquid product N2
45
12
LNG and purge gas heating (HE3 and HE4)
46
53
purge gas
5
28
18
49
27
Compression of N2 and O2
17
37
15
Main heat exchanger (MHE)
16
20
25
10
Cryogenic air separation (double-column distillation)
7
14
liquid product O2
LNG Pump
43
42
LNG
legend:
air
purge gas
nitrogen
oxygen
LNG

Figure 2.3: Conceptual design 1 - two-column ASU with LNG integrated in the MHE and gaseous product HE, Tesch et al. (2016).

2.2 Single-column processes

2.2.1 Single-column heat pump ASU and LNG cold recovery with cyclic nitrogen, Zheng et al. (2015)

Zheng et al. (2015) propose a configuration, shown on Fig. 2.5, to recover LNG cold exergy utilizing the single-column heat pump ASU described by Fu and Gundersen (2013). The process achieves a total exergy efficiency of 57.5 %. It is comparable in scale to the option described by Xu et al. (2014) with a small LNG flow rate (4.434 tons per hour) and low LNG feed pressure (1.1 bar), recovering high purity liquid and gaseous nitrogen (99.999 mol %) and liquid oxygen (99.8 mol %). Part of the nitrogen top product from the distillation column is compressed from 1.2 to 4.5 bar in the main compressor, then cooled in the MHE. It is condensed and liquefied against liquid nitrogen from the loop and the liquid oxygen reflux in a coupled condenser-reboiler. Finally, it is throttled down to the column pressure to be fed as reflux. Another part is extracted to recover LNG cold exergy in a pressurized liquid loop. The vapor nitrogen is compressed in two steps with inter-

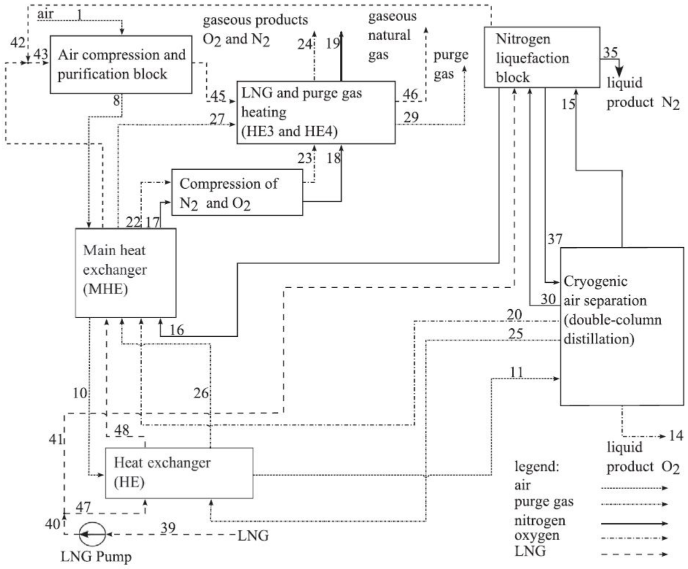
air
1
42
43
50
Air compression and purification block
8
gaseous products O_2 and N_2
24
19
gaseous natural gas
purge gas
Nitrogen liquefaction block
35
liquid product N_2
15
45
LNG and purge gas heating (HE3 and HE4)
46
27
29
23
18
Compression of N_2 and O_2
22
17
Main heat exchanger (MHE)
16
37
Cryogenic air separation (double-column distillation)
30
20
25
11
10
26
41
48
14
liquid product O_2
Heat exchanger (HE)
47
40
39
LNG
LNG Pump
legend:
air
purge gas
nitrogen
oxygen
LNG

Figure 2.4: Conceptual design 2 - two-column ASU with LNG integrated in all the heat exchangers, Tesch et al. (2016).

and after-cooling from 1.2 to 18 bar. It gasifies the LNG feed in two multi-stream HE before being sub-cooled and throttled down to 3.8 bar, feeding a flash-separator. The gas stream provides cold duty to the nitrogen loop and goes back to the second compressor of the cyle while the liquid stream is divided in three parts. One is used for cooling needs of the nitrogen reflux in the integrated condenser-reboiler and the MHE. The second is compressed by a pump up to 90 bar to liquefy the cyclic nitrogen and to extract power in turbo-expanders. The last part is expanded to atmospheric pressure in a JT-valve and stored as liquid nitrogen product.

2.2.2 Single-column ASU with LNG cold recovery and power cycle, Mehrpooya et al. (2015)

Mehrpooya et al. (2015) propose a single-column ASU with products heat recovery to avoid any utility consumption in the distillation column. The LNG cold is recovered in the MHE. In order to increase the efficiency of the total process and recover LNG cold exergy from -76 ^{o}C up to about ambient temperature, a carbon dioxyde power cycle is integrated to the configuration. The process achieves a high exergy efficiency of 67.1 % and produces high purity liquid and gaseous nitrogen (above 99 mol %) and liquid oxygen (100 mol %). Compared to the other propositions, this process is relevant for medium capacity LNG terminals with a LNG feed of 13.88 tons per hour and an inlet pressure of 70 bar.

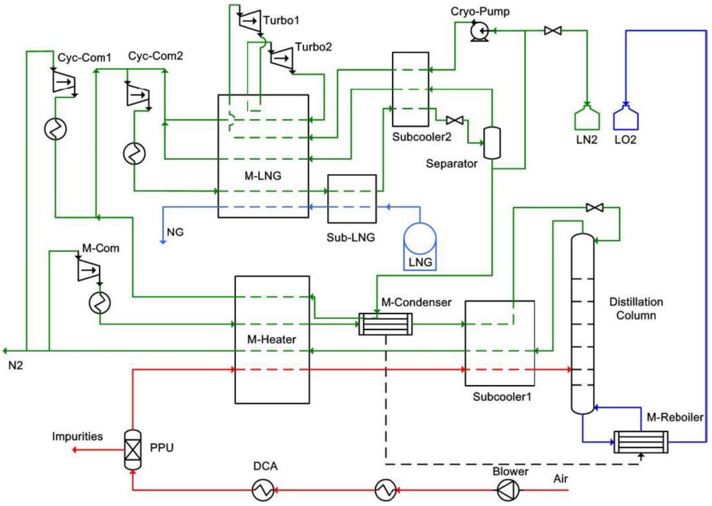
Turbo1
Cryo-Pump
Turbo2
Cyc-Com1
Cyc-Com2
Subcooler2
LN2
LO2
Separator
M-LNG
NG
Sub-LNG
LNG
M-Com
M-Condenser
Distillation
Column
M-Heater
N2
Subcooler1
M-Reboiler
Impurities
PPU
DCA
Blower
Air

Figure 2.5: Flowsheet of a single-column heat pump ASU with LNG cold recovery through nitrogen cycle, Zheng et al. (2015).

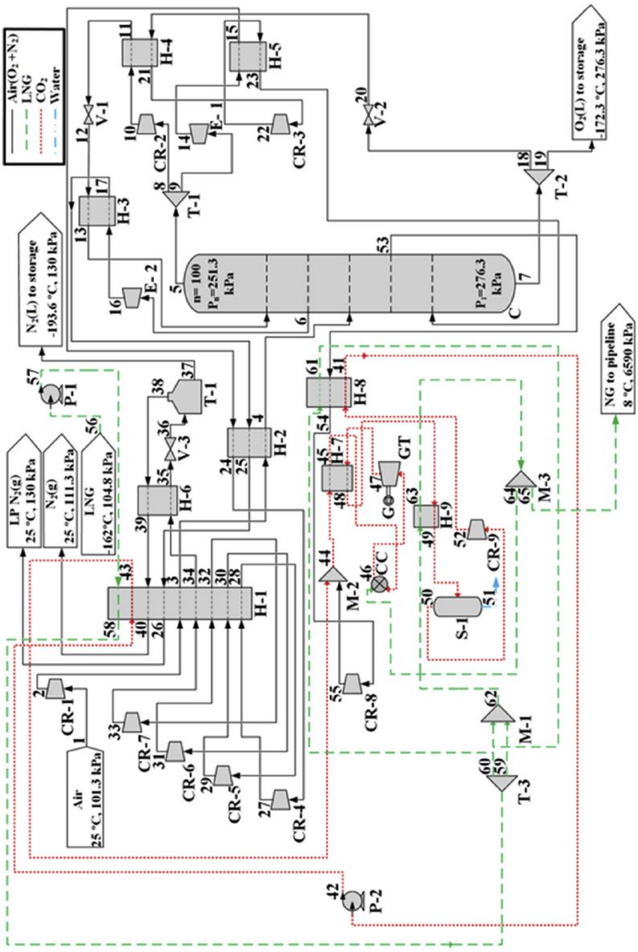
Air(O_2+N_2)
LNG
CO_2
Water
O_2(L) to storage -172.3 °C, 276.3 kPa
N_2(L) to storage -193.6 °C, 130 kPa
NG to pipeline 8 °C, 6590 kPa
LP N_2(g) 25 °C, 130 kPa
N_2(g) 25 °C, 111.3 kPa
LNG -162°C, 104.8 kPa
Air 25 °C, 101.3 kPa
n= 100
P_n=251.3 kPa
P_1=276.3 kPa
C
H-1
H-2
H-3
H-4
H-5
H-6
H-7
H-8
H-9
CR-1
CR-2
CR-3
CR-4
CR-5
CR-6
CR-7
CR-8
CR-9
E-1
E-2
V-1
V-2
V-3
T-1
T-2
T-3
M-1
M-2
M-3
P-1
P-2
GT
G
CC
S-1

Figure 2.6: Flowsheet of a single-column ASU with LNG cold recovery through nitrogen cycle and power cycle, Mehrpooya et al. (2015).

Chapter 3

Selection of processes and parameter sets for a fair comparison

3.1 Selection of ASU and LNG regasification configurations

As seen in the survey, the existing integrated configurations of ASU and LNG regasification use LNG cold exergy to cool down the air feed to the ASU and/or to liquefy the nitrogen product. The main difference among the options is in which heat exchanger LNG cold exergy is recovered: in the main heat exchanger (MHE) directly cooling down the air feed, or in the nitrogen loop heat exchangers (HE_{Loop}), or in all HEs over the process. This study will work to compare the configurations on the basis of the classification shown in Table 3.1. The configurations proposed by Tesch et al. (2016) will not be modelized due to time constraint and complexity.

Table 3.1: Classification of reviewed integrated ASU and LNG regasification configurations.

LNG in:	MHE	HE_{Loop}	All HEs
Single-column	Mehrpooya et al. (2015)	Zheng et al. (2015)	-
Two-column	Xu et al. (2014) novel	Xu et al. (2014) traditional	Tesch et al. (2016)

In addition, stand-alone ASU configurations will be studied to provide a reference for comparison to the integrated models. The single column ASU based on the work by Fu and Gundersen (2013) will be the comparison basis for sinlge column integrated models, as it is the reference for the integration work in the study by Zheng et al. (2015). The two-column ASU proposed by Ebrahimi et al. (2015), which is close to the one used by Xu et al. (2014), will be the reference for two-column integrated models. The regasification of LNG in non-integrated models will be performed by heat exchange with seawater in a vaporizer. LNG feed at 70 bar and -158.7 ^{o}C is warmed up to ambient temperature at 25 ^{o}C while water at atmospheric pressure is cooled down from 25 ^{o}C to 15 ^{o}C.

3.2 Method for the selection of parameter sets

The ASU products are varying from one configuration to another, so is the set of operating conditions for air feed and LNG feed. The main objective of this thesis is to find a simulation and calculation basis to be able to compare fairly the different configurations. The classic indicator to evaluate ASU designs is the work consumption per amont of liquid nitrogen or oxygen produced. As the amont of product recovered is dependent on the flow rate of feed air and the exergy available from the LNG feed, both the air feed and the LNG feed characteristics should be set for all cases. This will affect the performance of the models, as they were designed for different capacity of LNG and have thus widely different air flow to LNG flow ratio. As the compression work required is also varying depending on the amont of liquid produced by the ASU, one should set the produced flow rate of either liquid oxygen or nitrogen to be the same in all cases. The desired product purities are also changing the designs and work consumptions so they should be set the same for all cases. With these constraints, each model will be working outside its original designed conditions, which could lead to a lower performance than the reference, but the comparison with this indicator should be more fair. This study will focus on comparing the performances among the cases, operating with the defined set of constraints.

3.3 Inlet parameters

3.3.1 LNG feed specifications

In the reviewed studies, there are large differences in the feed LNG stream parameters. For comparison sake, the same feed specifications will be selected for all cases. In the studies, LNG inlet pressure after send out pumps is ranging from atmospheric up to 120 bar. According to Mokhatab et al. (2014), LNG is stored at around 130 kPa and -162 ^{o}C in receiving terminals, which will be the selected specifications for the model feed stream. The send out pump will be integrated in the models. The LNG flowrates vary greatly from less than 3 up to 113 tons per hour in the different studies. In the review of existing ASU integrated to LNG by Xu et al. (2014), the flow rates of LNG feed go from 8 for small scale integrated ASU and LNG regasification designs up to 68 tons per hour, larger scale being the latest trend. An intermediate flowrate of 50 tons per hour will be selected for the models. The studies are also using different LNG compositions, with

Lower Heating Values (LHV) ranging from 49.30 up to 49.62 MJ per kg. The LHV is a parameter depending on the regulation set by the country importing LNG. The LNG composition used in the specialization project, with a LHV of 49.28 MJ per kg, will be used in the models. It is shown on Table 3.2.

Table 3.2: LNG feed stream composition.

Components	Mole fractions
Nitrogen	0.0101
Methane	0.9160
Ethane	0.0493
Propane	0.0171
I-butane	0.0035
N-butane	0.0040
LNG molar flow [kmol/h]	2833

3.3.2 Air feed specifications

The air inlet flow rate should be taken in accordance to the selected LNG flow rate. As seen in the reviewed studies, it should be roughly 20 tons per hour higher than the LNG flow rate. So as a starting value for the models, the feed air flow rate will be 70 tons per hour. The aim of this project is to compare the optimized cases on the basis of exergy efficiency at process level using Exergy Transfer Effectivness (ETE). The standard air composition tabulated in the work by Szargut et al. (1988) has been used in the previous semester work to calculate the reference level of chemical exergy. Yet, most of the references found on integrated ASU and LNG regasification are neglecting noble gas fractions, as Helium, Krypton, Neon and Xenon, which all have a mole fraction below 0.0001 in air. Not all references consider the fraction of Argon, which is fairly low with 0.0093 mol $\%$. Moreover, Argon production is not treated in the reviewed sources. For simplification purpose, notably to facilitate the convergence of the distillation coulumns in the simulation, the air feed composition will be reduced to Nitrogen and Oxygen with the fractions presented in Table 3.3. Water and carbon dioxide traces are considered to have been removed from the air feed upstream of the models, in the air pre-treatment part of the ASU, which is not included in the simulations. With this chosen composition, the air feed has a non-zero chemical exergy value, which will be accounted for in exergy calculations. Finally, for simplification purpose in exergy calculation, the feed air temperature and pressure for the models will be 25 ^{o}C and 101.325 kPa, which are standard values for the environment conditions in exergy calculations.

Table 3.3: Air feed stream composition.

Components	Mole fractions
Nitrogen	0.7906
Oxygen	0.2094
Air molar flow [kmol/h]	2426

3.4 Product specifications

3.4.1 Regasified LNG

According to Gomez et al. (2014), the required natural gas pressure at the outlet of the LNG regasification terminal depends on the end user, ranging from 6-25 bar for power stations, 30 bar for local distribution, and up to 70 bar for long distance distribution. The outlet natural gas pressure in the reviewed studies are between atmospheric pressure and 65.9 bar. This parameter has a large influence on the integration design because the compression up to the selected distribution pressure is done by pumping work on the LNG feed, in order to save energy compared to gas compression at the outlet of the regasification process. Thus, the heat balances in the configurations are affected. The study will focus on long distance gas distribution, selecting a gas outlet pressure of 70 bar for the models, which is a medium value with regards to the pressure after send-out pumps in the survey. The gas outlet temperature specification is chosen at 25 ^{o}C, matching the ambient temperature. Additional heating in a water-vaporizer at the exit of the ASU-integrated LNG heating is set in the models in order to reach this specification. Water is cooled down from ambient temperature 25 ^{o}C to 15 ^{o}C.

3.4.2 ASU products

The reviewed studies propose models with varying product flow rates and purities. In order to set a fair comparison basis, the nitrogen liquid product specifications will be the same in all the simulations. This product was chosen as main parameter among the products because LNG regasification is often integrated to the liquid nitrogen loop. Liquid nitrogen production is also the part that requires the most compression work in ASU. Moreover compression work is the main term in exergy efficiency, as can be seen in the detailed results later in the report.

During the simulation work, the maximum flow rate that could be reached for liquid nitrogen was around 415 kmol per hour in the model based on the work by Mehrpooya et al. (2015). This value was used as specification for the other integrated models. The liquid nitrogen purities attained were between 99.34 and 99.52 mol %. Pure liquid oxygen is produced in all the models. The flow rate is varying from simulation to simulation, as it is constrained by the reflux need in the distillation columns (LP column for two-column models) and the heat balance of the integrated condenser-reboiler in two-column designs.

Not all the configurations produce vapor oxygen or vapor nitrogen. The novel model proposed by Xu et al. (2014) produces neither and the model based on the work by Zheng et al. (2015) produces only nitrogen gas. The flow rates of gas nitrogen and gas oxygen products are varying from model to model, as they are fixed by the previous constraints on liquid nitrogen. The purities attained are above 99 mol $\%$ and 100 mol $\%$ fo gas nitrogen and gas oxygen products respectively. All models, except the one based on the work by Zheng et al. (2015), produce a waste gaseous stream with a composition close to the feed air. The flow rate of the waste stream is varying from model to model. All products have a pressure constaint varying between 110 and 130 kPa. All the gaseous product streams have a temperature constraint of 25 ^{o}C.

The references used for stand-alone ASU simulations were not originally producing liquid nitrogen. After modifications, it was not possible to reach the liquid nitrogen flow rate constraint of 415 kmol per hour, due to lack of cold duty without LNG cold utilization. The maxima achieved were of 158 kmol/h based on the one-column ASU by Fu and Gundersen (2013) and 47.74 kmol/h based on the two-column model by Ebrahimi et al. (2015). In order to produce liquid nitrogen in stand-alone units, liquid oxygen production was not achieved. In both models, pure gaseous oxygen and gaseous nitrogen with a purity above 99.5 mol $\%$ are produced.

After setting both flow rate and composition of the liquid nitrogen product, there is limited margin to set specifications for the other products, as has just been described. Using ETE to compare the efficiency of the models will allow to account for varying compositions, flow rates and pressures of the product streams, thanks to the decomposition down to component partial chemical exergies, as will be explained in the exergy calculation method later on. The specifications for ASU products are summarized in table 3.4.

Table 3.4: Summary of specifications for ASU products.

Products	Liquid N_2	Liquid O_2	Gaseous N_2	Gaseous O_2
Pressure [kPa]	-	-	between 110 and 130	
Temperature [^{o}C]	-	-	25	25
Purity [mol $\%$]	$>$ 99.3	100	$>$ 99.3	100
Flow rate [kmol/h]	415	-	-	-

3.5 Machinery and equipment design

3.5.1 Compressors, pumps and expanders

There are differences again in the equipment efficiencies used in the reviewed models. For this project, the efficiencies used in the specialization project and by Marmolejo-Correa and Gundersen (2015), have been chosen. In the models, compressors and expanders have a polytropic efficiency of 78 % and pumps an adiabatic efficiency of 75 %. Except for the feed air compressor, all pressure ratio in compressors are kept slightly above or below 3.

3.5.2 Heat exchangers

In the specialization project, the pressure drop in heat exchangers was set to 5.5 % of the inlet pressure (Marmolejo-Correa and Gundersen (2015)). For this thesis, as the models are more complexe and not all reviewed references were considering pressure drop, a zero-pressure drop will be used in all heat exchangers, for simplification purpose. During simulation work, the minimum approach temperature of cryogenic heat exchangers was constrained to 1 ^{o}C.

3.5.3 Distillation columns

Pressure drop was neglected in all the distillation columns for simplification purpose. The numbers of stages are varying from model to model and were selected based on the litterature review.

Chapter 4

Modelization

The commercialized software Aspen HYSYS was used for modelling with the conventional equation of state Peng-Robinson. Eight cases were simulated. All the configurations are summarized in Table 4.1 and the models are explained below. IMHE stands for configurations with LNG streams integrated in the MHE, ILoop for cases with LNG streams integrated in the nitrogen loop and Alone for stand-alone ASU. 1C is for single column ASU designs and 2C for two-column ones. Exp means than expansion power was added compared to the original design.

Table 4.1: Summary of simulated cases.

Cases	Descriptions	References
IMHE-1C	single column ASU LNG integrated in the MHE	Mehrpooya et al. (2015)
IMHE-2C IMHE-2Cexp	two-column ASU LNG integrated in the MHE	Xu et al. (2014)
ILoop-1C	single column ASU LNG integrated in the nitrogen loop	Zheng et al. (2015)
ILoop-2C ILoop-2Cexp	two-column ASU LNG integrated in the nitrogen loop	Xu et al. (2014) Ebrahimi et al. (2015)
Alone-1C Alone-2C	single column stand-alone ASU two-column stand-alone ASU	Fu and Gundersen (2013) Ebrahimi et al. (2015)

4.1 Adaptation of integrated models from literature

The classification proposed for this study is only approximative as the nitrogen loops are not standardized among all selected models. Some designs include power generation to increase the overall process efficiency, through compression-expansion of nitrogen in case ILoop-1C or ASU column reflux streams in case IMHE-1C, while other designs use only expansion valves. Case IMHE-1C was even considering further recovery of LNG cold exergy through integration with a power cycle. The configuration of the cold box is varying for single column ASU: case IMHE-1C is based on heat integration between the column draw streams, while cases ILoop-1C and Alone-1C, both inspired from the ASU model by Fu and Gundersen (2013), rely on recuperative vapor recompression heat pump effect. The liquid nitrogen is obtained by different ways: through the liquefaction of ASU gas nitrogen product in the nitrogen loop for cases IMHE-1C, IMHE-2C, ILoop-1C, Alone-1C and IMHE-2Cexp; or directly as liquid product from the distillation column, as in cases ILoop-2C, Alone-2C and ILoop-2Cexp. The ideal work would have been to design standardized model for each configuration from the classification to achieve a fair comparison. However, such process design is not a feasible task for only one semester. Thus, the study focuses on adaptating the reviewed models, as presented in the following paragraphs.

Each reference uses its own set of feed and product parameters. Changing these parameters to a common set for all models has required modifications in order to achieve convergence of the distillation columns and reach balance in the heat exchangers. It has included for example changing draw streams of the distillation columns, changing pressure levels in columns and nitrogen loops, supressing heat exchangers or modifying their connexions, and other operations. These modifications were done step by step following trial and error method. It has been the main task of this thesis in terms of work load.

Recycle units were used in nitrogen loops and column reflux loops. As the studied ASU were designed to yield high purity products, the phase change in the product streams were occuring at almost constant temperature. As a consequence, slight temperature changes in the reflux loops had a major impact on the convergence of the columns. Thus, the recycle units failed to reach convergence on their own: the convergence of the distillation columns and their integration in the main flowsheets by closing the reflux loops had to be done manually.

Final models obtained for each case are explained below, as well as their modifications compared to the reference in studied literature.

4.1.1 CASE IMHE-1C - Single column ASU, LNG in the MHE, based on the work by Mehrpooya et al. (2015)

In the model proposed by Mehrpooya et al. (2015), the carbon dioxide power cycle was removed to work on a similar basis with the other models. As the feed flow rates were modified compared to the reference, there was a temperature cross in the air subcooler heat exchanger (H-2 on Fig. 2.6) and the integrated heat exchangers with the ASU product streams (H-3 to -5 on Fig. 2.6). Producing the selected flow rate and purity for the liquid nitrogen product also modified the convergence parameters of the distillation column, and then of the integrated heat exchangers. In order to achieve convergence of the column, the vapor fraction of the nitrogen reflux and of the air feed were changed, which impacted on the flow rates of the draw streams. To remove temperature crosses, the medium vapor oxygen draw (stream 53 on Fig. 2.6), initially used as feed in the power cycle, was integrated in the subcooler and the MHE after expansion to 130 kPa. The oxygen reflux and liquid oxygen product flow rates were reduced to generate an other oxygen cold stream (stream OX04a on Fig. 4.1) supplying the missing cold duty in one integrated ASU heat exchanger (H-5 on Fig. 2.6) as well as in the subcooler and the MHE. The use of these two streams, mixed in MIX-100, generated a pure vapor oxygen product (OX07 on Fig. 4.1). The high purity nitrogen heat exchanger (H-6 on Fig. 2.6) was merged with the air subcooler (H-2) in a single heat exchanger. LNG cold exergy is used from feed temperature up to -101.3 ^{o}C before it is vaporized in an additional heat exchanger. Recycle units were used for the air feed, the nitrogen reflux and the oxygen reflux.

4.1.2 CASE IMHE-2C - Two-column ASU, LNG in the MHE, based on the work by Xu et al. (2014)

In the novel design proposed by Xu et al. (2014), the HP distillation column pressure is 350 kPa. As with this pressure, there was a temperature cross in the integrated reboiler condenser, it had to be increased up to 415 kPa. Recycle units were used on the air feed stream to the HP column, on the nitrogen reflux to the HP colum, on the high purity nitrogen feed and low purity oxygen feed to the low pressure column and on the oxygen reflux to the LP column. Another recycle unit was used in the nitrogen loop, which was working in a reasonable range. In order to avoid temperature cross in the MHE and to fulfil the specifications on the liquid nitrogen product, the maximum pressure in the nitrogen loop was increased from the reference value of 1500 kPa to 2800 kPa. Two-stage (streams N03b - N03e) and three-stage (streams N11b - N11j) compressions were therefore needed as can be seen on Fig. 4.2. LNG was further integrated in an intercooler, raising its feed temperature to vaporizer from -97.83 ^{o}C (stream L03) up to -84.08 ^{o}C (stream L04).

4.1.3 CASE ILoop-1C - Single column ASU, LNG in the nitrogen loop, based on the work by Zheng et al. (2015)

In the reference work by Zheng et al. (2015), very few stream data were given so the start data for the distillation column were extracted from the original work by Fu and Gundersen (2013), quoted in the reference paper. Yet, the nitrogen reflux flow rate, temperature and purity as well as the air feed temperature to the distillation column were adapted to reach the specifications for the liquid nitrogen product. The oxygen reflux flow rate was constrained by the heat balance in the integrated condenser-reboiler. For the nitrogen loop, no other papers were found to gather more stream data so the flow rates in the loop were set without reference to fulfil the heat balance in the main LNG heat exchanger (LNG2 on Fig. 4.3) and to achieve a flow rate of 415 kmol/h for the liquid nitrogen product (stream N16 on Fig. 4.3). The maximum pressure in the nitrogen loop had to be increased from the reference 1800 kPa up to 7750 kPa obtained by three-stage compression to respect the limit of 3 for the pressure ratio of the compressors. A compressor aftercooler, obtained thanks to a second LNG heat exchanger (LNG1 on Fig. 4.3), was introduced to reduce the compression work, increasing the use of LNG cold from -62.18 ^{o}C up to -33.36 ^{o}C.

In the reference design, a LNG preheater was used (Sub-LNG on Fig. 2.5). As the LNG feed pressure in the simulation work is set to 7000 kPa instead of 110 kPa used in the design by Zheng et al. (2015), the compressed LNG temperature is raised from -162 ^{o}C up to -158.7 ^{o}C. This was increasing the duty required in the nitrogen loop subcooler of the original design (Subcooler2 on Fig. 2.5), which would have required to use unrealisticly high flow rates in the nitrogen loop. So in the adapted design, both the LNG preheater and the nitrogen subcooler were removed, keeping only the main LNG heat exchanger in the loop. Recycle units were used for the air feed, the oxygen and the nitrogen reflux in the ASU as well as on the three nitrogen loops (streams N14, N17 and N18 on Fig. 4.3).

4.1.4 CASE ILoop-2C - Two-column ASU, LNG in the nitrogen loop, based on the work by Xu et al. (2014) and Ebrahimi et al. (2015)

As there were no stream data for most of the distillation draw streams in the paper by Xu et al. (2014) in the traditional design, the start data where taken from the paper by Ebrahimi et al. (2015), which describes a similar two-column ASU. Compared to the original design, the gaseous nitrogen product, drawn from the LP distillation column was preheated in the subcooler (heat exchanger F on Fig. 2.1) before entering the MHE to be brought to 25 ^{o}C. The main difference is on the nitrogen reflux stream to the HP column. The maximum pressure was increased from 2600 kPa in the reference up to 3313 kPa in the model, in order to have sufficient driving forces in the LNG heat exchanger and in the integrated condenser-reboiler. To respect the maximum pressure ratio constraint, 2-stage compression was used. LNG was used in heat exchanger LNG-100 on Fig. 4.4 for after-cooling. Instead of feeding the HP column directly with stream N07f, it was expanded to a lower pressure than the HP column (518 kPa versus 560 kPa), bringing it to a temperature sufficiently low to ensure no temperature cross in the integrated condenser-reboiler. It was then fed to the subcooler and separated into gas and liquid fraction to compress it back to HP column pressure before warming it up to the nitrogen reflux temperature in the MHE. Recycles were used for the air feed to the HP column and the nitrogen and low purity oxygen feeds to the LP column as well as on the nitrogen reflux of the HP column and the oxygen reflux on the LP column.

4.2 Introduction of expansion work

After analyzing contributions to exergy efficiency, as will be described in details in the paragraph on result analysis, it was found that the dominant terms in ETE ratio were compression and expansion works. As a consequence, the models that did not include expanders had an exergy efficiency close to zero. In order to be able to compare the configurations fairly, those models were modified to produce expansion work.

4.2.1 CASE IMHE-2Cexp

Compared to case IMHE-2C, expanders were added on the feed streams to the nitrogen loop as can be seen on Fig. 4.5. Stream N11a, initially fed to the MHE at 130 kPa and -193.6 ^{o}C on Fig. 4.2, is expanded to 110 kPa reducing its temperature down to -195.1 ^{o}C. Stream N03a, fed to the MHE at 415 kPa and -181.3 ^{o}C in case IMHE-2C, is expanded to 130 kPa in case IMHE-2Cexp, decreasing its temperature to -193.5 ^{o}C. These modifications produced 88.26 kW of expansion work and allowed to reduce the maximum pressure in the nitrogen loop from 2800 kPa in case IMHE-2C down to 2630 kPa in case IMHE-2Cexp.

4.2.2 CASE ILoop-2Cexp

In case ILoop-2Cexp, expanders were added on product streams N03a and N05a from the LP column on Fig. 4.6, decreasing their pressure from 130 down to 110 kPa. Another expander was added on stream N07a, feed to the nitrogen loop, decreasing its pressure from 560 kPa to 110 kPa. The total expansion work produced is 156.5 kW. These modifications allowed to reduce the maximum pressure in the nitrogen loop from 3313 kPa in case ILoop-2C down to 3040 kPa in case ILoop-2Cexp. To avoid temperature cross in the integrated condenser reboiler due to the expansion, the nitrogen product from the HP column was splitted into an additional stream, N08, merged again with the nitrogen loop stream N07 before feeding the HP column. To optimize the feed air compression, two stages were used instead of one. An expansion valve was added on stream OX04a to standardize gaseous product pressure at 110 kPa.

4.3 Adaptation of stand-alone models

4.3.1 CASE Alone-1C - Single column ASU, based on the work by Fu and Gundersen (2013)

The basis for single column stand-alone ASU simulation was the model designed by Fu Chao displayed on Fig. 4.7. The adapted simulation design is shown on Fig. 4.8. Compared to the reference design, the maximum pressure level for the air feed out of the booster compressor was raised from 305 up to 480 kPa, which required to use two stages instead of one. The part of air flow going to the booster was raised from one third in the reference up to around 90 % of the total flow. The maximum pressure in the nitrogen loop was decreased from 475 to 450 kPa. The nitrogen reflux stream was split after being subcooled in the MHE in order to produce liquid nitrogen, contrary to the original design. The gaseous nitrogen product purity was raised from 99 up to 99.52 mol % and the oxygen product purity from 95 to 100 mol % to fulfil the specifications.

4.3.2 CASE Alone-2C - Two-column ASU, based on the work by Ebrahimi et al. (2015)

The basis for two-column stand-alone ASU simulation was the model designed by Ebrahimi et al. (2015) displayed on Fig. 4.9. The adapted simulation design is shown on Fig. 4.10. The proportion of feed air going through the booster compressor was raised from one third to 72 % of the total flow. The boosted air outlet pressure was decreased from 1200 down to 836 kPa. The expansion of boosted air through a JT valve was replaced by an expander followed by subcooling to the feed temperature thanks to the nitrogen product stream from the LP column (stream N03c on Fig. 4.10). This modification allowed to produce expansion work and reduce the duty of the MHE compared to the original design. The HP column pressure was decreased from 649 kPa down to 477 kPa. Excess heat from the nitrogen reflux outlet from the integrated condenser reboiler was used in the cryogenic heat exchanger. In order to achieve balance in the cryogenic heat exchanger, the oxygen bottom product from the HP column was expanded by a JT valve before being fed to the cryoHE instead of after. Contrary to the original design, a liquid nitrogen draw was obtained from the LP column (stream N05 on Fig. 4.10), while the liquid oxygen draw (stream 20 on Fig. 4.9) was removed in order to fulfil the liquid nitrogen production constraint. The nitrogen gaseous product from the LP column was expanded from 130 kPa, modified pressure of the LP coumn, down to 110 kPa in order to produce work.

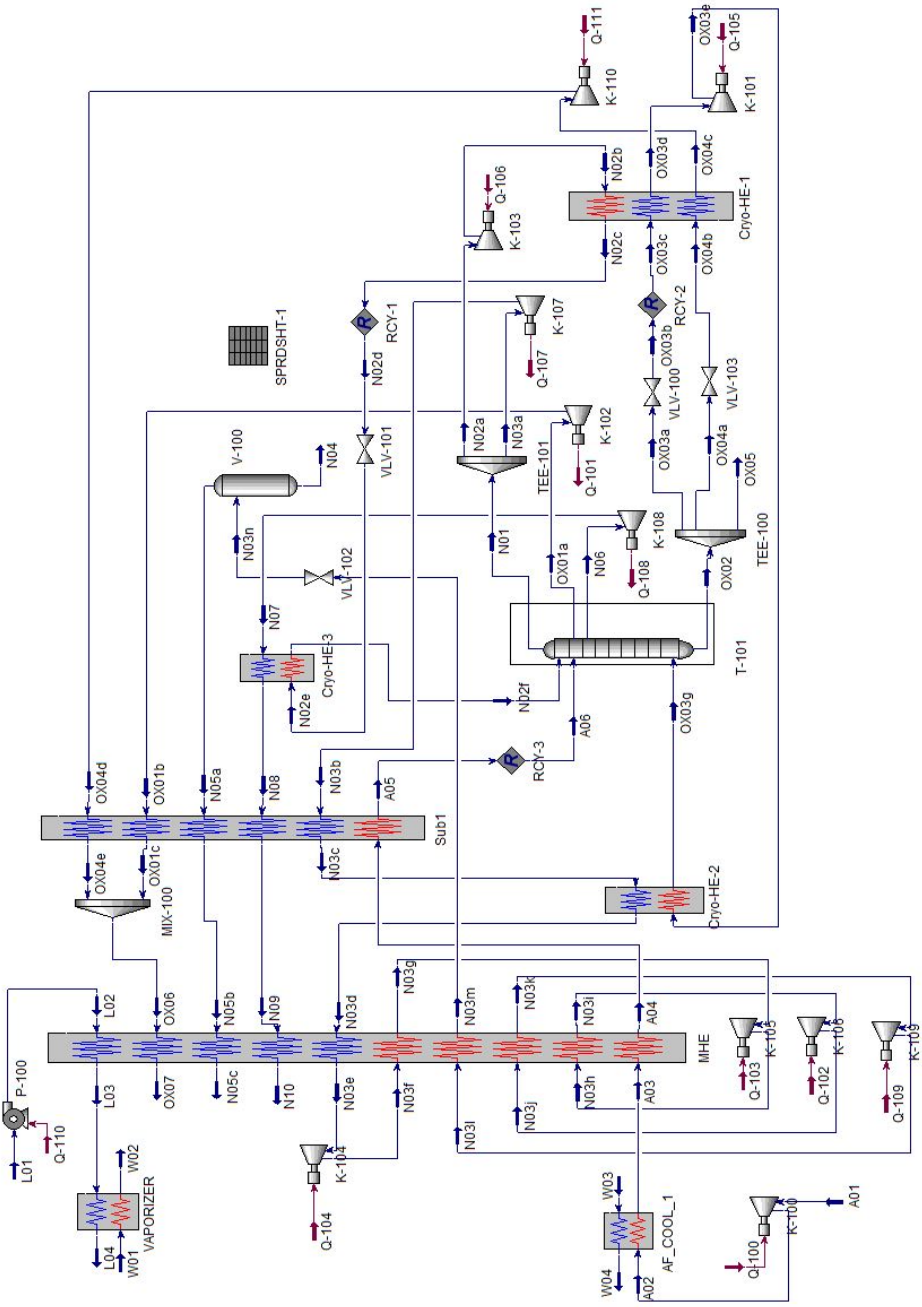
SPRDSHT-1
V-100
N04
VLV-101
N02d
RCY-1
K-103
Q-106
K-110
Q-111
K-101
Q-105
OX03e
N02b
OX03d
OX04c
Cryo-HE-1
N02c
OX03c
OX04b
RCY-2
OX03b
VLV-100
VLV-103
OX03a
OX04a
OX05
K-107
Q-107
N02a
N03a
TEE-101
K-102
Q-101
N01
OX01a
N06
K-108
Q-108
OX02
TEE-100
N03n
VLV-102
N07
Cryo-HE-3
N02e
N02f
T-101
A06
RCY-3
OX03g
OX04d
OX01b
N05a
N08
N03b
A05
Sub1
OX04e
OX01c
N03c
MIX-100
Cryo-HE-2
L02
OX06
N05b
N09
N03d
N03g
N03m
N03k
N03i
A04
MHE
L03
OX07
N05c
N10
N03e
N03f
N03l
N03j
N03h
A03
P-100
Q-110
L01
VAPORIZER
W02
L04
W01
K-104
Q-104
K-105
Q-103
K-106
Q-102
K-109
Q-109
W03
AF_COOL_1
W04
A02
K-100
Q-100
A01

Figure 4.1: CASE IMHE-1C - Flowsheet of a single column ASU with LNG integrated in the MHE, adapted from the work by Mehrpooya et al. (2015).

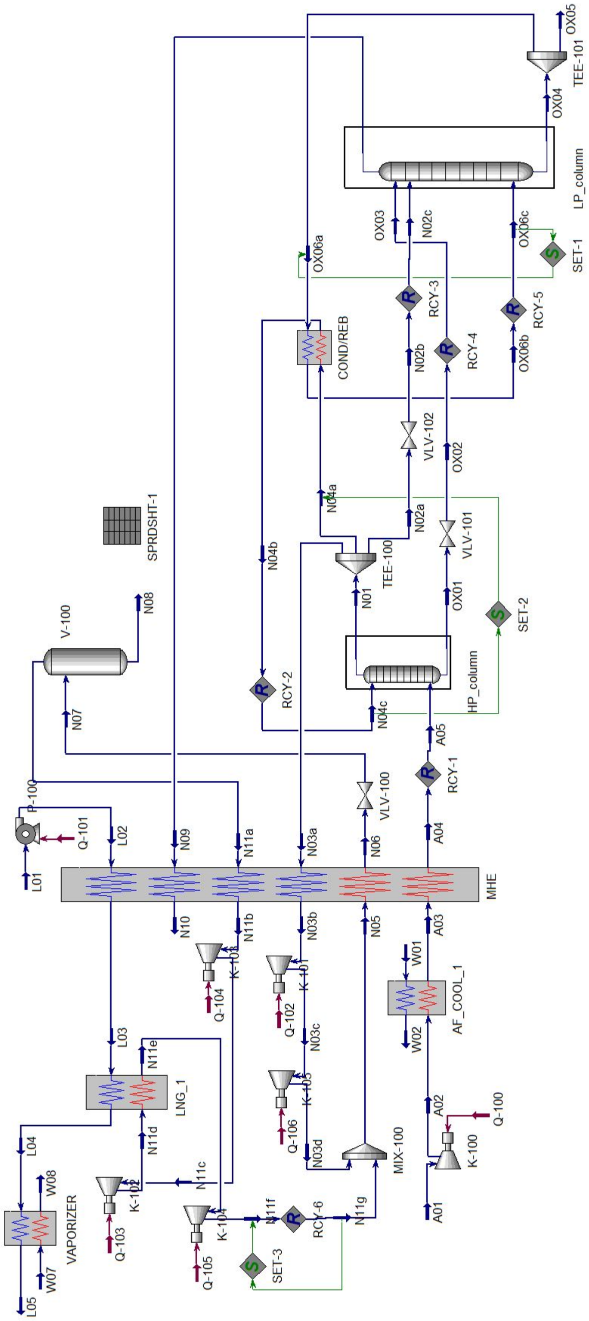
OX05
TEE-101
OX04
LP_column
OX03
N02c
OX06c
SET-1
OX06a
RCY-3
RCY-5
COND/REB
N02b
RCY-4
OX06b
VLV-102
OX02
N04a
N02a
VLV-101
SPRDSHT-1
N04b
TEE-100
N01
OX01
SET-2
V-100
N08
HP_column
RCY-2
N04c
N07
A05
RCY-1
P-100
Q-101
L02
N09
N11a
N03a
N06
VLV-100
A04
L01
MHE
N10
N11b
N03b
N05
A03
W01
K-103
Q-104
K-101
Q-102
N03c
AF_COOL_1
W02
L03
N11e
LNG_1
K-105
Q-106
N03d
MIX-100
A02
Q-100
K-100
L04
N11d
N11c
W08
K-102
Q-103
VAPORIZER
K-104
N11f
RCY-6
N11g
A01
Q-105
SET-3
W07
L05

Figure 4.2: CASE IMHE-2C - Flowsheet of a two-column ASU with LNG integrated in the MHE, adapted from the work by Xu et al. (2014).

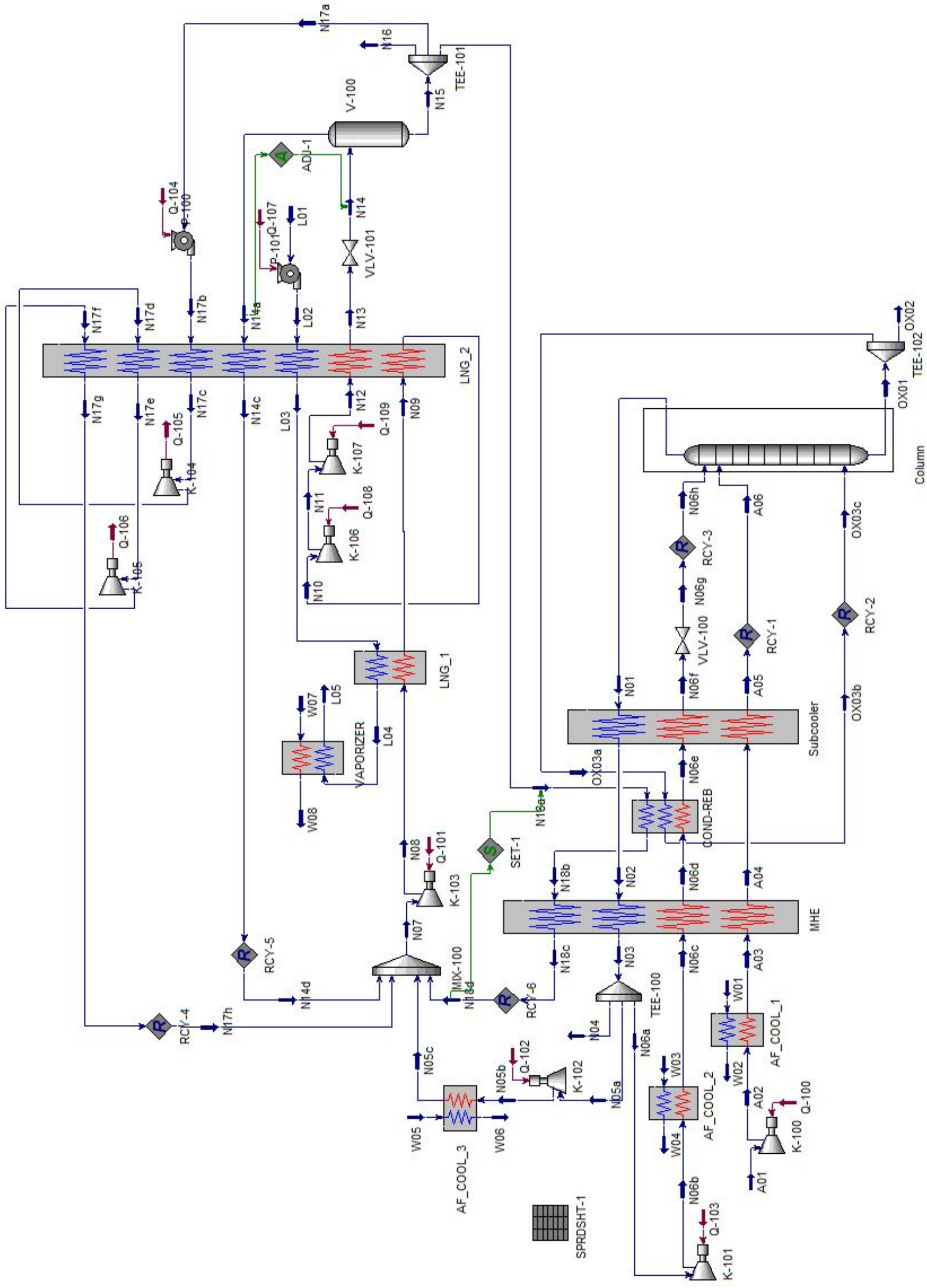
N17a
N16
TEE-101
N15
V-100
ADJ-1
N14
Q-104
P-100
Q-107
L01
P-101
VLV-101
N17f
N17d
N17b
N14a
L02
N13
LNG_2
N17g
N17e
N17c
N14c
L03
N12
N09
Q-109
Q-105
K-104
K-107
N11
Q-108
K-106
Q-106
K-105
N10
LNG_1
W07
L05
VAPORIZER
L04
W08
N08
Q-101
K-103
SET-1
N18a
N07
MIX-100
RCY-5
N14d
N18d
RCY-6
RCY-4
N17h
N05c
N05b
Q-102
K-102
N05a
W05
W06
AF_COOL_3
SPRDSHT-1
OX02
TEE-102
OX01
Column
N06h
A06
OX03c
RCY-3
N06g
RCY-2
VLV-100
RCY-1
N01
N06f
A05
OX03b
Subcooler
OX03a
N06e
COND-REB
N18b
N02
N06d
A04
MHE
N18c
N03
N06c
A03
TEE-100
N04
N06a
W01
AF_COOL_1
W03
W02
A02
Q-100
AF_COOL_2
W04
K-100
A01
N06b
Q-103
K-101

Figure 4.3: CASE ILoop-1C - Flowsheet of a single column ASU with LNG integrated in the nitrogen loop, adapted from the work by Zheng et al. (2015).

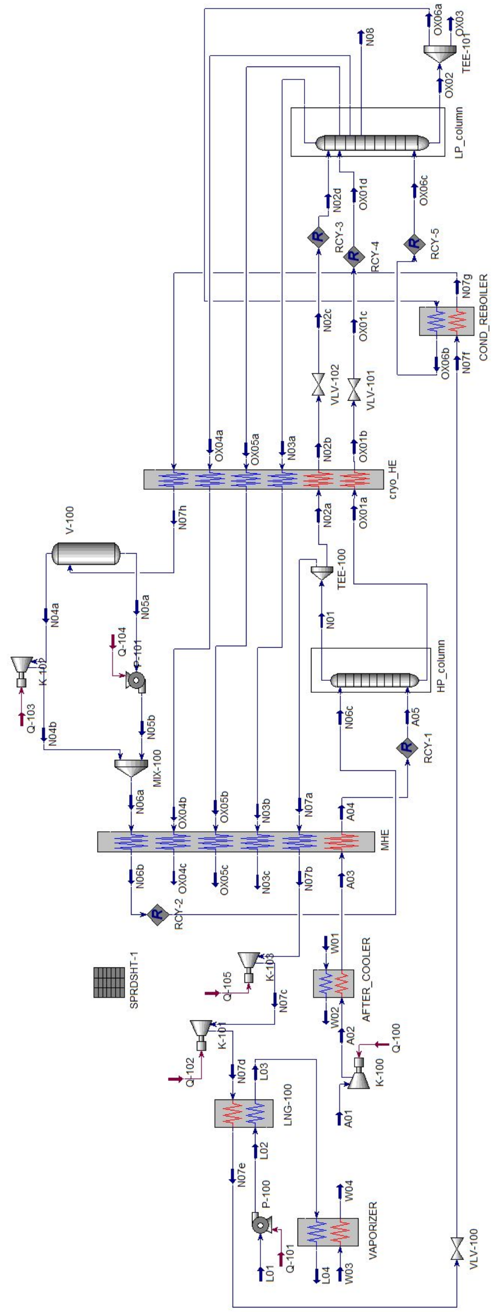
LP_column
HP_column
cryo_HE
MHE
COND_REBOILER
AFTER_COOLER
LNG-100
VAPORIZER
V-100
TEE-100
TEE-101
MIX-100
K-100
K-101
K-102
K-103
P-100
P-101
VLV-100
VLV-101
VLV-102
RCY-1
RCY-2
RCY-3
RCY-4
RCY-5
Q-100
Q-101
Q-102
Q-103
Q-104
Q-105
SPRDSHT-1
A01
A02
A03
A04
A05
W01
W02
W03
W04
L01
L02
L03
L04
N01
N02a
N02b
N02c
N02d
OX01a
OX01b
OX01c
OX01d
OX02
OX03
N03a
N03b
N03c
OX04a
OX04b
OX04c
OX05a
OX05b
OX05c
N04a
N04b
N05a
N05b
N06a
N06b
N06c
N07a
N07b
N07c
N07d
N07e
N07f
N07g
N07h
N08
OX06a
OX06b
OX06c

Figure 4.4: CASE ILoop-2C - Flowsheet of a two-column ASU with LNG integrated in the nitrogen loop, adapted from the work by Xu et al. (2014) and Ebrahimi et al. (2015).

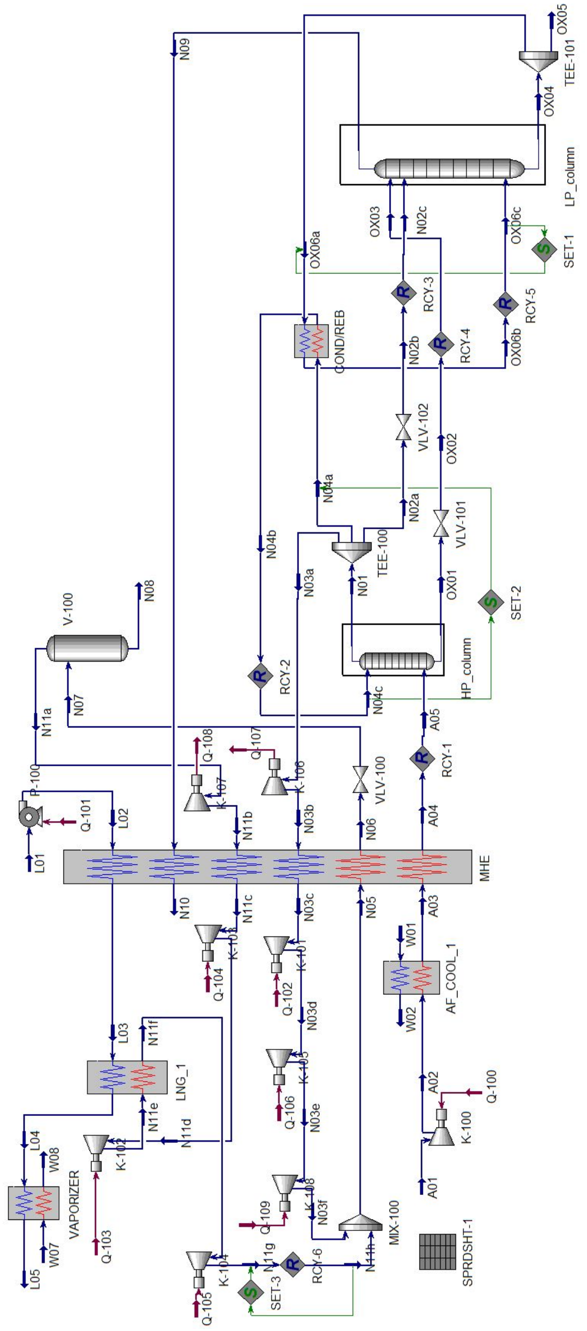
OX05
TEE-101
OX04
N09
LP_column
OX03
N02c
OX06c
SET-1
OX06a
RCY-3
RCY-5
N02b
RCY-4
OX06b
COND/REB
VLV-102
OX02
N04a
N02a
VLV-101
N04b
TEE-100
N03a
N01
OX01
SET-2
V-100
N08
RCY-2
HP_column
N04c
A05
N11a
N07
Q-108
Q-107
K-107
K-106
VLV-100
RCY-1
P-100
Q-101
L02
N11b
N03b
N06
A04
L01
MHE
N10
N11c
N03c
N05
A03
K-103
K-101
W01
Q-104
Q-102
AF_COOL_1
W02
L03
N11f
N03d
LNG_1
K-105
A02
Q-100
Q-106
N11e
N03e
K-100
L04
N11d
W08
K-102
VAPORIZER
A01
K-108
Q-109
N03f
MIX-100
W07
Q-103
N11g
RCY-6
N11h
K-104
SET-3
L05
Q-105
SPRDSHT-1

Figure 4.5: CASE IMHE-2Cexp - Flowsheet of a two-column ASU with LNG integrated in the MHE, adapted from the work by Xu et al. (2014).

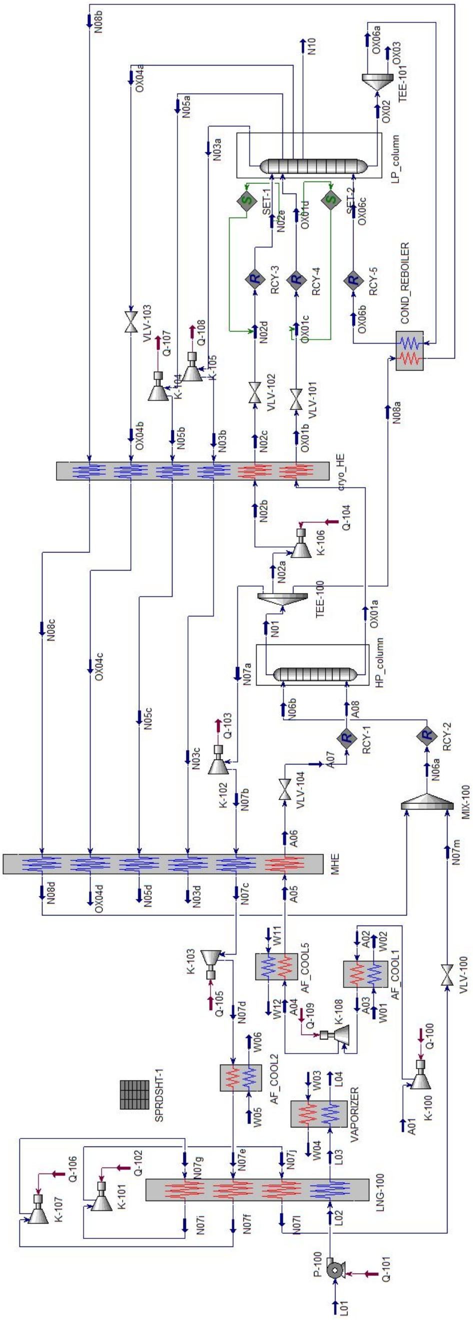
N08b
OX04a
N05a
N03a
N10
OX06a
OX03
TEE-101
OX02
LP_column
SET-1
SET-2
N02e
OX01d
OX06c
RCY-3
RCY-4
RCY-5
COND_REBOILER
VLV-103
Q-107
Q-108
K-104
K-105
N02d
OX01c
OX06b
VLV-102
VLV-101
N08a
OX04b
N05b
N03b
N02c
OX01b
cryo_HE
N02b
Q-104
K-106
N02a
TEE-100
N08c
OX04c
N05c
N03c
N01
OX01a
N07a
HP_column
Q-103
N06b
A08
RCY-1
RCY-2
K-102
A07
VLV-104
N07b
N06a
MIX-100
A06
MHE
N08d
OX04d
N05d
N03d
N07c
A05
N07m
W11
A02
W02
K-103
AF_COOL5
AF_COOL1
VLV-100
Q-105
W12
A04
A03
W01
Q-109
K-108
N07d
W06
Q-100
SPRDSHT-1
AF_COOL2
W03
L04
W05
VAPORIZER
A01
K-100
Q-106
Q-102
N07g
N07e
N07j
W04
L03
K-107
K-101
N07i
N07f
N07l
L02
LNG-100
P-100
Q-101
L01

Figure 4.6: CASE ILoop-2Cexp - Flowsheet of a two-column ASU with LNG integrated in the nitrogen loop, adapted from the work by Xu et al. (2014) and Ebrahimi et al. (2015).

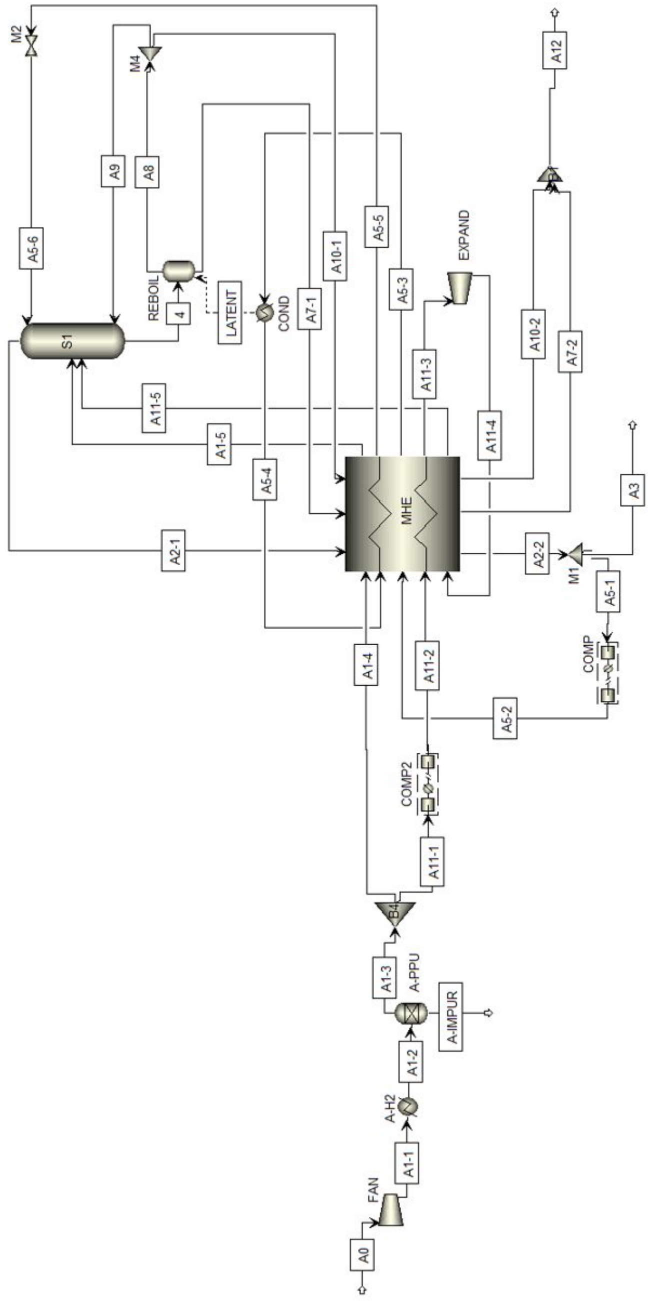
M2
M4
A9
A8
A5-6
REBOIL
4
LATENT
COND
S1
A10-1
A5-5
A7-1
A5-3
EXPAND
A11-3
A10-2
A7-2
A12
A11-5
A11-4
A1-5
A5-4
MHE
A2-1
A2-2
M1
A3
A5-1
COMP
A1-4
A11-2
A5-2
COMP2
A11-1
B4
A1-3
A-PPU
A-IMPUR
A1-2
A-H2
A1-1
FAN
A0

Figure 4.7: CASE Alone-1C - Original design of single column stand-alone ASU by Fu Chao.

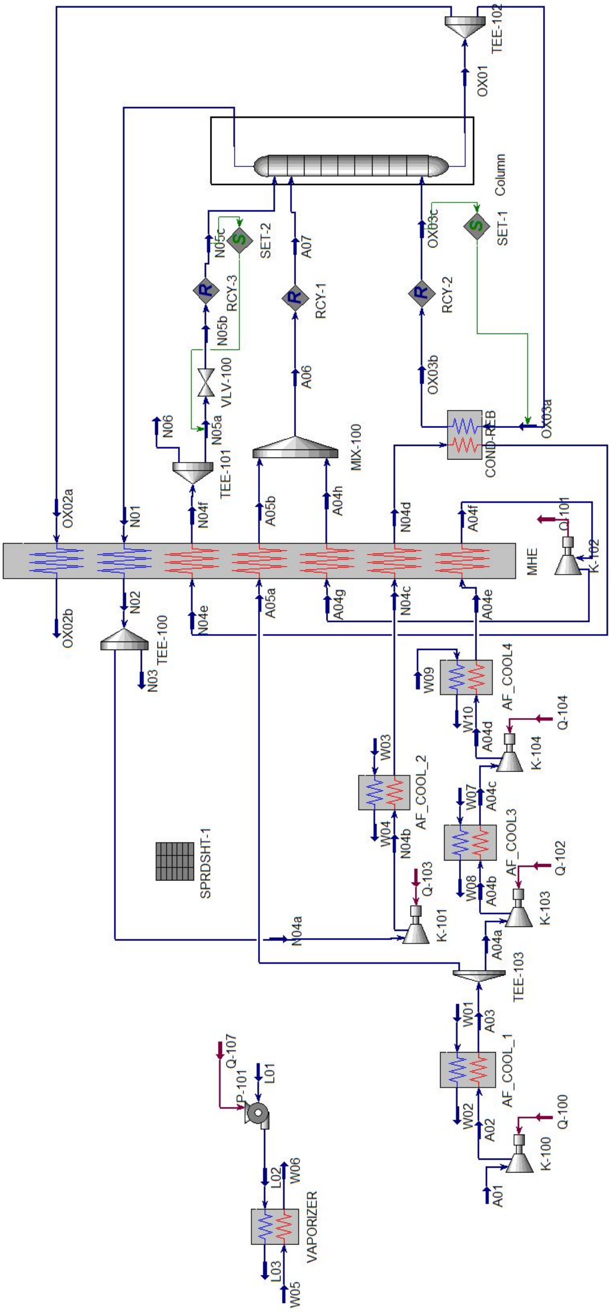
TEE-102
OX01
Column
OX02a
N01
N04f
A05b
A04h
N04d
A04f
MHE
OX02b
N02
N04e
A05a
A04g
N04c
A04e
TEE-100
N03
N06
N05a
TEE-101
VLV-100
N05b
RCY-3
N05c
SET-2
A07
RCY-1
A06
MIX-100
OX03c
SET-1
RCY-2
OX03b
COND-REB
OX03a
Q-101
K-102
W09
AF_COOL4
W10
A04d
K-104
Q-104
W03
AF_COOL_2
W04
N04b
W07
A04c
AF_COOL3
W08
A04b
Q-102
K-103
Q-103
K-101
N04a
A04a
TEE-103
W01
A03
AF_COOL_1
W02
A02
K-100
Q-100
A01
SPRDSHT-1
Q-107
P-101
L01
L02
W06
VAPORIZER
L03
W05

Figure 4.8: CASE Alone-1C - Flowsheet of a stand-alone single column ASU, adapted from the work by Fu and Gundersen (2013).

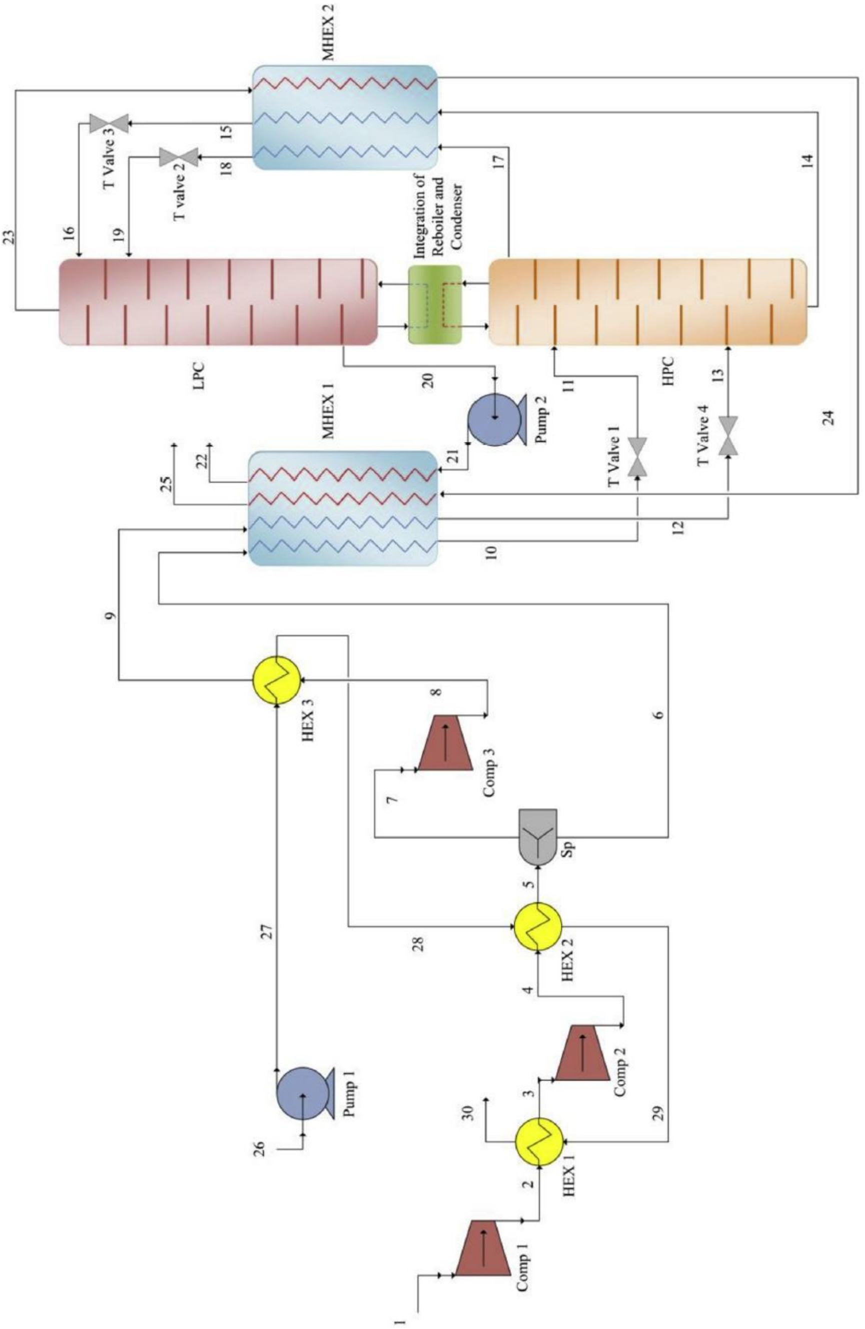
MHEX 2
T Valve 3
T valve 2
Integration of Reboiler and Condenser
LPC
HPC
MHEX 1
Pump 2
T Valve 1
T Valve 4
HEX 3
Comp 3
Sp
HEX 2
Comp 2
HEX 1
Comp 1
Pump 1
1
2
3
4
5
6
7
8
9
10
11
12
13
14
15
16
17
18
19
20
21
22
23
24
25
26
27
28
29
30

Figure 4.9: CASE Alone-2C - Original design of two-column stand-alone ASU, proposed by Ebrahimi et al. (2015).

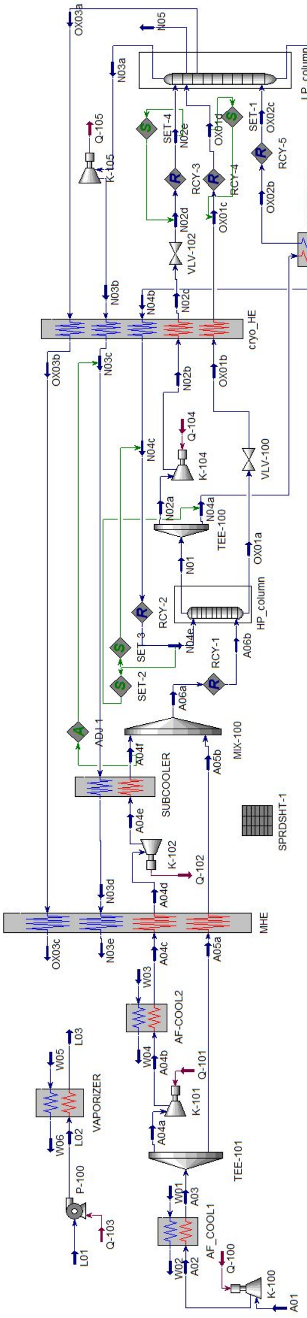
OX03a
N05
N03a
LP_column
OX02a
Q-105
K-105
SET-4
N02e
OX01d
SET-1
OX02c
RCY-3
RCY-4
RCY-5
OX02b
COND_REB
N02d
OX01c
VLV-102
N03b
N04b
N02c
cryo_HE
OX03b
N03c
N02b
OX01b
Q-104
N04c
K-104
VLV-100
N02a
N04a
TEE-100
N01
OX01a
RCY-2
HP_column
SET-3
N04e
RCY-1
A06b
SET-2
A06a
ADJ-1
A04f
MIX-100
A05b
SUBCOOLER
SPRDSHT-1
A04e
K-102
Q-102
N03d
A04d
MHE
OX03c
N03e
A04c
A05a
W03
AF-COOL2
L03
W05
W04
A04b
Q-101
VAPORIZER
K-101
W06
L02
A04a
TEE-101
P-100
W01
A03
AF_COOL1
Q-103
L01
W02
A02
Q-100
K-100
A01

Figure 4.10: CASE Alone-2C - Flowsheet of a stand-alone two-column ASU, adapted from the work by Ebrahimi et al. (2015).

Chapter 5

Cases comparison and performance indicator analysis

5.1 Utilization of LNG cold exergy

The main motivation of integrating LNG regasification to ASU design is to recover LNG temperature-based exergy, also referred to as cold exergy, in order to fulfil ASU cold duty requirements and reduce ASU work consumption. After pressurization from 130 kPa to 7000 kPa, the LNG temperature is raised from -162 up to -158.4 ^{o}C. The total amont of temperature-based exergy available from LNG on the whole range of temperature (-158.4 up to 25 ^{o}C) with the design flow rate is 5.72 MW. A portion of this exergy is used by ASU as LNG is partly regasified through heat exchange with ASU streams. The remaining amont is wasted to seawater through heat exchange in the vaporizer. The details of LNG cold exergy utilization are summarized for all cases on Fig. 5.1.

As the flow rate of liquid nitrogen product was constrained for all cases, the best performance for integrated models is obtained when the smallest amont of LNG cold exergy is used by the ASU process to produce the fixed amont of liquid nitrogen. In stand-alone processes, there was no heat exchange between ASU and LNG streams: the entire amont of LNG cold exergy was wasted to seawater.

Looking into details for integrated models, the amont of LNG cold used by ASU is correlated with the flow rate of the streams cooled by LNG. In case ILoop-1C, LNG is integrated in the nitrogen loop main heat exchanger and in the loop compressor aftercoolers. As this case has the highest flow rate in the nitrogen loop, the cold requirements are the highest. LNG is integrated with the same configuration in cases ILoop-2C and ILoop-2Cexp, but the nitrogen flow rates are reduced in these cases from case ILoop-1C design 4085 kmol/h down to 2000 kmol/h and 558 kmol/h respectively, which explain the decrease in cold duty requirements. As case ILoop-2exp has the smallest flow rate of nitrogen in LNG heat exchangers among all cases studied, this explain its lowest utilization of LNG cold exergy as seen on Fig. 5.1. In case IMHE-1C, nitrogen compression after-cooling is done directly in the MHE, where the LNG is integrated. Since the nitrogen flow rate is the second lowest, with 670 kmol/h, case IMHE-1C has the second lowest LNG cold exergy needs. In cases IMHE-2C and IMHE-2Cexp, LNG is integrated both in the MHE and in the nitrogen loop after coolers. The nitrogen flow rate in the loop is the same in both cases but the compression needs are higher for streams N11 (integrated in the LNG compressor after-cooler) as they are expanded in case IMHE-2Cexp. Thus, IMHE-2Cexp has a higher consumption of cold for the same amont of liquid nitrogen produced.

With the set of constraints used for modelization, case ILoop-2Cexp achieves the lowest consumption of LNG cold exergy to produce the fixed amount of liquid nitrogen. Yet, the models were not optimized in order to reduce the utilization of LNG cold exergy. Increasing the use of water after-coolers over LNG after-coolers in the nitrogen loop could reduce the consumption of LNG cold exergy without affecting the heat balance in the main heat exchangers or changing the ASU products. If the models were not scaled to fit the set of constraints for the sake of comparison with indicator $Work_{N_2}$, the LNG flow rate could have been increased to reduce the oulet temperature of the LNG stream out of the ASU heat exchangers. The amount of liquid nitrogen produced with the same use of LNG cold exergy could also have been increased for integrated cases, except for case IMHE-1C. Considering only LNG cold exergy consumption does not show the differences between cases in terms of ASU work requirements or value of the ASU products. Thus, the consumption of LNG cold exergy is not a sufficient and fair indicator of performance to compare the cases. It only gives a lead for further improvment of the models.

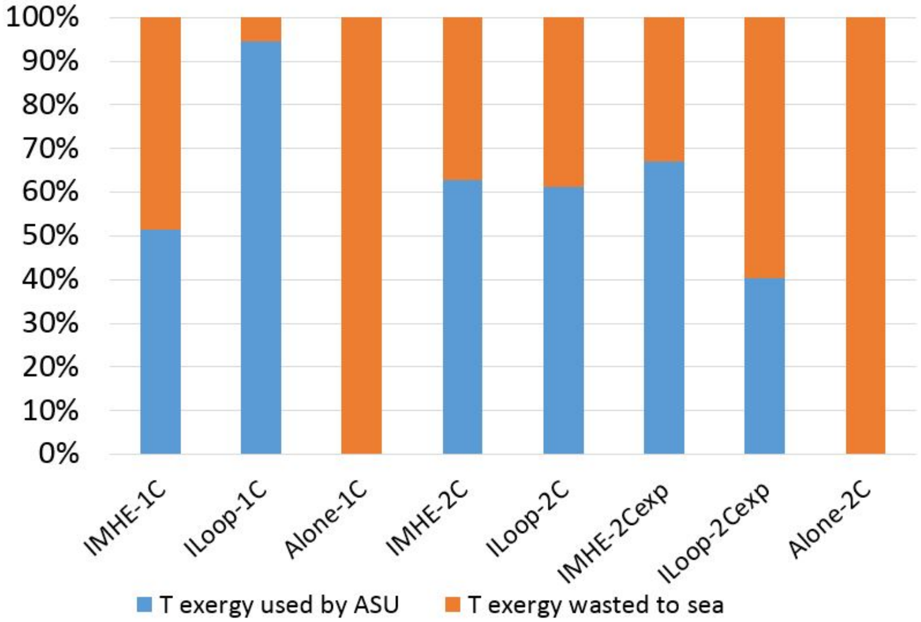

Figure 5.1: Details of LNG cold exergy utilization, in %.

5.2 Work per amont of liquid nitrogen produced

Traditionaly, the performance of ASU is measured through the work required per amont of liquid nitrogen or liquid oxygen produced. It is motivated as compression work is usually the dominant term in ASU. This indicator was calculated for all cases for liquid nitrogen production thanks to equation (5.1) as summarized in table 5.1. Liquid nitrogen was chosen over liquid oxygen to evaluate the work consumption of integrated ASU and LNG regasification designs since LNG is integrated in the nitrogen loop, which is the most energy intensive part in the models and is producing the desired liquid nitrogen. It is also a varying part between the integrted designs, while liquid oxygen production is achieved with the same configuration in all cases, by recovery of the distillation column (LP column for the two-column cases) bottom product.

$$Work_{N_2} = \frac{\sum_z W_{comp_z} - \sum_l W_{exp_l}}{\dot{m}_{N_2}} \tag{5.1}$$

where W_{comp_z} is the work consummed by compressor or pump *z* and W_{exp_l} the work produced by expander *l* in kW and $\dot{m}_{N_2}$ is the mass flow rate of liquid nitrogen produced by the model in ton per hour.

In order to be able to compare the cases with this indicator, all integrated models were set to produce the same amont of liquid nitrogen. Through simulation work, case IMHE-1C appeared to reach the lowest amont of liquid nitrogen produced, which was set as the common constraint. The production of other integrated models was scaled down to the constraint flow rate of 415 kmol/h of liquid nitrogen production, even though they were initially able to produce higher flow rates.

$Work_{N_2}$ does not take into account the purity, pressure and temperature of the liquid nitrogen produced by the ASU, neither does it account for these parameters for the other ASU products. Usually the products and their characteristics vary largely from one ASU design to another, as has been shown in the previous chapters through ASU review and the survey of integrated ASU and LNG regasification configurations. The constraints for modelization were chosen so that the models could be compared thanks to this common indicator with a defined purity of the produced liquid nitrogen for all models. Yet, these parameters could not be constrained for the other ASU products and are varying from cases to cases, making the comparison only partly fair with these figures.

As the flow rate constraint for liquid nitrogen production could not be reached for stand-alone configurations, but only lower flow rates were achieved, the work required in cases Alone-1C and Alone-2C are anormaly high compared to the other cases. So the comparison of integrated and stand-alone models by $Work_{N_2}$ is unfair.

Looking into details, the best performances for integrated models are correlated with the smallest flow rates in the nitrogen loop, except for case ILoop-2Cexp. Reducing nitrogen loop flow rates is decreasing radically the required compression power for the overall process as the nitrogen loop is one of the most energy intensive part of the ASU. ILoop-2Cexp is the only integrated configuration where the warm feed air is compressed over the HP column pressure, up to 8.6 bar, in order to balance the MHE, and expanded after being cooled down to cryogenic temperature. As the feed air compression is the second most energy intensive part of the ASU, this modification is increasing the necessary compression work for liquid nitrogen production, even though case ILoop-2Cexp has one of the lowest flow rate in the nitrogen loop (558 kmol/h).

Table 5.1: Work required per amont of liquid nitrogen produced, in kW per ton per hour.

Cases	IMHE-1C	ILoop-1C	Alone-1C	IMHE-2C
$Work_{N_2}$	317.1	745.5	1293	520.0

Cases	ILoop-2C	IMHE-2Cexp	ILoop-2Cexp	Alone-2C
$Work_{N_2}$	607.3	558.0	569.8	3922

Though the maximum pressure levels used in the nitrogen loops are higher for single column cases IMHE-1C (with 117 bar) and ILoop-1C (77.5 bar), the loop pressure levels do not seem to affect significantly indicator $Work_{N_2}$. Indeed, two-column integrated models require higher overall compression work for liquid nitrogen production than single column ones, except for case ILoop-1C. This can be explained as ILoop-1C has the biggest nitrogen loop flow rate of all the configurations with 4085 kmol/h, while the others vary between 558 and 2000 kmol/h.

5.3 Exergy efficiency

Exergy has been the main topic of the master specialization project. It is presented in details in Appendix for non-informed readers. This thesis is using only Exergy Transfer Effectivness (ETE) to evaluate the exergy efficiency of the overall integrated ASU and LNG regasification process. It has proved to be the best definition through the comparison of exergy efficiency definitions on the AP-DMR natural gas liquefaction process.

ETE has been introduced by the work of Marmolejo-Correa and Gundersen (2015). Yet, it was previously limited to the analysis of thermo-mechanical exergy, i.e. temprature and pressure changes. Through the master specialization project on the application of exergy efficiencies to chemical processes, with the help of Truls Gundersen and Donghoi Kim, ETE was extended to analyze the changes in chemical exergy, thanks to the introduction of mixing exergy terms. This extended definition is accounting for stream composition: higher stream purities are yielding higher mixing exergy values. Thus, this indicator is in theory able to evaluate ASU performance accounting for each product flow rate, purity, pressure and temperature, without the need to set product constraints or the limitation to evaluate only one product and ignore the value of the others like $Work_{N_2}$.

ETE analyzes exergy variations at stream level (ETE2) or at component level (ETE3). In the master specialization project, ETE2 and ETE3 were both applied to the AP-DMR natural gas liquefaction process. While they provided equal results for the overall process, where there is no chemical change, they produced different results at unit operation level. The largest differences were obtained for units operating at low temperatures in the process, like LNG heat exchangers and expansion valves in the cold mixed refrigerant loop, and for units presenting a chemical change (mixers and flash separators). For these cases, ETE2 had a tendency to over-evaluate the efficiencies and showed little changes through the sensitivity analysis, contrary to ETE3. Therefore, ETE3 is expected to give more consistant results for the analysis of the overall integrated ASU and LNG regasification process, where both low tempratures and chemical changes are involved. Yet, both ETE2 and ETE3 definitions have been applied to the studied cases in order to get a deeper understanding on the differences and confirm the superiority of ETE3 definition.

5.3.1 ETE calculation for the study

At each level, ETE is defined as the ratio between exergy sinks and exergy sources as shown by equation (5.2). The equations used to calculate the overall process effiency are an extended version of the formula proposed in the specialization project for flash separators operating below ambient temperature. They are described below for both levels.

$$ETE = \frac{Sinks}{Sources}, \tag{5.2}$$

All exergies transfered to water streams are considered as exergy losses for the efficiency of the overall process, because cooling- and vaporizing-water are not product streams as they are released in the sea without further use. Indeed, their outlet temperatures are not valuable enough, respectively 35 and 15^{o}C, to consider heat recovery. Thus, for the overall process no water exergy appears in the efficiency equations. On the other hand, the air feed and the ASU product streams, as well as the LNG inlet and outlet streams and the energy streams are taken into account for exergy calculations of the overall process. Equations (5.3) and (5.4) are used to calculate exergy sinks and exergy sources at stream level, to be used in ETE2 definition. Equations (5.5) and (5.6) are used to calculate exergy sinks and exergy sources at component level for ETE3 definition.

$$\begin{aligned} Sinks^{ETE2} &= \dot{n}_{L01} \sum_{j=T,P,CH} \begin{cases} [{e_x}^j_{L_{out}} - {e_x}^j_{L01}] & \text{if } {e_x}^j_{L_{out}} > {e_x}^j_{L01} \\ 0 & \text{if } {e_x}^j_{L_{out}} < {e_x}^j_{L01} \end{cases} \\ &+ \sum_{j=T,P,CH} \sum_i \begin{cases} \dot{n}_i [{e_x}^j_i - {e_x}^j_{A01}] & \text{if } {e_x}^j_i > {e_x}^j_{A01} \\ 0 & \text{if } {e_x}^j_i < {e_x}^j_{A01}. \end{cases} \\ &+ \sum_l W_l^{exp}, \end{aligned} \tag{5.3}$$

$$\begin{aligned} Sources^{ETE2} &= \dot{n}_{L01} \sum_{j=T,P,CH} \begin{cases} -[e_{x}{}^{j}_{L_{out}} - e_{x}{}^{j}_{L01}] & \text{if } e_{x}{}^{j}_{L_{out}} < e_{x}{}^{j}_{L01} \\ 0 & \text{if } e_{x}{}^{j}_{L_{out}} > e_{x}{}^{j}_{L01} \end{cases} \\ &+ \sum_{j=T,P,CH} \sum_{i} \begin{cases} -\dot{n}_i[e_{x}{}^{j}_{i} - e_{x}{}^{j}_{A01}] & \text{if } e_{x}{}^{j}_{i} < e_{x}{}^{j}_{A01} \\ 0 & \text{if } e_{x}{}^{j}_{i} > e_{x}{}^{j}_{A01}. \end{cases} \\ &+ \sum_{z} W_z^{comp}. \end{aligned} \tag{5.4}$$

where $\dot{n}_{L01}$ is the molar flow rate of the LNG feed stream in kmol per second, *T*, *P* and *CH* are indices for temperature-based, pressure-based and chemical exergy, $e_{x}{}^{j}_{L_{out}}$ is the molar exergy *j* of the LNG outlet stream in kJ per kmol, *i* are the product streams from the ASU, *l* are the expanders and W_l^{exp} the work produced in kW, *z* the pumps and compressors and W_z^{comp} the work consummed in kW.

$$
\begin{aligned}
Sinks^{ETE3} = & \sum_{j=T,P,CH} \sum_{k} \begin{cases} \dot{n}_{L01,k}[\tilde{ex}^{j}_{L_{out},k} - \tilde{ex}^{j}_{L01,k}] & \text{if } \tilde{ex}^{j}_{L_{out},k} > \tilde{ex}^{j}_{L01,k} \\ 0 & \text{if } \tilde{ex}^{j}_{L_{out},k} < \tilde{ex}^{j}_{L01,k} \end{cases} \\
& + \sum_{j=T,P,CH} \sum_{i} \sum_{k} \begin{cases} \dot{n}_{i,k}[\tilde{ex}^{j}_{i,k} - \tilde{ex}^{j}_{A01,k}] & \text{if } \tilde{ex}^{j}_{i,k} > \tilde{ex}^{j}_{A01,k} \\ 0 & \text{if } \tilde{ex}^{j}_{i,k} < \tilde{ex}^{j}_{A01,k}. \end{cases} \\
& + \sum_{l} W^{exp}_{l},
\end{aligned}
\tag{5.5}
$$

$$
\begin{aligned}
Sources^{ETE3} = & \sum_{j=T,P,CH} \sum_{k} \begin{cases} -\dot{n}_{L01,k}[\tilde{ex}^{j}_{L_{out},k} - \tilde{ex}^{j}_{L01,k}] & \text{if } \tilde{ex}^{j}_{L_{out},k} < \tilde{ex}^{j}_{L01,k} \\ 0 & \text{if } \tilde{ex}^{j}_{L_{out},k} > \tilde{ex}^{j}_{L01,k} \end{cases} \\
& + \sum_{j=T,P,CH} \sum_{i} \sum_{k} \begin{cases} -\dot{n}_{i,k}[\tilde{ex}^{j}_{i,k} - \tilde{ex}^{j}_{A01,k}] & \text{if } \tilde{ex}^{j}_{i,k} < \tilde{ex}^{j}_{A01,k} \\ 0 & \text{if } \tilde{ex}^{j}_{i,k} > \tilde{ex}^{j}_{A01,k}. \end{cases} \\
& + \sum_{z} W^{comp}_{z}.
\end{aligned}
\tag{5.6}
$$

where *k* are the components, $\dot{n}_{L01,k}$ is the molar flow rate of component *k* in the LNG feed stream in kmol per second, and $\tilde{ex}^{j}_{L_{out},k}$ is the partial molar exergy j of component *k* in the LNG outlet stream in kJ per kmol.

5.3.2 ETE result analysis

Calculation results are displayed in table 5.2 and table 5.3 below. ETE2 values are systematically above ETE3 values, and both set of results show the same tendencies. The first analysis show that:

- for each configuration, one-column ASU models show higher efficiencies than the same configuration two-column models,
- for single column cases, integration of ASU and LNG regasification shows better performances than the stand-alone case only when the LNG stream is used in the nitrogen loop,
- cases IMHE-2C and ILoop-2C, which are not producing any expansion power, have efficiencies close to zero,
- for two-column models, integration of LNG regasification to ASU is beneficial in neither cases, the stand-alone model having the highest efficiency,
- in integrated models, both for single and two-column ASU, integration of the LNG stream in the nitrogen loop show higher efficiency than integration in the MHE.

It was expected that integrated models would have higher efficiencies than stand-alone models, independently of the configuration. Indeed, they recover LNG cold exergy, which is supposed to reduce energy requirements to achieve the same ASU product specifications than stand-alone designs. It is difficult to explain the differences between ETE2 and ETE3 without going into more details. Therefore, the results will be further analyzed thanks to the decomposition of exergy sink and source terms into the contribution of ASU streams, LNG streams and energy streams. The detailed figures are shown in tables 7.1 and 7.2 in Appendix.

Compression and expansion works are the same in ETE2 and ETE3. LNG sinks and sources are also the same for ETE2 and ETE3: though LNG streams go through low temperatures, there is no composition change so it seems normal that stream and component level exergy efficiencies are the same. Moreover, LNG terms are the same for all cases as both LNG feed and outlet streams are totally defined by the modelization constraints and set the same for all cases. The only varying terms between ETE2 and ETE3 results are ASU sink and source terms. Yet, the differences are barely shown as compression and expansion works are too big compared to the other terms. It is displayed on Fig. 5.2 and Fig. 5.3, showing relative contribution of ASU, LNG and energy terms to ETE3 sinks and ETE3 sources.

Table 5.2: Exergy efficiency at stream level, with sinks and sources in TW and ratio ETE2 in %.

	Units	IMHE-1C	ILoop-1C	Alone-1C	IMHE-2C	ILoop-2C	IMHE-2Cexp	ILoop-2Cexp	Alone-2C
Sinks	TW	0.962	4.33	1.92	0.0574	0.128	0.375	0.691	0.754
Sources	TW	15.3	37.9	23.5	22.8	26.6	24.8	25.6	20.7
ETE2	%	**6.30**	**11.42**	**8.15**	**0.25**	**0.48**	**1.52**	**2.70**	**3.65**

Table 5.3: Exergy efficiency at component level, with sinks and sources in TW and ratio ETE3 in %.

	Units	IMHE-1C	ILoop-1C	Alone-1C	IMHE-2C	ILoop-2C	IMHE-2Cexp	ILoop-2Cexp	Alone-2C
Sinks	TW	0.925	4.26	1.83	0.0391	0.0402	0.357	0.603	0.661
Sources	TW	15.2	37.8	23.5	22.8	26.5	24.7	25.5	20.6
ETE3	%	**6.09**	**11.27**	**7.79**	**0.17**	**0.15**	**1.44**	**2.37**	**3.21**

Sink terms are exergy increase. In all cases except IMHE-2C and ILoop-2C which have no expanders, the dominant term by above 89 % share is expansion power. LNG sink terms are increase in pressure-based exergy due to the compression from the storage pressure of 130 kPa up to the long distance distribution network pressure of 7000 kPa. ASU sink terms are mostly due to the production of high purity oxygen and nitrogen, which yields an increase in component partial molar mixing exergies compared to the ASU air feed values. The partial molar temperature-based exergies are also increased in liquid nitrogen and liquid oxygen product streams compared to the air feed, as their temperatures, around -180-190 °C, are far below ambient.

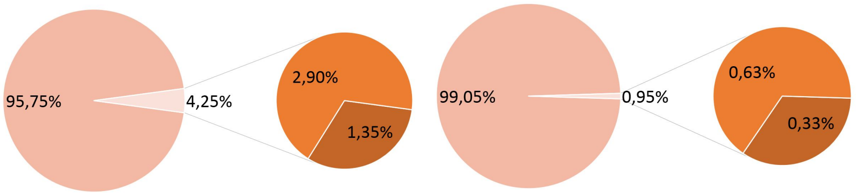

(a) Case IMHE-1C **(b)** Case ILoop-1C

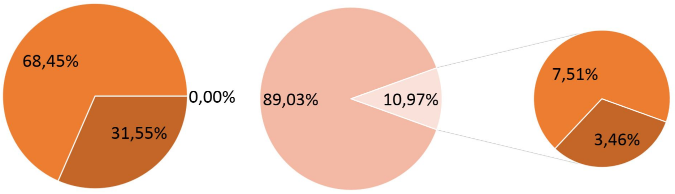

(c) Case IMHE-2C **(d)** Case IMHE-2Cexp

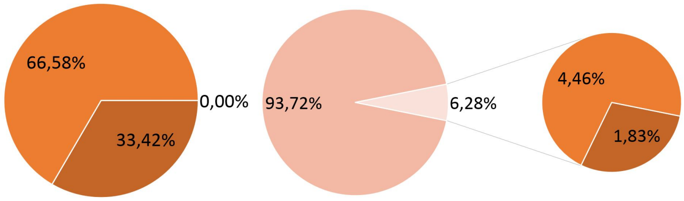

(e) Case ILoop-2C **(f)** Case ILoop-2Cexp

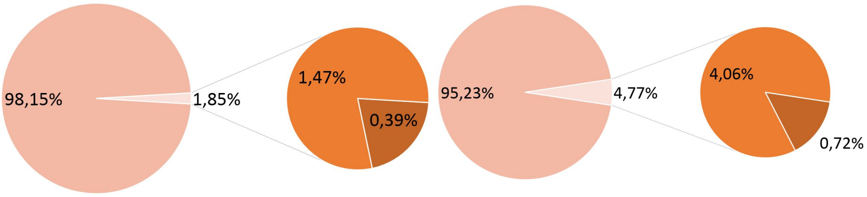

(g) Case Alone-1C **(h)** Case Alone-2C

■ ASU sinks ■ LNG sinks ■ Expansion work

Figure 5.2: Decomposition of ETE3 sink terms, in %.

Source terms are exergy decrease. Since the ASU compression needs are really high, varying between 15 and 38 TW (= 10^{12} W) in the studied cases, they are overweighting all the source terms with a share over 99.6 %. LNG source terms are due to the decrease in temperature-based exergy with the raise in temperature from -162 ^{o}C up to ambient in all cases. ASU source terms are due to the decrease in some component partial molar mixing exergies in the nitrogen product streams and in the waste streams compared to the feed air and have almost no share.

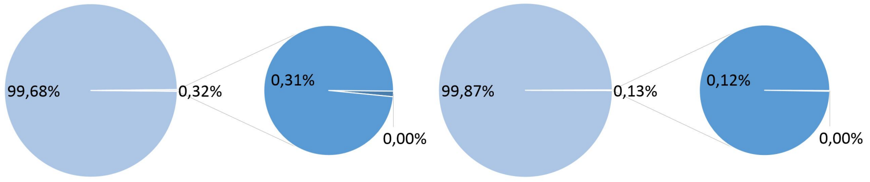

(a) Case IMHE-1C **(b)** Case ILoop-1C

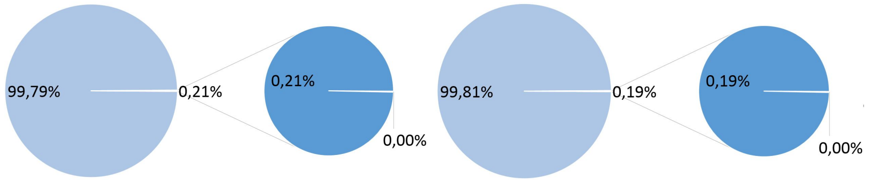

(c) Case IMHE-2C **(d)** Case IMHE-2Cexp

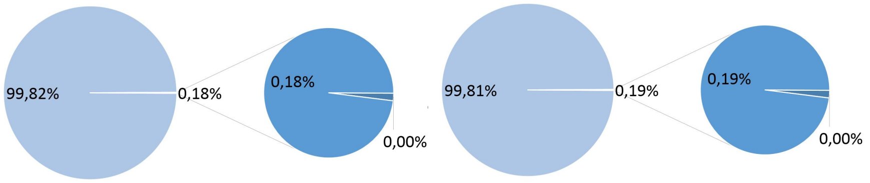

(e) Case ILoop-2C **(f)** Case ILoop-2Cexp

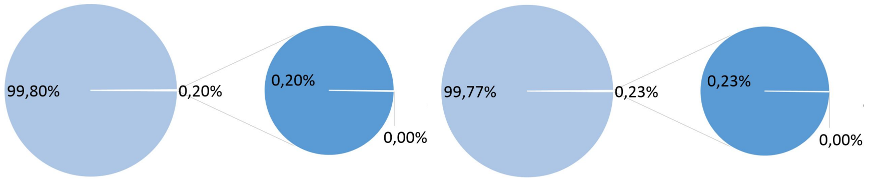

(g) Case Alone-1C **(h)** Case Alone-2C

Figure 5.3: Decomposition of ETE3 source terms, in %.

The previous diagrams confirm that sink terms are dominated by the expansion power produced and source terms by the compression power needs. Thus, ETE2 and ETE3 values are almost equivalent to the ratio of expansion to compression work, as shown on Fig. 5.4. The main idea in utilizing ETE was to be able to evaluate the performance of ASU designs with different products, which other indicators are failing to show, so the cases could be compared fairly, but it is not achieved as chemical exergy changes are overweighted by energy contributions in exergy efficiency calculations.

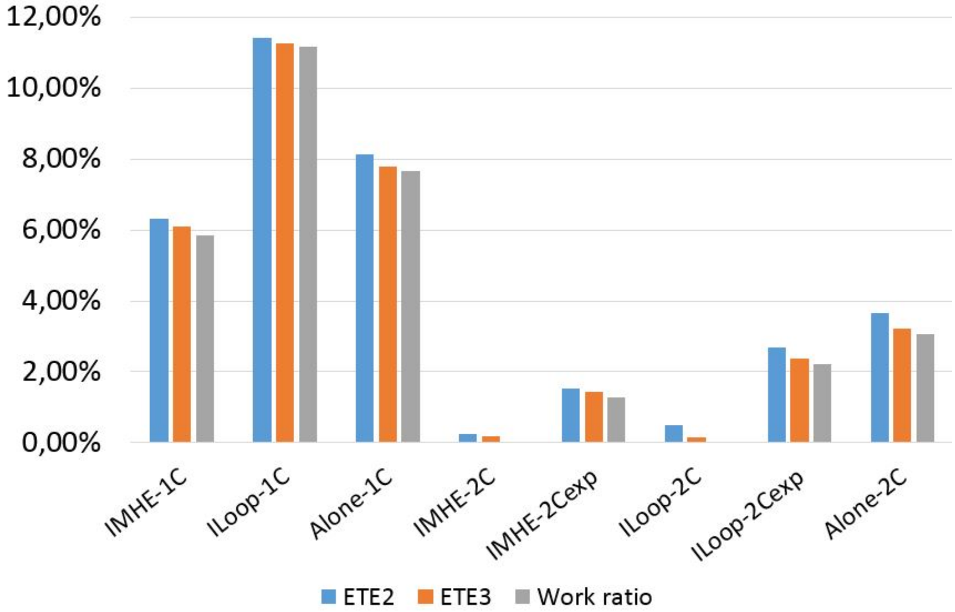

Figure 5.4: ETE2, ETE3 and work ratio, in %.

5.4 Material stream exergy ratio

In order to focus on comparing the different ASU products in all cases, another ratio can be evaluated in paralell of ETE: the ratio of material stream exergies, i.e. the ratio of LNG and ASU sinks to LNG and ASU sources. Equations (5.7) and (5.8) are used to calculate the material exergy ratio at stream level and at component level respectively. The values of this new ratio are summarized in table 5.4 both at stream and component level and displayed on Fig. 5.5.

$$\text{Material exergy ratio at stream level} = \frac{Sinks^{ETE2} - \sum_l W_l^{exp}}{Sources^{ETE2} - \sum_z W_z^{comp}}, \tag{5.7}$$

$$\text{Material exergy ratio at component level} = \frac{Sinks^{ETE3} - \sum_l W_l^{exp}}{Sources^{ETE3} - \sum_z W_z^{comp}}. \tag{5.8}$$

Since LNG feed and outlet exergies are the same in all cases, as they are defined in the simulation constraints, the material exergy ratio does not show the benefit of integrating LNG regasification to ASU. Yet, it highlights the result differences between exergy

Table 5.4: Material stream exergy ratio, in %.

Material exergy ratio	IMHE-1C	ILoop-1C	Alone-1C	IMHE-2C
Stream level	90.33	77.01	90.29	85.45
Component level	82.59	85.88	71.45	82.70

Material exergy ratio	IMHE-2Cexp	ILoop-2C	ILoop-2Cexp	Alone-2C
Stream level	85.49	94.87	94.27	88.76
Component level	82.70	85.09	83.56	66.70

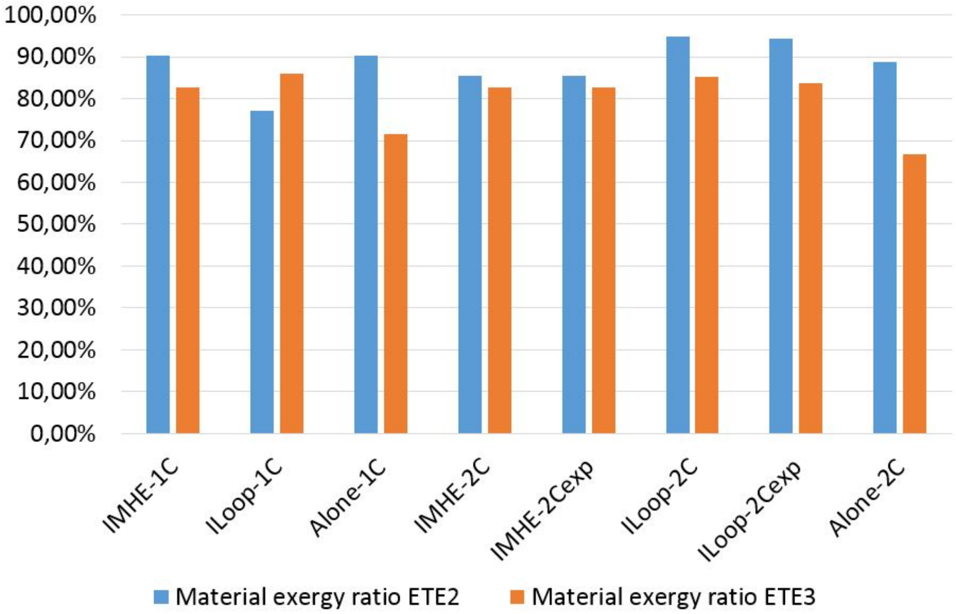

Figure 5.5: Comparison of material exergy ratio based on stream-level (ETE2) and component-level (ETE3) exergy terms, in %.

calculation at stream level and at component level. Stream level material exergy ratio is higher than the component level ratio in all cases, except in case ILoop-1C. In addition, the differences between cases for stream level ratio are lower than for component level ratio. Especially, component level material exergy ratio are lower for stand-alone cases than for integrated designs, as it was expected because the former achieved far lower amonts of high purity liquid nitrogen production. On the contrary, both integrated and stand-alone material exergy ratio have close values at stream level, which is surprising.

The decomposition of ASU sinks and sources for the different products at stream level is shown on Fig. 5.6 and Fig. 5.8, and at component level on Fig. 5.7 and Fig. 5.9. These graphs are also compared with regards to the calculation files used to obtain molar and partial molar temperature-based, pressure-based and mixing exergies for each product stream in each studied case. These detailed data are available in Appendix.

For liquid nitrogen product streams, the flow rates are the same for all cases in integrated models and lower for stand-alone cases. The purity is almost the same in all cases. The pressure levels are varying depending on the pressure of the distillation columns where the draw is taken from. The temperatures are saturation temperares corresponding to the pressure level, as the liquid nitrogen products are saturated liquids. The lower flow rates in cases Alone-1C and Alone-2C explains that they have lower sink values than integrated models. In case ILoop-1C, the sink value is lower than for other integrated cases since the pressure level is higher (380 kPa) leading to a higher temperature (from -193.6 ^{o}C at 130 kPa up to -182.4 ^{o}C at this pressure), thus decreasing largely the temperature-based exergy. Between cases IMHE-2C, IMHE-2Cexp, ILoop-2C and ILoop-2Cexp, only the purity of the stream is changing: 99.52 mol % for cases IMHE-2C and IMHE-2Cexp versus 99.34 mol % for cases ILoop-2C and ILoop-2Cexp. This small purity difference is accentuated at component level on Fig. 5.7, while it is almost non-visible at stream level on Fig. 5.6. This difference between stream and component level exergy values with purity variations can be explained looking at the variations of partial molar mixing exergies: they are increasing when the molar fraction of the component is increasing in the product stream compared to the feed stream. Thus, in liquid nitrogen product streams where the molar fraction of nitrogen is increased and the oxygen's one is decreased compared to the air feed, the partial molar mixing exergies of nitrogen are increasing as does the molar mixing exergy at stream level but the partial molar mixing exergies of oxygen are decreasing.That is why they are reduced sink values at component level compared to stream level and non-zero source terms at component level on Fig. 5.9, while they are equal to zero at stream level on Fig. 5.8. Case IMHE-1C has a considerably higher source value than all the other cases. Looking into details, it is due to a large decrease of the partial molar temperature-based exergy of nitrogen compared to the air feed. This is surprising as the product stream temperature is decreased considerably under ambient, which should lead to a temperature-based exergy increase. As the liquid nitrogen product comes directly from a flash separtor, it is close to phase change in case IMHE-1C. This could explain the unexpectedly large variation of temperature-based partial molar exergy of nitrogen. Yet, this could also be due to uncertainties for nitrogen and oxygen components, linked to the use of the equation of state Peng-Robinson during the simulation, which is originaly designed for hydrocarbons.

For liquid oxygen product streams, the purity is 100 mol % in all cases. The pressure levels are varying depending on the pressure of the distillation column where the draw stream is taken, and the temperature levels are varying accordingly as the liquid is saturated. The flow rates have the largest variations between cases with zero in stand-alone models up to 499.2 kmol/h in case ILoop-1C. The exergy values are similar at stream level and component level for all cases except for ILoop-1C, where the sink value is more than two times higher at stream level than at component level. Looking into details, the pressure-based contribution is the same for both levels, while the temperature-based term is around five times higher at stream level than at component level and the mixing term is three times higher at component level than at stream level. It seems to confirm that component level exergy is accentuating the mixing exergy value variation compared to stream level exergy.

The variations are also different at stream and component levels in ASU waste streams. Nitrogen partial molar mixing exergy increases and oxygen partial molar mixing exergy decreases when the molar fraction of nitrogen increases compared to the feed air composition, as in case IMHE-1C (stream N10). The opposite happens when the molar fraction of nitrogen decreases in the waste stream compared to the feed air, as in cases IMHE-2C, ILoop-2C, IMHE-2Cexp and ILoop-2Cexp. On the other hand, there is almost no source term at stream level, except for cases IMHE-2C and IMHE-2Cexp, where there is a small decrease in mixing exergy compared to the air feed. This could be explained as the largest variation in composition between the air feed and the waste stream occures in cases IMHE-2C and IMHE-2Cexp, so they could be spotted at stream level mixing exergy variations, while the other cases composition variations were too small to be seen at stream level.

For gaseous nitrogen product streams, the temperature is ambient, so temperature-based exergy variation is zero compared to feed air. Cases IMHE-2C and IMHE-2Cexp do not produce gaseous nitrogen. In other cases, the pressure levels are varying between 120 and 130 kPa. The purities are varying slightly between 99.52 mol % for cases ILoop-1C and Alone-1C, and 99.81 mol % for cases IMHE-1C, ILoop-2C, ILoop-2Cexp and Alone-2C. The flow rate variations are the largest between cases with a production of 256 kmol/h for case IMHE-1C up to 1875 kmol/h for case Alone-2C. The tendencies in the sink value results are the same at component and at stream level. In addition, they are consistant with the conditions of the gaseous nitrogen product streams for all cases. Yet, the sink values are lower at component level than at stream level and there is no source term at stream level, while there are at component level. The main difference is for mixing exergy terms: as the mole fraction of nitrogen is increased compared to the air feed, the partial molar exergy values of nitrogen are increasing, while the ones of oxygen are decreasing.

Cases ILoop-1C, IMHE-2C and IMHE-2Cexp are not producing gaseous oxygen. In other cases, its temperature is ambient so there is no temperature-based exergy variation compared to the air feed. Its pressure is varying between 120 and 130 kPa and its purity is 100 mol %. The main changing parameter is the production flow rate from 143 kmol/h for case IMHE-1C up to 504 kmol/h for case Alone-2C. The variation tendencies between cases are the same at component and at stream level, but the sink values are lower at stream level than at component level. Looking at detailed data, the mixing exergy variations are higher at component level.

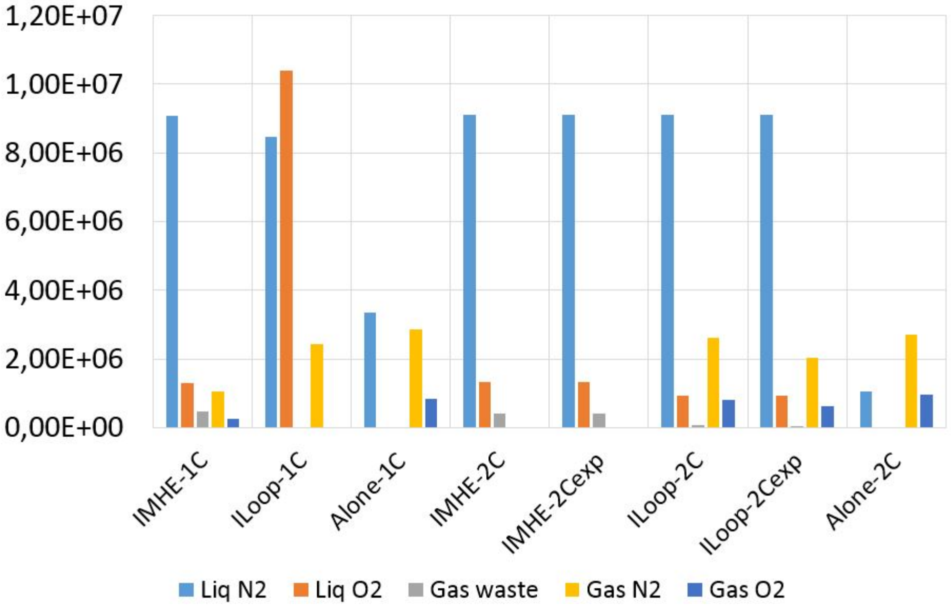

Figure 5.6: ASU sink decomposition per product at stream level (ETE2), in kW.

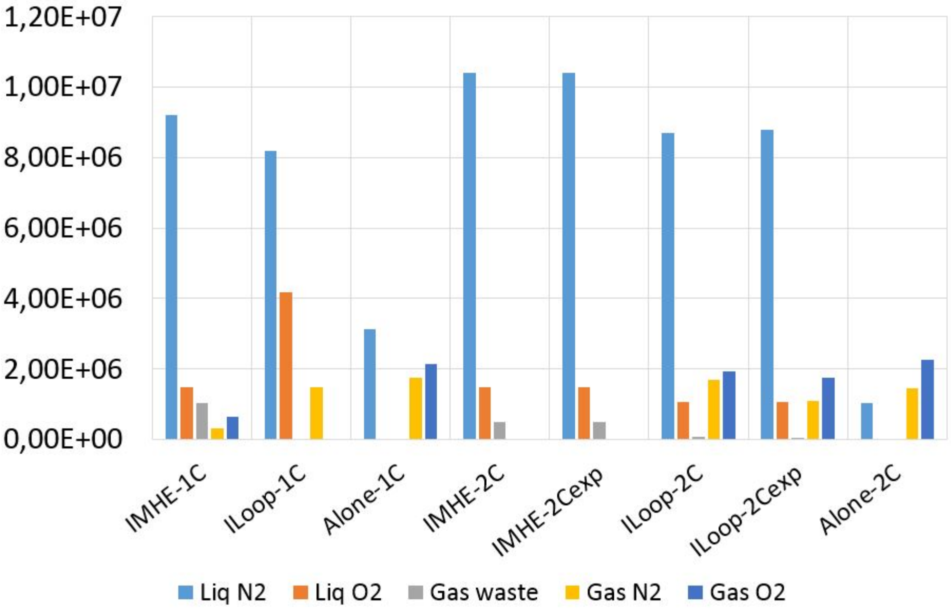

Figure 5.7: ASU sink decomposition per product at component level (ETE3), in kW.

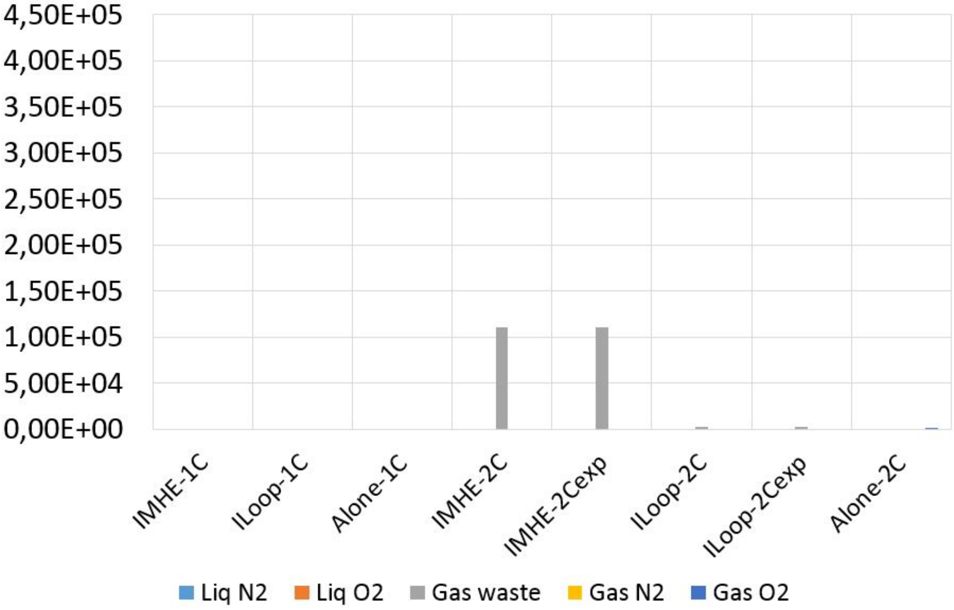

Figure 5.8: ASU source decomposition per product at stream level (ETE2), in kW.

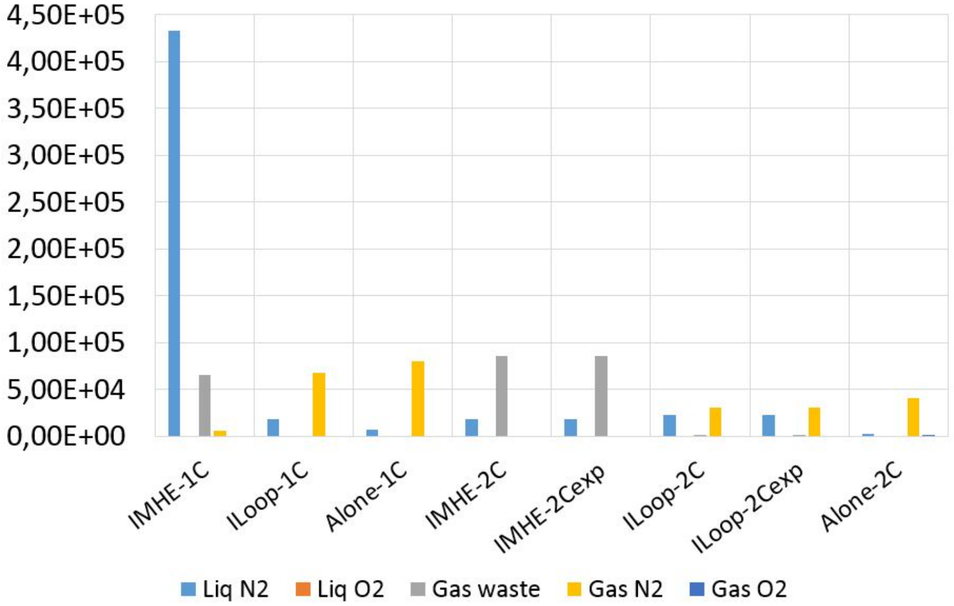

Figure 5.9: ASU source decomposition per product component level (ETE3), in kW.

Chapter 6

Conclusion

6.1 Key results and comments

Integrated ASU and LNG regasification have been evaluated with various performance indicators.

ASU uses LNG cold exergy in the lower range of the available temperature-based exergy, from a storage temperature of -162 ^{o}C in the receiving terminal up to outlet temperatures varying between -116 ^{o}C for the best case (ILoop-2Cexp) or an average temperature around -87 ^{o}C. Thus, ASU integration can be coupled with other applications, in order to use the rest of the available LNG cold exergy, like power production by Rankine cycle or refrigeration. The possibility to integrate several applications of LNG cold recovery in a cold industrial facility is already applied at Senboku LNG terminal and is a promising way to decrease exergy losses to seawater or air during LNG regasification. In ASU, LNG cold exergy consumption is correlated with the flow rates of integrated streams to LNG heat exchangers. A way to reduce this consumption can be to minimize the flow rate of the nitrogen loop or to increase LNG flow rate if the capacity of the receiving terminal is sufficient. The use of LNG cold exergy in compressor after-cooling should be limited when it does not lead to lack of cold duty in the heat balance of the main heat exchangers.

The work requirement per amont of liquid nitrogen produced is a constraining indicator, as it requires to scale the configurations to the same flow rate of liquid nitrogen produced to be able to compare them fairly. Thus, stand-alone ASU required more than two times higher $Work_{N_2}$ than integrated models average because they could not achieve the specified flow rate of liquid nitrogen production. This indicator provides a restrictive mean of comparison as it evaluates the work requirements for only one ASU product, disregarding the other products which are varying between designs. ASU work consumption is correlated to the flow rates in the nitrogen loop. So minimizing the work requirements can be achieved by reducing those flow rates.

Exergy Transfer Effectiveness, extended to analyze mixing exergy variations, does not require to rescale the ASU configurations to a constrained production rate, contrary to $Work_{N_2}$. Moreover, it provides a mean to evaluate the performance of ASU with regards to the exergy values of all the products, increasing the fairness of the comparison between the different designs compared to the other performance indicators. Yet, as the work requirements in ASU processes are overweighting the exergy flow variations in material streams, ETE is almost equivalent to the ratio of expansion work production to compression work needs. The strategies used by the studied cases were different in terms of optimization of work requirements, so ETE was not fully satisfying to give a general comparison of integrated ASU according to the classification proposed in this study, even though it increased the accuracy of the comparison. The superiority of all integrated cases compared to stand-alone designs, in terms of achieved ASU liquid production rates, was conter-balanced by work requirements, thus diverging from the expected results for the exergy efficiencies: only the single column ASU with LNG integrated in the nitrogen loop performed better than stand-alone designs. To validate the tendencies of the results obtained for the general classification, more designs should be studied for each possible case or the cases should be optimized. For now, the solid conclusion is that the best performance among integrated cases was achieved by recuperative vapor recompression ASU design using heat pumping effect proposed by Fu and Gundersen (2013), followed by the use of integrated column draws coupled to compression-expansion proposed by Mehrpooya et al. (2015). Both designs were relying on single column ASU configurations, which suggests that single column ASU can achieve better performances than two-column designs.

To focus on exergy flow variations between ASU products and to compare the consistancy of the results between ETE at stream level and at component level, the ratio of material stream sinks to sources were evaluated in all cases. Both levels showed that the highest value product in terms of exergy was the liquid nitrogen stream, for the set of constraints used in the study. But the analysis at stream level was not consistant because it did not show that integrated models have a higher performance than stand-alone models, even though the later achieve only a lower production of liquid nitrogen. When looking down to the decomposition of exergy flow variations per ASU product stream, it appears that stream level calculation under-evaluates the influence of stream composition variations on exergy compared to component level analysis. It can then be confirmed than component level exergy analysis is more consistant than stream level calculation for the evaluation of processes with chemical changes. A limitation of this result is the introduction of uncertainties for streams containing oxygen and nitrogen by the use of Peng-Robinson equation of state during modelization, as it is originally designed for hydrocarbons only.

6.2 Further work

A limitation in the comparison of the studied cases according to the proposed classification of integrated ASU and LNG regasification designs is the lack of optimization work. Though it was originally planed by the thesis description, it could not be performed due to lack of time and the complexity of the processes, notably because of cryogenic distillation with high purity products. It could be implemented in further work in order to validate the results from ETE3 calculations on the higher efficiency of single column ASU. It should be linked to the elaboration of standard design for each classification case.

To provide further tools for the improvement of overall ASU designs, unit operation ETE3 calculation could be performed. It would allow to spot exergy losses at unit level in the overall designs.

Bibliography

Agrawal, R., Herron, D. M., 2000. Encyclopedia of separation science, Chapter 3, AIR LIQUEFACTION: DISTILLATION. ELSEVIER.

Beysel, G., 2009. Enhanced cryogenic air separation a proven process applied to oxyfuel - linde. In: First Oxyfuel Combustion Conference. Cottbus.

Ebrahimi, A., Meratizaman, M., Reyhani, H. A., Pourali, O., Amidpour, M., 2015. Energetic, exergetic and economic assessment of oxygen production from two columns cryogenic air separation unit. Energy 90, 12981316.

Efrat, T., 2011. Utilizing available ”coldness” from lng regasification process for seawater desalination. In: IDA World Congress. Perth Convention and Exhibition Centre (PCEC), Perth, Western Australia.

Egashira, S., 2013. Lng vaporizer for lng re-gasification terminal. KOBELCO TECHNOLOGY REVIEW 32, 64–69.

Fu, C., Gundersen, T., 2013. Recuperative vapor recompression heat pumps in cryogenic air separation processes. Energy 59, 708–718.

Gomez, M. R., F., G. R., Gomez, J. R., Carril, J. C., 2014. Review of thermal cycles exploiting the exergy of liquefied natural gas in regasification process. Renewable and Sustainable Energy Reviews 38, 781–795.

IGU, 2016. 2016 world lng report. In: LNG 18 Conference and Exhibition Edition. Fornebu, Norway.

La Rocca, V., 2011. Cold recovery during regasification of lng part two: Applications in an agro food industry and a hypermarket. Energy Review 36, 4897–4908.

Marmolejo-Correa, D., Gundersen, T., 2015. A new efficiency parameter for exergy analysis in low temperature processes. Int. J. Exergy 17 (2), 135170.

Mehrpooya, M., Sharifzadeh, M. M. M., Rosen, M. A., 2015. Optimum design and exergy analysis of a novel cryogenic air separation process with lng cold energy utilization. Energy 90, 2047–2069.

Mokhatab, S., Mak, J., Valappil, J., Wood, D. A., 2014. Handbook of Liquefied Natural Gas. ELSEVIER.

Moll, A., 2014. Distillastion: Operation and Applications, Chapter 6 - Air Distillation. ELSEVIER.

Moran, M. J., Shapiro, H. N., Boettner, D. D., Bailey, M. B., 2011. Fundamentals of engineering thermodynamics, 7th Edition. John Wiley and Sons, Inc.

Nguyen, T., Voldsund, M., Elmegaard, B., Ertesvaag, I., Kjelstrup, S., 2014. On the definition of exergy efficiencies for petroleum systems: Application to offshore oil and gas processing. Energy 73, 264282.

Patel, D., Mak, J., Rivera, D., Angtuaco, J., 2013. Lng vaporizer selection based on site ambient conditions. In: Gas Processor Association, 30th annual conference, Fluor. Edinburgh.

Sato, N., 2004. Chemical Energy and Exergy: An Introduction to Chemical Thermodynamics for Engineers. 1st ed. Elsevier.

Szargut, J., Morris, D. R., Steward, F. R., 1988. Exergy analysis of thermal, chemical, and metallurgical processes. Hemisphere Publishing Corporation.

Tesch, S., Morosuk, T., Tsatsaronis, G., 2016. Advanced exergy analysis applied to the process of regasification of lng integrated into an air separation process. Energy 117, 550–561.

Uwitonze, H., Han, S., Jangryeok, C., Hwang, K. S., 2014. Design process of lng heavy hydrocarbons fractionation: Low lng temperature recovery. Chemical engineering and processing: process intensification 85, 187–195.

Xu, W., Duan, J., Mao, W., 2014. Process study and exergy analysis of a novel air separation process cooled by lng cold energy. Journal of Thermal Science 23, 77–84.

Zheng, J., Li, Y., Li, G., Si, B., 2015. Simulation of a novel single-column cryogenic air separation process using lng cold energy. Physics Procedia 67, 116–122.

Chapter 7

Appendix

7.1 Exergy presentation

The exergy concept dates back to the mid 20^{th} century. The term exergy comes from the Greek words ex (external) and ergos (work) and it is defined by Moran et al. (2011) : exergy is the maximum theoretical work obtainable from an overall system consisting of a system and the environment as the system comes into equilibrium with the environment.

As two systems in different states are brought into interaction, there is a potential to develop work when they converge to a state of equilibrium with each other. The maximum amount of that work, when all the processes involved are reversible, is exergy, also described as available energy or availability. The potential irreversibilities cause losses or exergy destruction, which is a partial inability to produce work. The environment should be defined with care as it is the reference state for zero exergy. A standard environment is defined with a reference pressure, temperature and chemical composition. In the study, environment conditions have been set as atmospheric pressure 1 bara and atmospheric temperature 25 ^{o}C. Air is set as the environment with its reference chemical composition defined by Szargut et al. (1988). Reaching equilibrium is achieved by exchange of energy and/or matter between the system and its surroundings. In order to characterize these exchanges, exergy is decomposed into several terms.

Various decomposition have been proposed. This study relies on the one described by Marmolejo-Correa and Gundersen (2015), as it is the basis for ETE. Its full version is shown on Fig. 7.1. The terms relevant for this thesis are thermo-mechanical exergy and chemical exergy, both carried by matter, and work carried by energy streams.

Thermo-mechanical exergy is commonly decomposed into temperature- and pressure-based molar exergies, which are calculated thanks to equations (7.1) and (7.2) at stream level. The temperature-based part is defined by bringing the system from its initial temperature T to the environment temperature T_0 at constant initial pressure p while the pressure-based part is bringing the system from p to p_0 at constant temperature T_0. Yet, this decomposition is not unique as there are an infinite number of paths for the system to go from p and T state to p_0 and T_0.

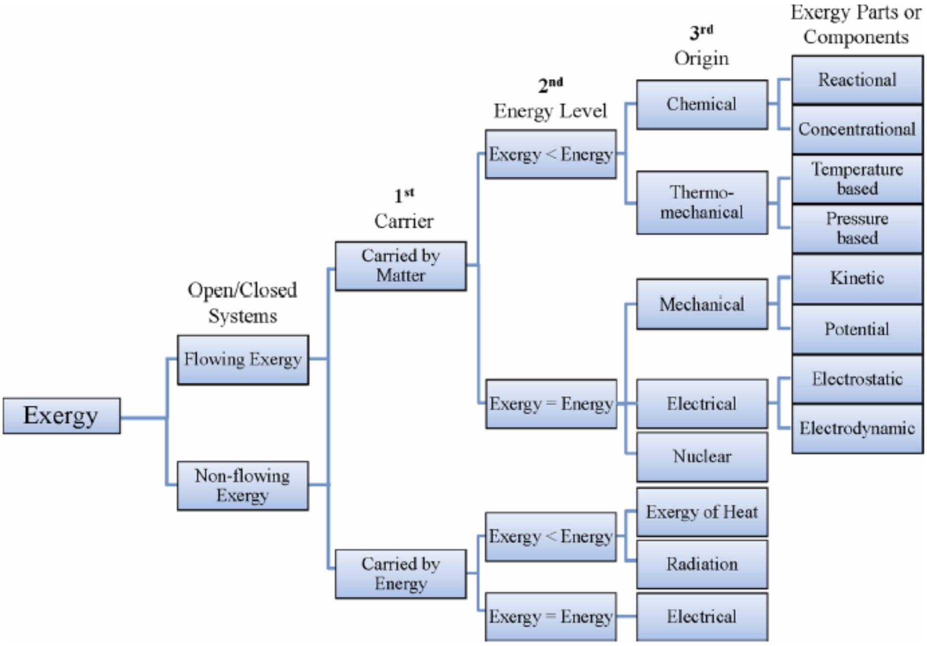
Exergy
Open/Closed Systems
Flowing Exergy
Non-flowing Exergy
1st Carrier
Carried by Matter
Carried by Energy
2nd Energy Level
Exergy < Energy
Exergy = Energy
Exergy < Energy
Exergy = Energy
3rd Origin
Chemical
Thermo-mechanical
Mechanical
Electrical
Nuclear
Exergy of Heat
Radiation
Electrical
Exergy Parts or Components
Reactional
Concentrational
Temperature based
Pressure based
Kinetic
Potential
Electrostatic
Electrodynamic

Figure 7.1: Decomposition of exergy proposed by Marmolejo-Correa and Gundersen (2015).

$$e_x^T = [h(T,p) - h(T_0,p)] - T_0[s(T,p) - s(T_0,p)], \tag{7.1}$$

$$e_x^P = [h(T_0,p) - h(T_0,p_0)] - T_0[s(T_0,p) - s(T_0,p_0)]. \tag{7.2}$$

where h is the molar enthalpy in kJ per kmol and s the molar entropy in kJ per kmol per K at the temperature and pressure expressed in the parenthesis. T_0 is there expressed in K.

The chemical exergy of a system refers to the deviation in its chemical composition from reference substances in the environment. The chemical exergy of a mixture at stream level as given by Sato (2004) is:

$$e_x^{CH} = \underbrace{\sum_i x_i e_{x_{i,0}}^{CH}}_{I} + \underbrace{(\sum_i x_i(h_i - h_{i,0})) - T_0(\sum_i x_i(s_i - s_{i,0}))}_{II}\,. \tag{7.3}$$

where *i* are the components of the mixture, $e_{x_{i,0}}^{CH}$, $h_{i,0}$ and $s_{i,0}$ the molar chemical exergy, enthalpy and entropy of component *i* pure, h_i, s_i and x_i the molar enthalpy, molar entropy and mole fraction of component *i* in the mixture. Term I represents the chemical exergy of each pure component and term II the reduction in chemical exergy due to the mixture effect.

Exergy can be calculated down to chemical component variations for each exergy category, thanks to partial molar exergies. Equation (7.4), described by Nguyen et al. (2014), is used for this purpose. The partial molar exergy of component *i* in stream *k* is calculated by partially derivating the exergy of stream *k* with respect to the molar quantity of component *i* in the stream, holding temperature, pressure and other component molar quantities in the stream constant.

$$\tilde{e}^{j}_{x_{k,i}} = (\frac{\partial E^{j}_{x_j}}{\partial n_{k,i}})_{T,P,n_{k,\neq i}}, \tag{7.4}$$

where *j* stands for temperature-based, pressure-based or compositional, $E^{j}_{x_j}$ is the *j* exergy of stream *k* calculated as explained in the previous paragraphs, $n_{k,i}$ is the molar quantity of component *i* in stream *k*. Equation (7.5) allows to go back to the exergy of stream *k* by summation of the partial molar exergies times molar quantities.

$$E^{j}_{x_k} = \sum_{i} n_{k,i} \tilde{e}^{j}_{x_{k,i}}. \tag{7.5}$$

7.2 Decomposition of exergy sinks and sources of the overall process into ASU, LNG and energy contributions

Table 7.1: ETE2 decomposition in GW.

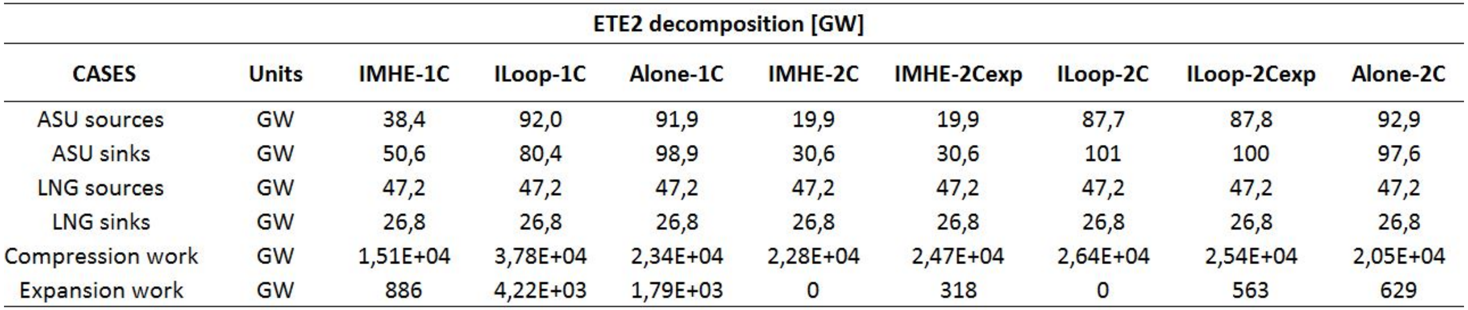

ETE2 decomposition [GW]									
CASES	**Units**	**IMHE-1C**	**ILoop-1C**	**Alone-1C**	**IMHE-2C**	**IMHE-2Cexp**	**ILoop-2C**	**ILoop-2Cexp**	**Alone-2C**
ASU sources	GW	38,4	92,0	91,9	19,9	19,9	87,7	87,8	92,9
ASU sinks	GW	50,6	80,4	98,9	30,6	30,6	101	100	97,6
LNG sources	GW	47,2	47,2	47,2	47,2	47,2	47,2	47,2	47,2
LNG sinks	GW	26,8	26,8	26,8	26,8	26,8	26,8	26,8	26,8
Compression work	GW	1,51E+04	3,78E+04	2,34E+04	2,28E+04	2,47E+04	2,64E+04	2,54E+04	2,05E+04
Expansion work	GW	886	4,22E+03	1,79E+03	0	318	0	563	629

Table 7.2: ETE3 decomposition in GW.

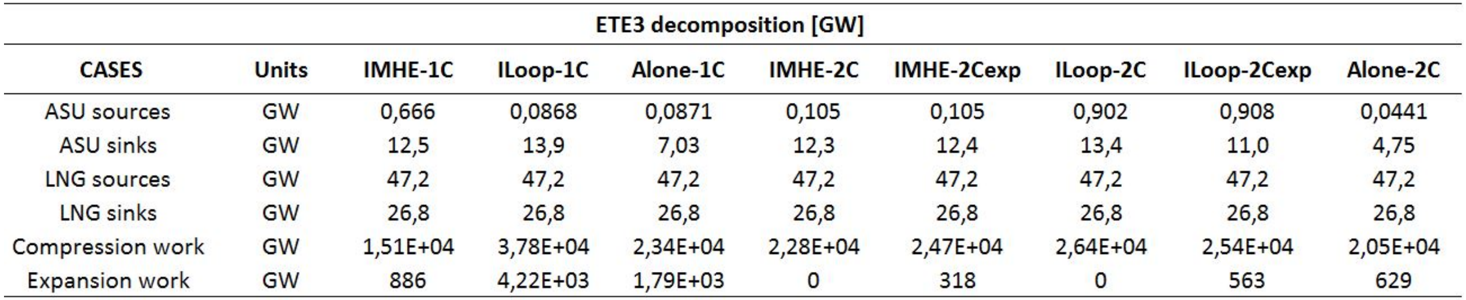

ETE3 decomposition [GW]

CASES	Units	IMHE-1C	ILoop-1C	Alone-1C	IMHE-2C	IMHE-2Cexp	ILoop-2C	ILoop-2Cexp	Alone-2C
ASU sources	GW	0,666	0,0868	0,0871	0,105	0,105	0,902	0,908	0,0441
ASU sinks	GW	12,5	13,9	7,03	12,3	12,4	13,4	11,0	4,75
LNG sources	GW	47,2	47,2	47,2	47,2	47,2	47,2	47,2	47,2
LNG sinks	GW	26,8	26,8	26,8	26,8	26,8	26,8	26,8	26,8
Compression work	GW	1,51E+04	3,78E+04	2,34E+04	2,28E+04	2,47E+04	2,64E+04	2,54E+04	2,05E+04
Expansion work	GW	886	4,22E+03	1,79E+03	0	318	0	563	629

7.3 Decomposition of exergy contribution per exergy term per ASU product stream at stream level and at component level

The following tables show the molar and partial molar exergy variations between the air feed and each ASU product times its molar flow rate. Each of these terms is either contributing as a source (negative) or a sink (positive) to ETE.

Table 7.3: Decomposition of exergy flow terms for ASU products at stream level in case IMHE-1C, in kW.

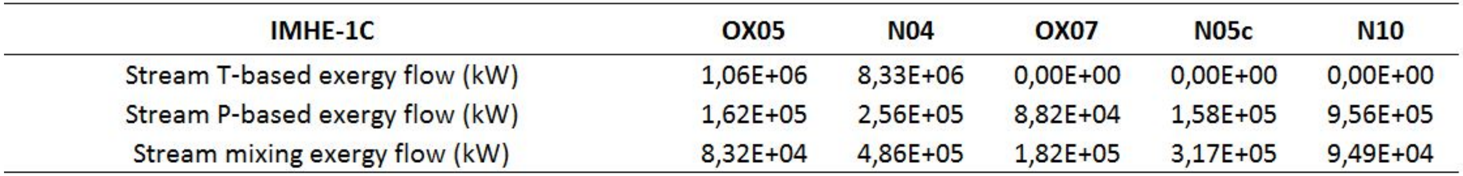

IMHE-1C	OX05	N04	OX07	N05c	N10
Stream T-based exergy flow (kW)	1,06E+06	8,33E+06	0,00E+00	0,00E+00	0,00E+00
Stream P-based exergy flow (kW)	1,62E+05	2,56E+05	8,82E+04	1,58E+05	9,56E+05
Stream mixing exergy flow (kW)	8,32E+04	4,86E+05	1,82E+05	3,17E+05	9,49E+04

Table 7.4: Decomposition of exergy flow terms for ASU products at component level in case IMHE-1C, in kW.

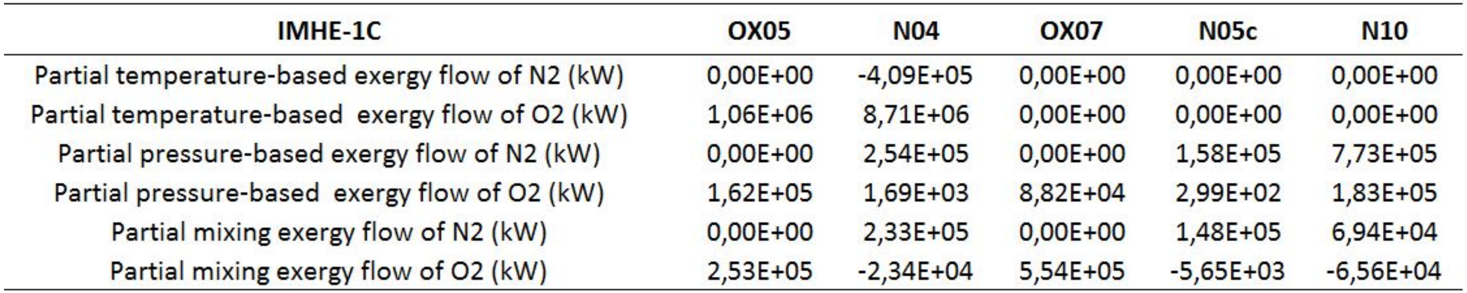

IMHE-1C	OX05	N04	OX07	N05c	N10
Partial temperature-based exergy flow of N2 (kW)	0,00E+00	-4,09E+05	0,00E+00	0,00E+00	0,00E+00
Partial temperature-based exergy flow of O2 (kW)	1,06E+06	8,71E+06	0,00E+00	0,00E+00	0,00E+00
Partial pressure-based exergy flow of N2 (kW)	0,00E+00	2,54E+05	0,00E+00	1,58E+05	7,73E+05
Partial pressure-based exergy flow of O2 (kW)	1,62E+05	1,69E+03	8,82E+04	2,99E+02	1,83E+05
Partial mixing exergy flow of N2 (kW)	0,00E+00	2,33E+05	0,00E+00	1,48E+05	6,94E+04
Partial mixing exergy flow of O2 (kW)	2,53E+05	-2,34E+04	5,54E+05	-5,65E+03	-6,56E+04

Table 7.5: Decomposition of exergy flow terms for ASU products at stream level in case ILoop-1C, in kW.

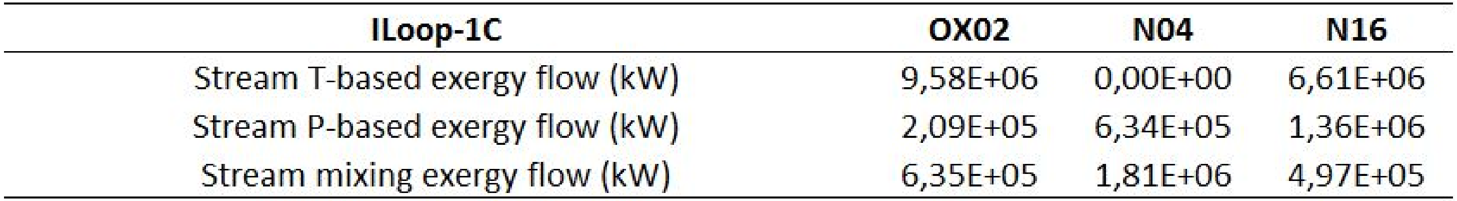

ILoop-1C	OX02	N04	N16
Stream T-based exergy flow (kW)	9,58E+06	0,00E+00	6,61E+06
Stream P-based exergy flow (kW)	2,09E+05	6,34E+05	1,36E+06
Stream mixing exergy flow (kW)	6,35E+05	1,81E+06	4,97E+05

Table 7.6: Decomposition of exergy flow terms for ASU products at component level in case ILoop-1C, in kW.

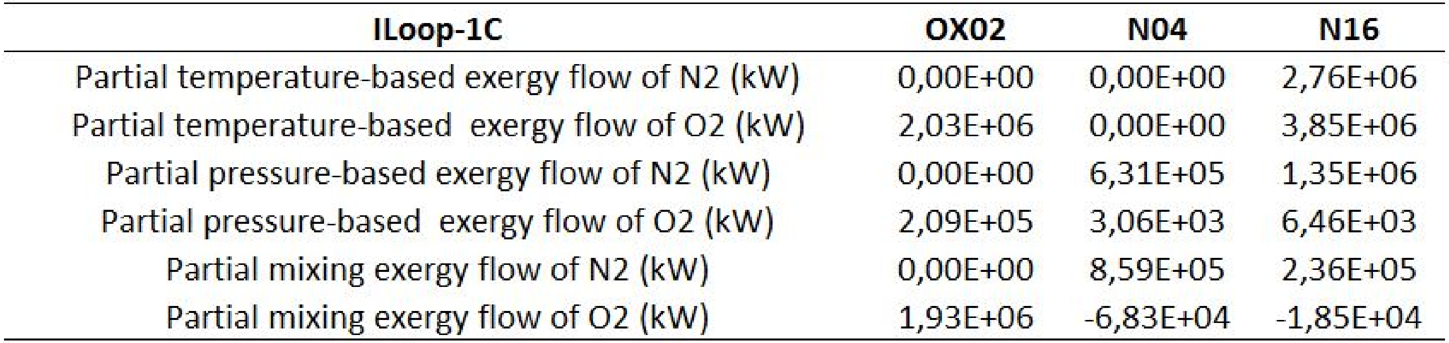

ILoop-1C	OX02	N04	N16
Partial temperature-based exergy flow of N2 (kW)	0,00E+00	0,00E+00	2,76E+06
Partial temperature-based exergy flow of O2 (kW)	2,03E+06	0,00E+00	3,85E+06
Partial pressure-based exergy flow of N2 (kW)	0,00E+00	6,31E+05	1,35E+06
Partial pressure-based exergy flow of O2 (kW)	2,09E+05	3,06E+03	6,46E+03
Partial mixing exergy flow of N2 (kW)	0,00E+00	8,59E+05	2,36E+05
Partial mixing exergy flow of O2 (kW)	1,93E+06	-6,83E+04	-1,85E+04

Table 7.7: Decomposition of exergy flow terms for ASU products at stream level in case Alone-1C, in kW.

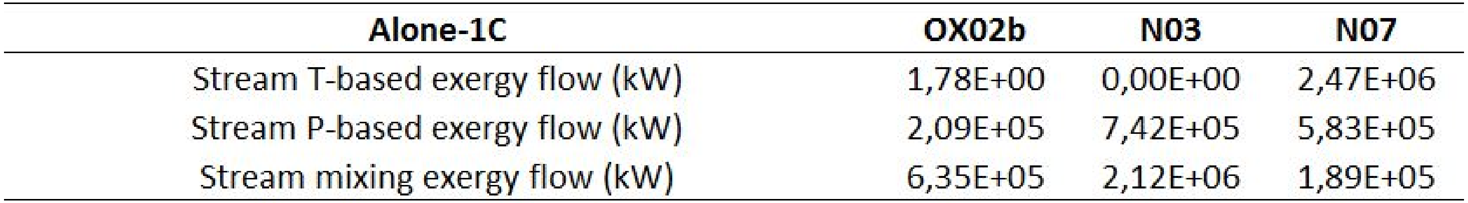

Alone-1C	OX02b	N03	N07
Stream T-based exergy flow (kW)	1,78E+00	0,00E+00	2,47E+06
Stream P-based exergy flow (kW)	2,09E+05	7,42E+05	5,83E+05
Stream mixing exergy flow (kW)	6,35E+05	2,12E+06	1,89E+05

Table 7.8: Decomposition of exergy flow terms for ASU products at component level in case Alone-1C, in kW.

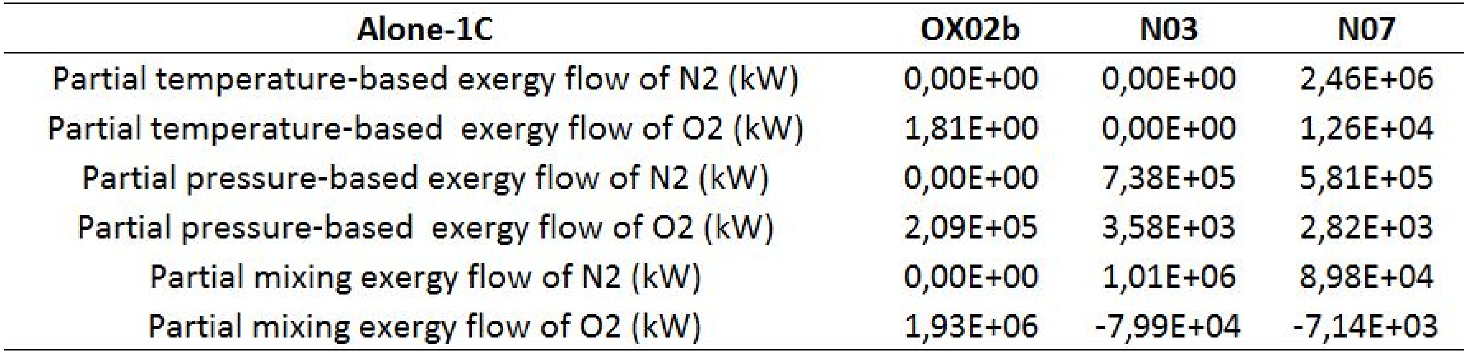

Alone-1C	OX02b	N03	N07
Partial temperature-based exergy flow of N2 (kW)	0,00E+00	0,00E+00	2,46E+06
Partial temperature-based exergy flow of O2 (kW)	1,81E+00	0,00E+00	1,26E+04
Partial pressure-based exergy flow of N2 (kW)	0,00E+00	7,38E+05	5,81E+05
Partial pressure-based exergy flow of O2 (kW)	2,09E+05	3,58E+03	2,82E+03
Partial mixing exergy flow of N2 (kW)	0,00E+00	1,01E+06	8,98E+04
Partial mixing exergy flow of O2 (kW)	1,93E+06	-7,99E+04	-7,14E+03

Table 7.9: Decomposition of exergy flow terms for ASU products at stream level in case IMHE-2C, in kW.

IMHE-2C	OX05	N08	N10
Stream T-based exergy flow (kW)	1,22E+06	8,35E+06	0,00E+00
Stream P-based exergy flow (kW)	1,28E+04	2,56E+05	3,97E+05
Stream mixing exergy flow (kW)	7,98E+04	4,97E+05	-1,11E+05

Table 7.10: Decomposition of exergy flow terms for ASU products at component level in case IMHE-2C, in kW.

IMHE-2C	OX05	N08	N10
Partial temperature-based exergy flow of N2 (kW)	0,00E+00	5,50E+06	0,00E+00
Partial temperature-based exergy flow of O2 (kW)	1,22E+06	4,39E+06	0,00E+00
Partial pressure-based exergy flow of N2 (kW)	0,00E+00	2,55E+05	3,06E+05
Partial pressure-based exergy flow of O2 (kW)	1,28E+04	1,22E+03	9,02E+04
Partial mixing exergy flow of N2 (kW)	0,00E+00	2,36E+05	-8,64E+04
Partial mixing exergy flow of O2 (kW)	2,43E+05	-1,86E+04	9,11E+04

Table 7.11: Decomposition of exergy flow terms for ASU products at stream level in case IMHE-2C exp, in kW.

IMHE-2Cexp	OX05	N08	N10
Stream T-based exergy flow (kW)	1,23E+06	8,35E+06	0,00E+00
Stream P-based exergy flow (kW)	1,28E+04	2,56E+05	3,97E+05
Stream mixing exergy flow (kW)	7,99E+04	4,97E+05	-1,11E+05

Table 7.12: Decomposition of exergy flow terms for ASU products at component level in case IMHE-2C exp, in kW.

IMHE-2Cexp	OX05	N08	N10
Partial temperature-based exergy flow of N2 (kW)	0,00E+00	5,51E+06	0,00E+00
Partial temperature-based exergy flow of O2 (kW)	1,23E+06	4,39E+06	0,00E+00
Partial pressure-based exergy flow of N2 (kW)	0,00E+00	2,55E+05	3,06E+05
Partial pressure-based exergy flow of O2 (kW)	1,28E+04	1,23E+03	9,02E+04
Partial mixing exergy flow of N2 (kW)	0,00E+00	2,36E+05	-8,64E+04
Partial mixing exergy flow of O2 (kW)	2,43E+05	-1,86E+04	9,11E+04

Table 7.13: Decomposition of exergy flow terms for ASU products at stream level in case ILoop-2C, in kW.

ILoop-2C	OX03	OX04c	N03c	OX05c	N10
Stream T-based exergy flow (kW)	8,56E+05	0,00E+00	0,00E+00	0,00E+00	8,35E+06
Stream P-based exergy flow (kW)	2,79E+04	2,65E+05	8,70E+05	7,85E+04	2,56E+05
Stream mixing exergy flow (kW)	5,76E+04	5,47E+05	1,74E+06	-2,49E+03	4,87E+05

Table 7.14: Decomposition of exergy flow terms for ASU products at component level in case ILoop-2C, in kW.

ILoop-2C	OX03	OX04c	N03c	OX05c	N10
Partial temperature-based exergy flow of N2 (kW)	0,00E+00	0,00E+00	0,00E+00	0	3,81E+06
Partial temperature-based exergy flow of O2 (kW)	8,56E+05	0,00E+00	0,00E+00	0	4,41E+06
Partial pressure-based exergy flow of N2 (kW)	0,00E+00	0,00E+00	8,68E+05	61631,484	2,55E+05
Partial pressure-based exergy flow of O2 (kW)	2,79E+04	2,65E+05	1,65E+03	16913,987	1,69E+03
Partial mixing exergy flow of N2 (kW)	0,00E+00	0,00E+00	8,13E+05	-1896,6052	2,33E+05
Partial mixing exergy flow of O2 (kW)	1,75E+05	1,67E+06	-3,11E+04	1931,0795	-2,35E+04

Table 7.15: Decomposition of exergy flow terms for ASU products at stream level in case ILoop-2C exp, in kW.

ILoop-2Cexp	OX03	OX04d	N03d	N05d	N10
Stream T-based exergy flow (kW)	8,59E+05	0,00E+00	0,00E+00	0,00E+00	8,35E+06
Stream P-based exergy flow (kW)	2,80E+04	8,75E+04	2,87E+05	2,58E+04	2,56E+05
Stream mixing exergy flow (kW)	5,78E+04	5,47E+05	1,74E+06	-2,22E+03	4,87E+05

Table 7.16: Decomposition of exergy flow terms for ASU products at component level in case ILoop-2C exp, in kW.

ILoop-2Cexp	OX03	OX04c	N03c	OX05c	N10
Partial temperature-based exergy flow of N2 (kW)	0,00E+00	0,00E+00	0,00E+00	0	3,90E+06
Partial temperature-based exergy flow of O2 (kW)	8,59E+05	0,00E+00	0,00E+00	0	4,41E+06
Partial pressure-based exergy flow of N2 (kW)	0,00E+00	0,00E+00	2,86E+05	20276,373	2,55E+05
Partial pressure-based exergy flow of O2 (kW)	2,80E+04	8,75E+04	5,42E+02	5543,312	1,69E+03
Partial mixing exergy flow of N2 (kW)	0,00E+00	0,00E+00	8,13E+05	-1686,7057	2,33E+05
Partial mixing exergy flow of O2 (kW)	1,76E+05	1,67E+06	-3,11E+04	1714,0477	-2,35E+04

Table 7.17: Decomposition of exergy flow terms for ASU products at stream level in case Alone-2C, in kW.

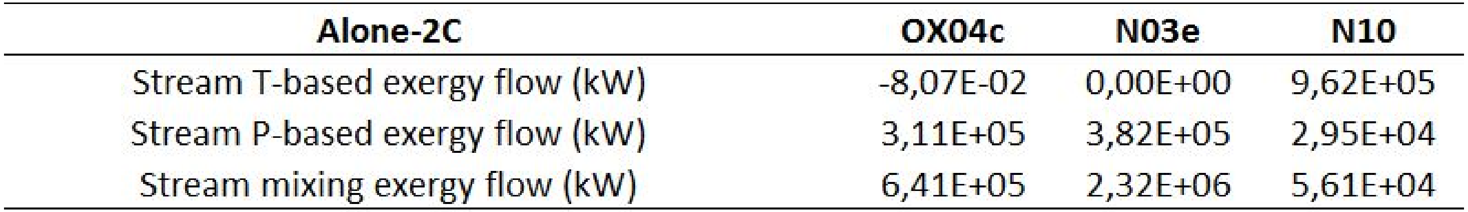

Alone-2C	**OX04c**	**N03e**	**N10**
Stream T-based exergy flow (kW)	-8,07E-02	0,00E+00	9,62E+05
Stream P-based exergy flow (kW)	3,11E+05	3,82E+05	2,95E+04
Stream mixing exergy flow (kW)	6,41E+05	2,32E+06	5,61E+04

Table 7.18: Decomposition of exergy flow terms for ASU products at component level in case Alone-2C, in kW.

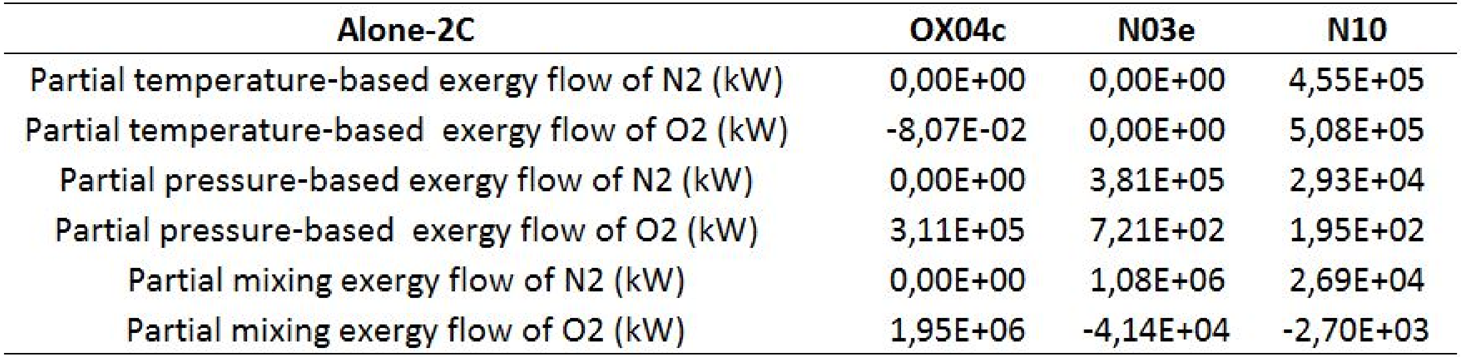

Alone-2C	**OX04c**	**N03e**	**N10**
Partial temperature-based exergy flow of N2 (kW)	0,00E+00	0,00E+00	4,55E+05
Partial temperature-based exergy flow of O2 (kW)	-8,07E-02	0,00E+00	5,08E+05
Partial pressure-based exergy flow of N2 (kW)	0,00E+00	3,81E+05	2,93E+04
Partial pressure-based exergy flow of O2 (kW)	3,11E+05	7,21E+02	1,95E+02
Partial mixing exergy flow of N2 (kW)	0,00E+00	1,08E+06	2,69E+04
Partial mixing exergy flow of O2 (kW)	1,95E+06	-4,14E+04	-2,70E+03